UNIVERSITY OF SOUTHAMPTON

QUANTIFICATION OF MYOCARDIAL BLOOD FLOW AND FUNCTION : AN EXPERIMENTAL STUDY

Soroosh Firoozan BM (Hons) MRCP

Dissertation Submitted for the Degree of
Doctor of Medicine

Health Sciences Centre
University of Virginia
Charlottesville, Virginia

March 2000

UNIVERSITY OF SOUTHAMPTON

ABSTRACT

FACULTY OF MEDICINE

SCHOOL OF MEDICINE

Doctor of Medicine

QUANTIFICATION OF MYOCARDIAL BLOOD FLOW AND FUNCTION : AN EXPERIMENTAL STUDY

by Soroosh Firoozan BM(Hons) MRCP

The appropriate management of patients with dysfunctional myocardium in the setting of coronary artery disease continues to challenge cardiologists. The causes of ischaemic myocardial dysfunction appear to be relatively straightforward. The myocardium is either scarred and irreversibly damaged (non-viable) or it is not (viable). In the latter, myocardial blood flow at rest is either normal (stunned) or below normal (hibernating). Repetitive ischaemia and chronic down-regulation of myocardial function respectively, have been held responsible for the observed dysfunction. The identification of viable myocardium leads to more accurate targeting of revascularization strategies.

The assessment of regional microvascular myocardial blood flow is likely to predict the outcome of revascularization procedures. The problem has been the adequate assessment of flow. Furthermore, the lack of a suitable experimental model that mimics chronic human coronary disease has made the pathophysiology of dysfunctional myocardium more difficult to understand.

In a series of experiments the application of myocardial contrast echocardiography (MCE) in the quantification of regional myocardial blood flow was examined. Using this method, the passage of intravenously injected microbubbles can be imaged through the myocardium with echocardiography. The conditions allowing quantifiable assessment of myocardial opacification were identified in the preliminary studies. In experimental models of coronary disease, this method was used to both detect and judge the severity of epicardial coronary stenoses. Using MCE, the physiology of coronary autoregulation was studied and a method was proposed for the measurement of absolute regional myocardial blood flow. MCE -derived myocardial blood flow measurements were validated against radiolabeled microsphere-derived blood flow in these studies. These experiments have contributed to the development of non invasive and repeated assessment of regional myocardial blood flow in patients with coronary artery disease.

In a further series of studies, the first large animal model of multivessel coronary disease was developed. The relation between myocardial blood flow and function, both on a regional and global basis, were studied using this model. It is hoped that this model will make the further study of the pathophysiology of dysfunctional myocardium, its response to stress and the outcome of revascularization possible.

List of Contents

List of Figures

List of Tables

PREFACE

The appropriate management of patients with dysfunctional myocardium in the setting of coronary artery disease continues to challenge cardiologists. The causes of ischaemic myocardial dysfunction appear to be relatively straightforward. The myocardium is either scarred and irreversibly damaged or it is not. Where irreversible damage has not occurred, myocardial blood flow at rest is either normal (stunned) or below normal (hibernating). In these settings it is held that repetitive ischaemia and chronic down-regulation of myocardial function respectively, are responsible for the observed dysfunction. It is important to determine the extent to which each entity contributes to myocardial dysfunction because the expected response to revascularization procedures depends upon it.

As myocardial function is exquisitely linked to microvascular perfusion, an assessment of regional myocardial blood flow is likely to predict the outcome of revascularization procedures. The problem has been the adequate assessment of flow. The lack of a suitable experimental model that mimics chronic human coronary disease has led to deficiencies in the understanding of the pathophysiology of dysfunctional myocardium. Characterisation of myocardial flow/function relationships at rest and during stress in such a model and observing the effect of revascularization in the light of this information could have important implications in clinical practice.

The first series of experiments examined the application of myocardial contrast echocardiography in the quantification of regional myocardial blood flow. Using this method, the passage of intravenously injected microbubbles can be imaged through the myocardium with

echocardiography. The echo system and contrast agent requirements allowing quantifiable assessment of myocardial opacification were identified in the preliminary studies. It was shown that providing a linear relation is maintained between videointensity and microbubble concentration, myocardial blood flow can be quantified with bolus injections of contrast. In an experimental model of coronary disease, this method was used to both detect and judge the severity of epicardial coronary stenoses. The ratios of myocardial blood flows to the normal and stenosed coronary beds correlated closely with the ratio of videointensities in those beds. There was a good negative correlation between the trans-stenotic gradient and the videointensity ratios between the beds. In a further experiment where coronary blood flow could be set to the desired level using a pump, using a modified imaging protocol and a continuous infusion of contrast, absolute myocardial blood flow was calculated from the contrast enhanced images. This estimate of myocardial blood flow correlated well with the rate set by the pump. These experiments have paved the way towards the non invasive and repeated assessment of regional myocardial blood flow in man.

The second series of experiments examine the relation between myocardial blood flow and function in a chronic canine model of progressive coronary stenosis and dysfunction. Left ventricular size doubles over the course of the observation period (mean 6 weeks) and ejection fraction halves. While regional function is severely reduced in this model, the pathophysiologic basis varies between different segments. Some segments show no reduction in blood flow (stunning), while in others the reduction in function is closely coupled to the reduction in blood flow (hibernation). In segments that show an ultimate reduction in blood flow, a decrease in function always precedes the reduction in blood flow.

This model may facilitate further studies into the pathophysiology of dysfunctional myocardium and its response to revascularization.

ACKNOWLEDGEMENTS

The work upon which this thesis is based, was conducted between August 1995 and August 1997, during my appointment as Research Fellow in the Health Sciences Centre, University of Virginia, Charlottesville, Virginia. For most of this period I was supported by a British Heart Foundation Junior Research Fellowship. I am particularly grateful to Professor Sanjiv Kaul, Director of Cardiac Imaging and Professor of Cardiology, for his guidance in the planning and execution of this research. I am also grateful to Dr J Colin Forfar, Consultant Cardiologist, John Radcliffe Hospital, Oxford for his support during this time.

The research presented in this thesis is my own work but would not have been possible without the support and collaboration of my colleagues, in particular, Kevin Wei, Andre Linka, Danny Skyba, Jiri Sklenar, Gursel Ates, Craig Goodman and Ranjith Jayaweera. My thanks to the late Dr Michael Gaffey for his contribution to the histopathological analysis.

I wish to pay special tribute to Dr Grace Ding for her tremendous support and patience throughout the time it has taken to complete this work.

Abbreviations

2DE	Two-dimensional echocardiography
CAD	Coronary artery disease
CBV	Coronary blood volume
CBF	Coronary blood flow
cm	Centimetre
CSA	Cross-sectional area
dB	Decibels
ECG	Electrocardiogram
ESWS	End-systolic wall stress
F	French gauge
g	Gram
IV	Intravenous
kg	Kilogram
L	Litre
LA	Left atrium
LAD	Left anterior descending coronary artery
LCx	Left circumflex coronary artery
LV	Left ventricle
LVEDA	Left ventricular end-diastolic area
LVESA	Left ventricular end-systolic area
m	Metre
MBF	Myocardial blood flow
MBV	Myocardial blood volume
MCE	Myocardial contrast echocardiography
MHz	Mega hertz
min	minute
mL	millilitre
mm	millimetre
ms	Millisecond
μg	Microgram
PET	Positron emission tomography
PTCA	Percutaneous trans-coronary angioplasty
PI	Pulsing interval
VI	Videointensity
WT	Wall thickening

CHAPTER 1

ASSESSMENT OF MYOCARDIAL PERFUSION AND FUNCTION: AN OVERVIEW

Myocardial function is exquisitely linked to microvascular perfusion. In a tissue with close to 100% oxygen extraction, changes in function with reduction in blood supply precede both electrophysiological changes and symptoms (Tennant *et al.* 1935; Hauser *et al.* 1985). Absence of detectable blood flow in a dysfunctional segment implies scarring and irreversible damage, whereas the presence of blood flow implies some viability and the possibility of restoration of function with revascularization. The problem has been the adequate assessment of flow (Ludman *et al.* 1993).

To achieve this, a tracer is needed that remains entirely within the intravascular space and transits the myocardial microcirculation as red cells. Furthermore, it needs to be stable in the circulation, mix rapidly and uniformly in blood, be haemodynamically inert and have a negligible volume compared with that of the system (Lindner *et al.* 1995). Due to limitations of resolution , coronary angiography provides no information on the integrity of the myocardial microcirculation as vessels below 100 μm are not visualised (Gensini 1969; Cohen 1985) . In addition, radio-opaque dyes have measurable haemodynamic effects, displace volume and mix inadequately with blood (Ikeda *et al.* 1986; Hess *et al.* 1990).

Current tracers used in nuclear imaging mainly rely on the integrity of cell membrane function and uptake within the myocardial cell. This is a rate-

limiting step which may underestimate viability in chronically hypoperfused myocardium where membrane function may be down regulated (Leppo *et al.* 1989). Evaluation of flow using positron emission tomography (PET) is equally complex. Flow measurement with the PET tracers rubidium and cationic ammonia depends upon uptake across the cell membrane and intracellular retention of the tracer (Fukuyama *et al.* 1978; Bergmann *et al.* 1980; Rauch *et al.* 1985; Anderson *et al.* 1994). Therefore, similar limitations apply as with nuclear imaging. In addition, extraction depends on myocardial metabolic status with incorporation of the tracers into metabolic pathways further confounding flow measurement (Bergmann *et al.* 1989).

For some years tracers that mostly fulfil the above criteria have been available: ultrasound microbubble contrast agents. The passage of microbubbles through the coronary microcirculation can be visualised with echocardiography. The first such tracers used in myocardial contrast echocardiography (MCE) were simply sonicated radio-opaque dyes injected directly into the coronary artery at cardiac catheterization. These agents did not have the rheology of red cells because increasing bubble size due to coalescence impeded the passage of the contrast agent through the microcirculation. However, due to the exclusively intravascular nature of these contrast agents, accurate spatial information on myocardial blood flow became available , namely the size of perfusion beds, the 'coronary risk' area and the extent of collaterals (Sabia *et al.* 1992). With the advent of sonicated air-filled albumin microbubbles, which have been shown to have similar intravascular rheology to red blood cells (Keller *et al.* 1989; Jayaweera *et al.* 1994 ; Ismail *et al.* 1996 ; Skyba *et al.* 1996), information could be obtained on both spatial and temporal aspects of myocardial blood flow. The volume of the contrast agent required is negligible

compared to the blood pool, it mixes thoroughly with blood and has no haemodynamic effects (Keller *et al.* 1988). However, the requirement for intracoronary injection of this contrast agent and its relative fragility when exposed to the arterial circulation limited the use of this agent to catheterization laboratories with an interest in the physiology of myocardial blood flow. Initial attempts to bring about myocardial opacification from intravenous injections of air-filled sonicated albumin microbubbles were disappointing. Although left ventricular opacification was possible, myocardial opacification proved elusive.

More recently, a number of important advances have made it possible to achieve reproducible myocardial opacification from intravenous injection of microbubble contrast agents during echocardiography.

The first advance is in microbubble engineering. Second generation agents are phospholipid microbubbles that are filled with heavy gases such as perfluorocarbons. As these gases are less soluble and diffusible than air and remain within the microbubble as it traverses the pulmonary circulation, bubbles can be delivered in large enough size and numbers to enable myocardial opacification. Preservation of bubble size is important because backscatter from the bubble is related, amongst other factors, to the sixth power of its radius.

The second advance is harmonic imaging (Burns *et al.* 1996). An ultrasound field consists of bands of contraction and rarefaction. Microbubbles oscillate linearly within this field. At a given frequency and power, however, bubble oscillation becomes non-linear (deJong 1993). This is called the resonant frequency. Backscatter from such microbubbles contains not only the resonant frequency, but also harmonics of that frequency (Figure 1.1). These harmonic frequencies are multiples of the resonant frequency: if the resonant frequency is 2MHZ, the harmonic frequency would be 4MHz. As microbubbles resonate

significantly more than tissue or red blood cells and hence emit more harmonics, this form of imaging increases the signal to noise ratio by receiving only the harmonic frequency . This enables more specific detection of the microbubbles.

Recently it has been shown that when microbubbles are subjected to ultrasound, particularly at their resonant frequency, they are destroyed (Wei, Skyba *et al.* 1997). The degree of destruction depends upon the frequency and power output of ultrasound (Figure 1.2), the properties of the microbubble and most importantly on the duration of ultrasound exposure. By limiting the exposure of microbubbles to ultrasound it is possible to prolong and increase their back scatter from the myocardium (Porter *et al.* 1995). The third advance, which follows on from this observation, is intermittent imaging: instead of imaging continuously, pulsed ultrasound transmission gated to the electrocardiogram improves myocardial opacification by limiting ultrasound induced microbubble destruction (Wei, Skyba et al. 1997).

In Chapter 2, the technical requirements for the performance of successful myocardial contrast echocardiography are examined. The use of microbubbles as surrogates for red cells and assessment of myocardial blood flow depends entirely on the interpretation of video intensity data processed by echocardiographic systems. These systems have evolved to serve the needs of structural and doppler echo. In structural echo it is desirable to have sharply defined images to delineate structural borders. To achieve this, echo systems use inbuilt algorithms that discard much of the data received by the transducer and amplify the difference between low and high intensity signals. In MCE the converse is more desirable. Here, as much of the data as possible should be included to maintain a near linear relation between videointensity and microbubble concentration. Currently, echosystems allow only a small linear range of microbubble

concentration to video intensity. All quantification in the temporal domain with MCE depends on this linear relation and it is important to choose a dose of agent that does not fall outside this range. Systems with more linear processing and wider dynamic range are being developed to accommodate the needs of contrast echocardiography. One of the limitations in this regard is the relatively small range of intensities that can physically be displayed on an echo monitor screen. Echosystems squeeze or compress the wide range of signal intensities received by the transducer in order to display it on the monitor. Algorithms are being developed that enable access to the raw uncompressed data in formats that can be analysed straightforwardly.

Currently, the quantification process requires off-line analysis. It is desirable to subtract background videointensity from the contrast enhanced images to enable the detection of subtle changes in intensity and images should be aligned to correct for respiratory movement. As the human eye is unable to distinguish between the many shades of grey that are displayed on black and white monitors, it may be advantageous to apply a colour coding algorithm to these images (Kaul 1995-1). Humans are capable of distinguishing many more colours than shades of grey. The degree of contrast enhancement can be quantified providing a linear relation is maintained between microbubble concentration and videointensity. The quantification approach is likely to gain acceptance as interpretation of the data becomes more operator-independent and reproducible.

The spatial resolution of echocardiography can be used in MCE to define the spatial distribution of myocardial blood flow. During coronary occlusion, MCE during aortic root injection of contrast can identify the area of myocardium at risk (Firschke *et al.* 1997-1). This risk area correlates well with technetium autoradiography, performed during

coronary occlusion. Immediately following coronary reperfusion infarct size is underestimated by MCE (Villanueva *et al.* 1996). However, if MCE is performed during coronary hyperaemia, by unmasking the coronary reserve abnormalities in the infarct zone, the size of the infarct can be more accurately estimated (Villanueva, Camarano et al. 1996). In patients undergoing coronary revascularization after myocardial infarction, MCE in the catheterization laboratory has been shown to predict recovery of dysfunctional myocardium (Sabia, Powers et al. 1992). If perfusion was detected by MCE, recovery occurred and if not functional recovery was not observed. Intracoronary MCE has been used to assess the outcome of dysfunctional myocardium in patients undergoing primary angioplasty or thrombolysis after myocardial infarction. Where "no-flow" is demonstrated with MCE, indicating a loss of integrity of the coronary microcirculation, function is less likely to improve despite establishment of antegrade flow in the epicardial coronary artery (Ito *et al.* 1992; Ito *et al.* 1995). The appropriate placement of venous and arterial grafts during bypass surgery has been assessed using injections of contrast into the grafts to delineate their perfusion territories (Spotnitz *et al.* 1988; Villanueva *et al.* 1992). MCE has also been shown to be a reliable intraoperative method of monitoring tissue delivery of cardioplegia during bypass surgery (Goldman *et al.* 1984; Keller *et al.* 1990).

MCE can be used to quantify a relative measure of regional myocardial blood flow (Jayaweera, Edwards et al. 1994; Lindner *et al.* 1997). Classic indicator dilution theory can be applied to the passage of contrast agents through the myocardial microcirculation provided two conditions are met. First, the agents need to have a rheology similar to red cells and second they should be administered as an instantaneous bolus. In a series of connected compartments with a given flow rate, a tracer introduced instantaneously to the first compartment (the coronary artery) will decay

according to an exponential function and will transit subsequent compartments (the myocardial bed) according to a gamma variate function (Figure 1.3). Increasing flow or reducing volume in these subsequent compartments will narrow the gamma variate curve increasing transit rate and peak concentration of the tracer. Conversely, reducing flow or increasing the volume (Figure 1.4) will widen the gamma variate reducing the transit rate and peak concentration of the tracer. With bolus intracoronary injections of sonicated albumin the myocardial blood flow (MBF) to myocardial blood volume (MBV) relation has been studied in the setting of non-flow limiting coronary stenoses at rest (Lindner, Skyba et al. 1997). As the stenosis severity increases, blood flow is maintained by distal autoregulation, and myocardial blood volume initially increases. Therefore, for the same resting myocardial blood flow, the transit of a given dose of contrast agent through the bed is prolonged and peak concentration is reduced compared to a bed subtended by a non-stenosed coronary artery (Lindner, Skyba et al. 1997).

During coronary hyperaemia, stenoses that are not flow limiting at rest become flow limiting (Gould *et al.* 1974). As a consequence a flow mismatch occurs between the MBF of normal and stenosed beds. MCE performed during aortic root injection of contrast can identify the stenosed bed and provide valuable information on the functional significance of the coronary stenosis (Firschke, Lindner et al. 1997-2). As MBF and MBV are interdependent variables, and the value of neither can be measured in isolation, MCE can only quantify the relation between the two. In the experimental laboratory, if one variable is held constant then the transit rate of the contrast agent reflects changes in the other.

With intravenous bolus injections of contrast, the accuracy of the spatial information is not diminished. It is still possible to define risk area accurately during coronary occlusion and to estimate final infarct size

using MCE (Firschke *et al.* 1997-2). However, measurement of the relation between myocardial blood volume and flow is not possible with intravenous boluses of contrast. When the contrast agent is administered as an intravenous bolus, it progressively mixes with blood through the venous circulation, right heart and pulmonary circuit before its arrival in the left ventricle. Therefore it no longer fulfils the instantaneous input function criterion described above. As a consequence classic indicator theory has limited application to the interpretation of contrast transit time through the myocardium. Despite this, the severity of coronary stenoses has been shown to correlate with the peak videointensity over a myocardial bed during coronary hyperaemia (Firschke, Lindner et al. 1997-2) and the ratio of video- intensities between beds correlates well with the ratios of their blood flows and the trans-stenotic gradient (Wei, Firoozan *et al.* 1997-1). This is because coronary hyperaemia maximises flow mismatch between the normal and stenosed beds: fewer bubbles transit the stenosed bed resulting in a lower peak videointensity compared to the normal bed. Without an absolute measure of MBF and without the benefit of a "normal" bed to compare, however, this method has significant limitations in the assessment of regional myocardial blood flow. Microbubbles are destroyed by ultrasound, once regarded a nuisance in MCE, reducing both the duration and intensity of myocardial opacification from intravenous injections of contrast. However, this interaction between microbubbles and ultrasound can be used positively to derive an absolute measure of blood flow using intravenous MCE. This property of microbubbles is examined in Chapter 3. If a contrast agent is administered as a constant infusion until a steady state is achieved , and a single pulse of ultrasound destroys all bubbles within the elevation (thickness) of the echo beam, the video intensity during a subsequent pulse will be proportional to the extent to which the elevation has been replenished in

the time period between the two pulses. If the interval between pulses is lengthened until the whole elevation is replenished with bubbles at the steady state concentration, video intensity will not rise any further. If the beam thickness and the time taken to fully replenish it are known, microbubble, and therefore blood velocity can be calculated. In an animal model where coronary flow could be controlled this technique has been successful in measuring regional MBF (Wei, Firoozan *et al.* 1997-3). Although the quantification of absolute regional myocardial blood flow with steady-state intravenous infusion of contrast agent has the potential to have a major impact on the assessment of ischaemic heart disease, this method has some limitations. Beam thickness is privileged information and is not divulged with other specifications of echo systems. Beam width also changes with distance from the transducer . In order to calculate flow, the beam width needs to be known. In a set up where the flow is known, beam width can be deduced but this is a laborious process and currently impractical. The industry is addressing these difficulties and it may soon be possible to set the beam width. All the difficulties of performing adult transthoracic echocardiography will apply to this new methodology. Problems with poor acoustic windows and chest wall attenuation will affect the quality of the studies. The development of harmonic transoesophageal probes may help overcome some of these difficulties.

In chapter 4, both continuous infusions and boluses are used to determine the severity of epicardial coronary stenoses. In this chapter the relative merits and pitfalls of either method are directly studied. The choice of method depends almost entirely on the clinical setting. Where assessment of coronary occlusion is required, such as during myocardial infarction, it is likely that the more expedient bolus infusion will be more useful. However, if an accurate assessment of the severity of coronary stenoses is

required, it may be advantageous to use the more robust infusion method. In a setting of stress myocardial echocardiography, where blood flow and function are changing, an infusion will be more appropriate.

MCE has great potential in diagnostic cardiology. Its development over the last few years has been swift and clinical trials to test its efficacy in detecting perfusion defects in patients with previous infarction are underway. Further studies are planned to test the ability of the method to diagnose infarction at the bedside in patients presenting with chest pain and to assess the efficacy of reperfusion strategies. It has the potential to diagnose non-invasively and quantify the functional severity of epicardial coronary artery stenoses and may be useful in the evaluation of patients representing with chest pain after PTCA. Work is underway to determine the usefulness of intravenous MCE in the assessment of myocardial viability, an important issue in the appropriate targeting of revascularization procedures.
The technology is ubiquitous and relatively cheap when compared to other methods of assessing myocardial perfusion. The contrast agents are well tolerated with little in the way of side effects and the MCE examination can be performed repeatedly. MCE has the potential to make widely available the rapid, repeated and non invasive measurement of regional myocardial blood flow at the bedside.

The study of the pathophysiology of ischaemic dysfunctional myocardium has been , until now, disabled by the lack of a suitable chronic large animal model of progressive myocardial ischaemia. Previous attempts have either been very short (hours to days) or involved only one coronary territory (Shen *et al.* 1995). Because of the efficient development of coronary collaterals, these models have not been able to accurately mirror

the clinical condition of multivessel disease in man. In Chapter 5 such a model is described and myocardial flow-function relations in it are characterised. This model is currently being utilised to study the pathophysiology of stress in ischaemic myocardium and perfusion imaging with echo contrast agents has already begun. The model allows the close study of the effects of revascularization and the infusion of angiogenic growth factors on myocardial blood flow and function.

In this thesis the physiology and pathophysiology of myocardial blood flow and function has been studied using a novel imaging method that in itself affords insights into the intricacies of the coronary microvascular circulation.

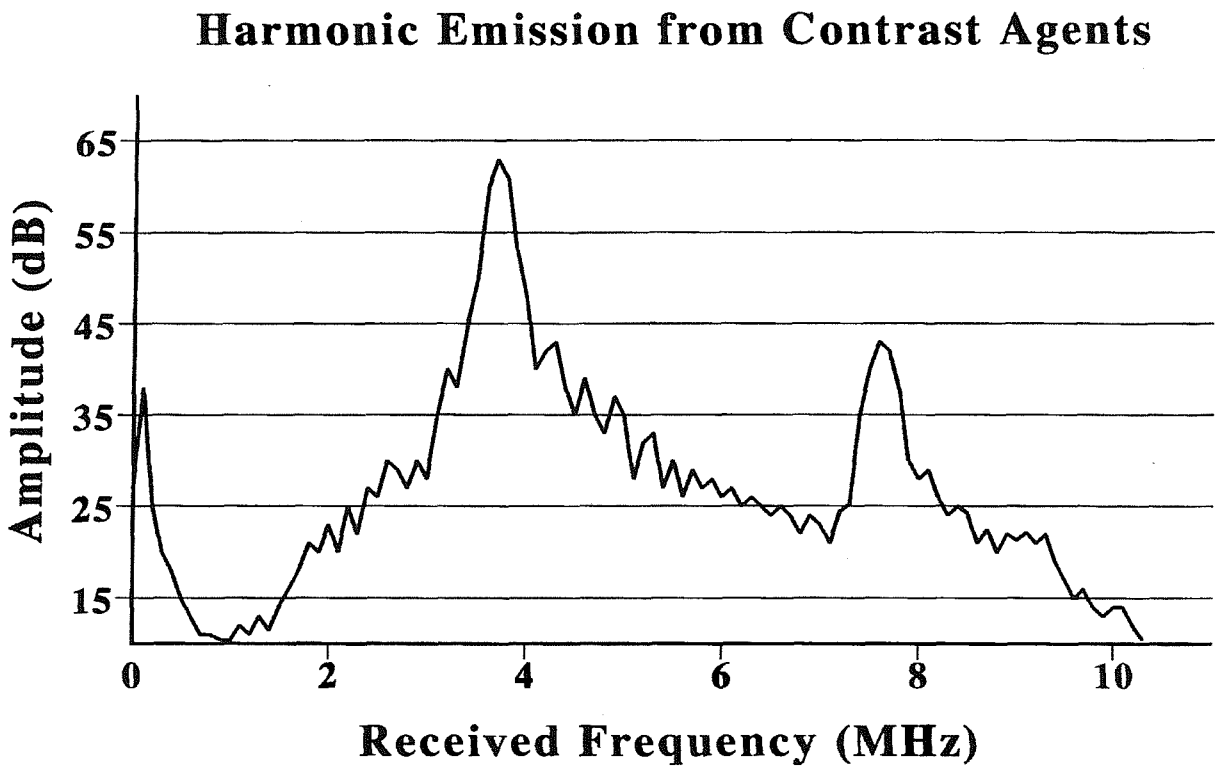
Harmonic Emission from Contrast Agents
Amplitude (dB)
65
55
45
35
25
15
0
2
4
6
8
10
Received Frequency (MHz)

Figure 1.1

Figure 1.1

This figure shows a plot of videointensity (y-axis) against the frequency of back scatter (x-axis). Microbubbles in a saline solution have been insonated with a fundamental frequency of 4MHz and a smaller harmonic of this frequency at 8MHz can be detected from them. The smaller magnitude of the harmonic frequency explains why receive gains need to maximised to detect the signal from microbubbles. See text for details.

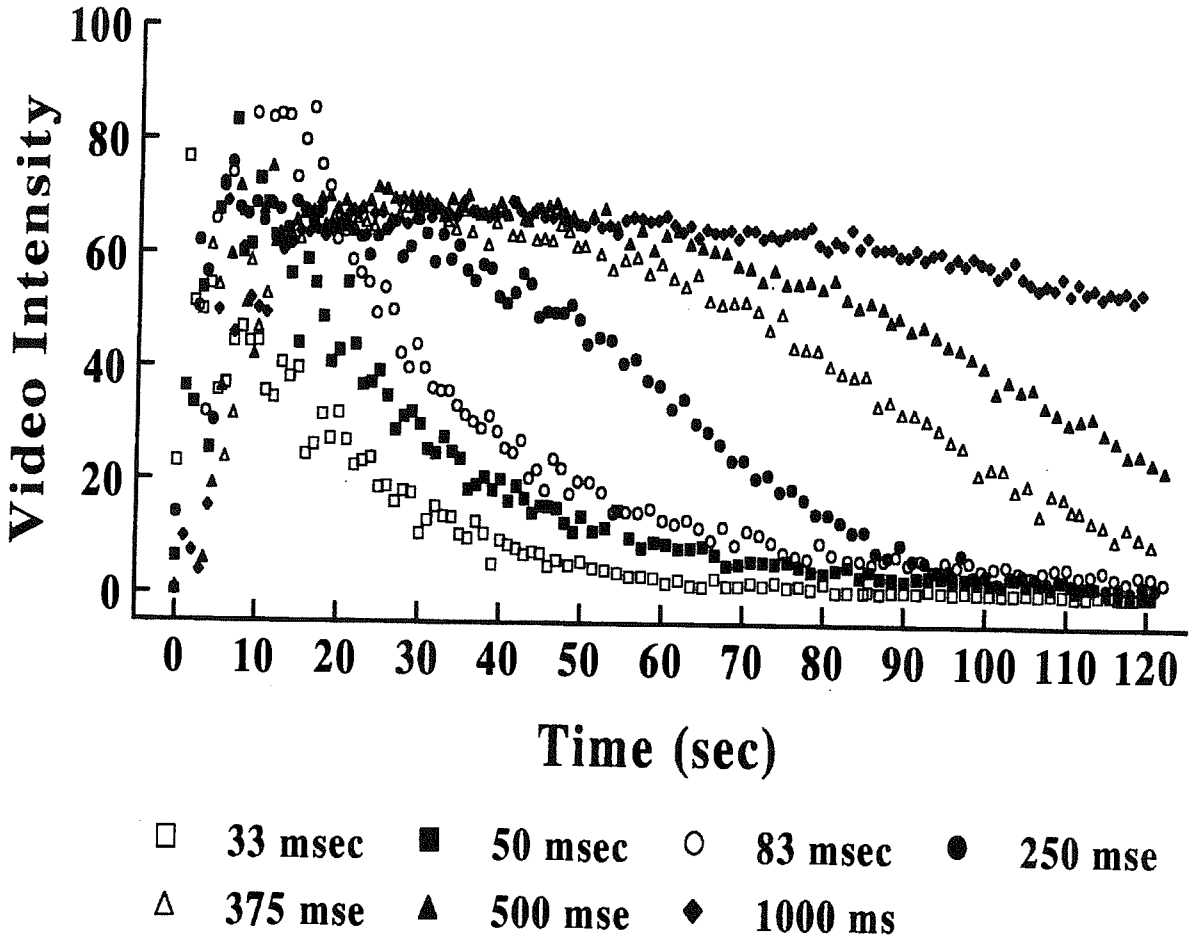
Video Intensity
100
80
60
40
20
0
0 10 20 30 40 50 60 70 80 90 100 110 120
Time (sec)
33 msec
50 msec
83 msec
250 mse
375 mse
500 mse
1000 ms

Figure 1.2

Figure 1.2

In this figure time (x-axis) is plotted against videointensity (y-axis). The effect of imaging rate on the persistence of microbubble in an invitro preparation can be observed. As the imaging interval is prolonged, the videointensity is seen to persist longer indicating a reduction in destruction rate by ultrasound. See text for details.

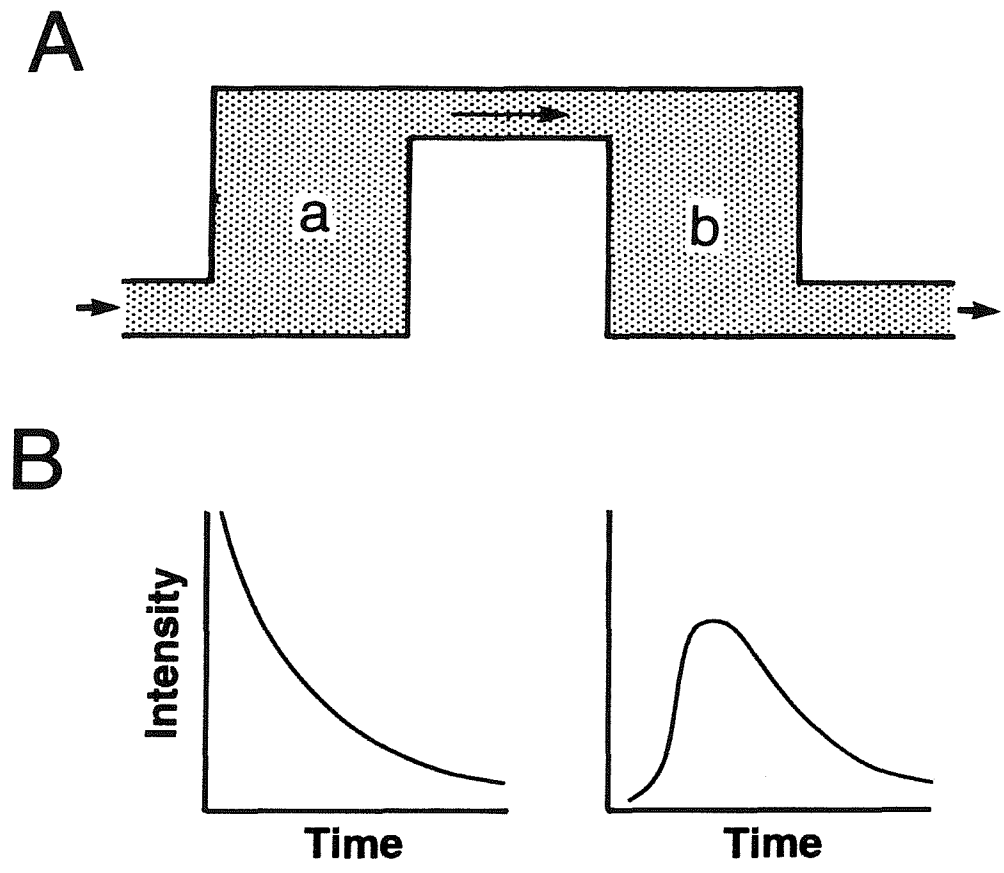

Figure 1.3

Figure 1.3

A) A model that describes the decay of a tracer introduced into the coronary artery (a) as an instant input and its subsequent transit through the myocardial bed (b).
B) Graphical display of the decay (a mono-exponential function) and transit (a gamma variate function) of the tracer in the corresponding compartments. Time is along the *x*-axes and videointensity along the *y*-axes. See text for details.

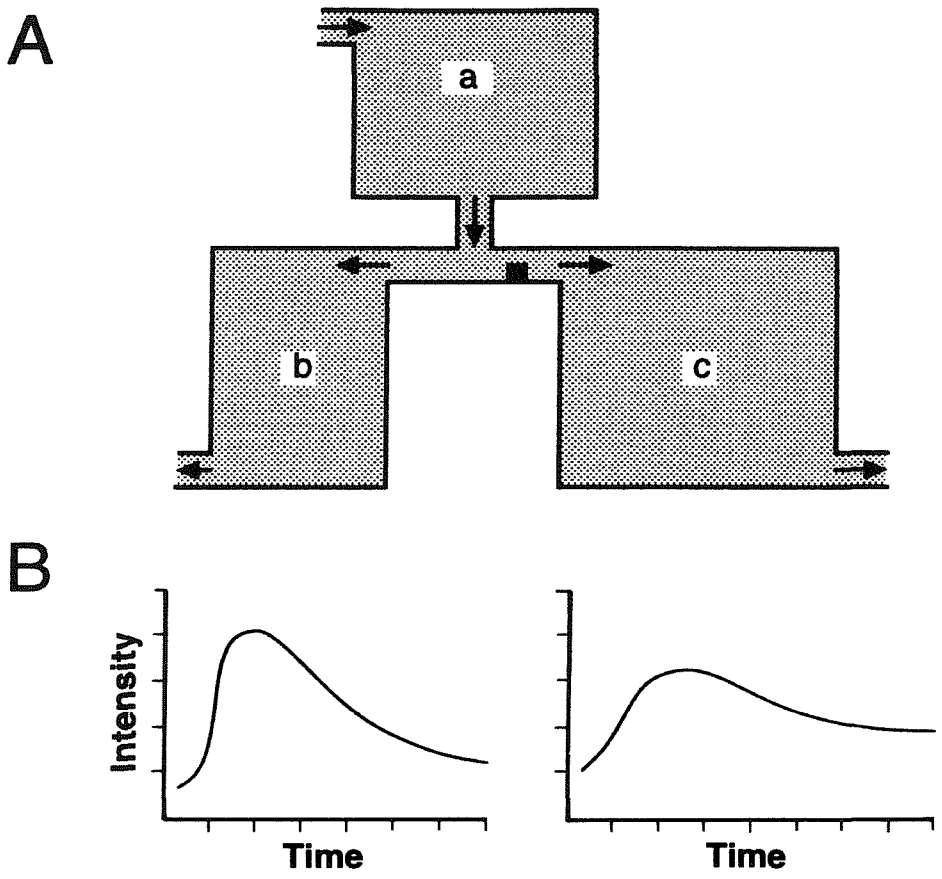

Figure 1.4

Figure 1.4

A) Compartment (a) represents the left main stem, (b) the left anterior descending bed and (c) the circumflex bed. The model assumes equal flow through the beds and a non-flow limiting stenosis in the proximal circumflex coronary artery.

B) The graphs show the transit of the tracer through the beds. As the coronary blood volume is increased in the stenosed bed (autoregulated to maintain flow), the transit rate is decreased and the peak intensity is lower compared to the normal bed. Time is along the x-axes and videointensity along the y-axes. See text for details.

CHAPTER 2 :

REQUIREMENTS FOR THE QUANTIFICATION OF MYOCARDIAL PERFUSION WITH MYOCARDIAL CONTRAST ECHOCARDIOGRAPHY DURING VENOUS INJECTION OF CONTRAST

2.1 Introduction

The detection of myocardial perfusion from a venous injection of contrast has recently become feasible with the development of two advances in ultrasound imaging. The first is intermittent imaging (Porter and Xie 1995) With intermittent ultrasound exposure gated to the electrocardiogram, myocardial opacification is much greater with intravenous contrast than during continuous imaging. This enhanced signal is thought to be due to minimisation of bubble destruction by limiting exposure to ultrasound. The second advance is harmonic imaging. Since an ultrasound field consists of bands of compression and rarefaction, bubbles in this field may alternately contract and expand. When exposed to a specific frequency (the resonant frequency) bubble oscillations become non-linear (Burns *et al.* 1996). When this occurs the bubbles emit not only the fundamental frequency to which they were exposed, but also harmonics of that frequency. Transducers have been designed that emit such fundamental frequencies but receive only the harmonic frequency generated by the microbubbles. Since microbubbles resonate significantly more than surrounding tissue or blood, the backscatter from the bubbles compared to the background is considerably greater at the resonant frequency, which results in an increased signal-to-noise ratio during harmonic imaging(Burns, *et al.* 1996).

The purpose of this study was to define the optimum dose of contrast agent capable of myocardial opacification without attenuation and thus to equate peak myocardial videointensity directly with epicardial coronary flow rate which in turn is proportional to myocardial nutrient flow. It has been previously demonstrated that when blood flow through a coronary artery is selectively altered without a change in MBV, the transit rate of microbubbles injected directly into the coronary on MCE correlates with regional MBF measured with radiolabeled microspheres (Kaul *et al.* 1989; Jayaweera, Edwards et al. 1994). In addition it has been shown that in the presence of infused phenylephrine, MBF and MBV are closely coupled during left atrial injections of contrast and MBV correlates very closely with peak background subtracted videointensity in the anterior myocardium. Given that the dogs used in this study are essentially similar in terms of weight, heart rate and cardiac output, the concentration of microbubbles in the arterial blood will have similar profiles. The number of microbubbles entering the coronary circulation will depend upon the fraction of cardiac output to the coronary circulation which is essentially coronary flow. During inotrope infusion, as the increase in MBF is closely coupled to an increase in MBV (Marcus 1983) the ratio of intravascular to myocardial volume will rise leading to an increase in measured videointensity.

To determine the relationship between microbubble concentration and videointensity in-vitro and in-vivo experiments were performed. The data was used to determine an optimal administration dose for the in-vivo studies with which videointensity changes could be measured over a linear range at widely different coronary flows. The aim was to correlate peak background subtracted videointensity with epicardial coronary flow rate. MBF and MBV were coupled through the administration of epinephrine.

2.2 Objectives

The purpose of this study was to establish the requirements that enable quantification of myocardial blood flow with MCE. The first part of the study was an in vitro study to determine the relation between videointensity and microbubble concentration. The aim was to examine the effect of dynamic range in distinguishing between different concentrations of microbubbles and to determine the range of microbubble concentrations over which there is a linear relation between videointensity and microbubble concentration.

The second part of the study examined the relation between myocardial videointensity and increasing administered doses of contrast agent at a low and high coronary flow rate to identify an optimum dose of contrast agent in vivo.

The third part of the study aimed to correlate myocardial videointensity measurements to myocardial blood flow. Whilst myocardial blood flow was increased, and the dose of contrast agent kept constant, videointensity was correlated to the myocardial blood flow.

2.3 Methods

2.3.1 Contrast agent

The echo contrast agent used in these experiments was MRX-115 (ImaRx Corp, Tuscon, Arizona) which is a 8nm thick phospholipid microbubble filled with perfluoropropane, with a mean diameter of 2.5 μm and a concentration of 1.2×10^9 ml^{-1}. This agent has been shown to pass through the pulmonary circulation, opacify the myocardium and have no effect on systemic or coronary haemodynamics (Lindner *et al.* 1998).

2.3.2 In Vitro Experiments

Increasing doses of the contrast agent were mixed with 4 L of normal saline in a glass beaker. A magnetic stirrer at the bottom of the beaker ensured thorough mixing of the solution. The transducer was clamped in a fixed position in the beaker, 2cm into the solution, and adjusted to minimise artefacts from the stirrer and the edges of the beaker. Two-dimensional echocardiographic (2DE) imaging was performed with harmonic imaging at two dynamic ranges (35 and 60 dB). Incremental doses of the contrast agent were micropippeted into the saline followed by a fifteen second period during which ultrasound was suspended to ensure thorough mixing.

2.3.3 In-Vivo Experiments:

The study protocol was approved by the Animal Research Committee at the University of Virginia and conformed to the American Heart Association Guidelines for Use of Animals in Research. Six male adult mongrel dogs were anaesthetised with 30mg•kg^{-1} of sodium pentobarbital (Abbott Laboratories, North Chicago, IL),intubated and ventilated with a respirator pump (model 607, Harvard Apparatus, Natick, MA). Additional anaesthesia was administered during the experiment as needed. Fluids were administered, as needed, via 7F catheters placed in right and left femoral veins. Arterial pressure was monitored and recorded from a 7F femoral arterial line connected to a fluid filled transducer, itself connected to a multi-channel recorder (Gould. ES 2000 MD).
A left lateral thoracotomy was performed and the heart was suspended in a pericardial cradle. A portion of the left anterior descending (LAD) artery was dissected free and a 2mm time of flight coronary flow probe (Series SB, Ithaca, NY) was placed around the vessel. This was connected to a

digital flow meter (model T206, Transonics). Contrast agent was administered through a right internal jugular catheter.

At baseline, with stable recordings of coronary flow rate, incremental doses of contrast agent were administered to enable construction of a dose response curve. Following this, an appropriate constant dose (0.1 mL) of contrast agent was used in all dogs throughout the study. Coronary flow rate was then increased by administration of incremental doses of epinephrine through a femoral venous line. Imaging was performed at baseline and following stabilisation at each new coronary flow rate.

2.3.4 Contrast Echocardiography:

Contrast echocardiography was performed using a prototype phased-array system (ATL-Interspec Corp., Bothell, WA) with continuous and intermittent harmonic imaging capabilities. The transducer emits at 2.3MHz and receives at 4.6MHz. Gain settings were optimised separately for the in-vivo and in-vitro studies but kept constant throughout the study thereafter. The dynamic range was maximised in all the studies (60dB) except where otherwise stated . All in-vivo imaging was gated to the electrocardiogram to occur at end systole. In-vitro imaging was performed after allowing thorough mixing of the contrast agent during suspension of ultrasound. Data were recorded on 1.25 cm video tape using an S-VHS recorder (Panasonic model AG6200, Matsushita Electrical Co., Japan) for later analysis.

For the in vitro studies, 12 doses of MRX-115 ranging from 0.5 to 30 microlitres were used. For the in-vivo studies, 0.1 ml of the contrast agent was injected intravenously at each of the 4 to 5 coronary flows achieved with infused epinephrine.

Images were analysed as previously described (Jayaweera *et al.* 1990). In brief, they were transferred from videotape to an off-line image analysis

system (Mipron, Kontron Electronics, Eching, Germany) in a 244x244x8 bit format.

For the in-vitro experiments, a large region of interest (at least 3000 pixels) was defined around the focal point of the transducer with care taken to avoid the edges of the beaker. Videointensity was measured and averaged in 5 pre-contrast and 10 post-contrast frames. The background-subtracted data thus obtained was then plotted against the dose of contrast agent added to the beaker.

For the in-vivo experiments, consecutive end-systolic frames, which included the period from just before contrast injection until 10s thereafter, were recorded during suspension of ventilation. A large transmural region-of-interest was defined over the anterior myocardium and care was taken to avoid the specular epicardial and endocardial borders. The average videointensity for the region-of-interest was determined for all end-systolic frames. The videointensity from several frames prior to the appearance of contrast in the myocardium was considered to represent background. Peak videointensity measurements were identified from the background subtracted data and plotted against the dose of contrast agent administered to identify the linear portion of this relation. At each coronary flow rate, following 0.1 ml injection of MRX-115, peak background subtracted videointensity was plotted against coronary flow rate.

2.4 Results

2.4.1 Relation Between Microbubble Concentration and Video Intensity

Figure 2.1 illustrates the relation between microbubble concentration and videointensity 15 seconds after each dose of microbubbles was added to the beaker during the in-vitro experiments. As expected, this relationship is exponential, with a the most linear relation demonstrated at the lower concentrations. It is important to note that the extent and slope of this linear relationship is primarily a function of system specific post-processing and varies from one echocardiographic system to another (Jayaweera *et al.* 1995); i.e. it would need to be determined individually for each machine. This figure also depicts plots of videointensity against microbubble concentration at two different dynamic ranges (60 and 35dB). The receive gain was kept constant between the two stages and as can be seen peak background subtracted videointensities are higher at the lower compression, but this improved detection of microbubbles is most apparent only over the non-linear portion of the curve and as such is of limited practical use. Over the linear range, microbubble detection is not improved at lower compression.

In the in-vivo experiments, when increasing doses of intravenous contrast agent are plotted against peak background subtracted myocardial videointensity in one dog, a similar graph is obtained. The results are presented in Figure 2.2. As expected, the graph demonstrates that the range of microbubble concentrations over which videointensity is linearly proportional to concentration is dependent upon the coronary (in this setting, nutrient) flow. At baseline with a flow of 40 mL/min the curve demonstrates a linear relation between administered microbubble dose and measured videointensity over a wide range of doses. However, in the

same animal with inotrope stimulation and a flow rate of 160 mL/min the linear portion of the curve is restricted to administered doses of less than 0.1 ml of contrast agent. At this flow, the echo machine simply cannot display higher videointensity from the myocardium at any higher dose of contrast agent. The difference in video intensity at any given dose of contrast agent at the two flows is as a result of change in myocardial blood volume.

2.4.2 Relation Between Coronary Flow and Videointensity

On the basis of the in-vitro and in-vivo experiments, the optimum dose of MRX-115 was determined. In order to improve sensitivity at the lower coronary flows, it was decided to use a 0.1 ml dose of MRX-115. Clearly, this would restrict the linear range of flow to videointensity to below 160ml/min. As figure 2.3 shows, the correlation between flow in the LAD and videointensity from the anterior bed is excellent up to a flow of around 160 ml/min. Above this flow, bubble saturation does not allow the display of any higher videointensity values. In this model with normal coronary arteries, it can be assumed that a rise in epicardial blood flow is directly proportional to an increase in MBF.

2.5 Discussion

2.5.1 Quantification of Myocardial Perfusion

It has previously been shown that in the absence if changes in blood volume, the mean transit rate of microbubbles injected into a coronary artery at different flows correlates closely with regional MBF (Kaul, Kelly et al. 1989; Jayaweera, Edwards et al. 1994). The scenario with a venous injection is very different. The bolus is progressively diluted through the right sided heart chambers, the pulmonary circulation and the left heart. It

is no longer a tight bolus, essential if dye dilution principles are to be applied to the kinetics of transit through the myocardium. Furthermore, with such a bolus, microbubbles are detectable in the myocardium for only a small fraction of the time they are present in the left ventricular cavity. This is because of the smaller number of bubbles and the higher thresholding in the myocardium. As the time course of the transit curves are so dissimilar between the myocardium and left ventricle, it is not possible to derive microbubble transit rate in the myocardium by deconvolving it from the left ventricular transit curve. Transit rate of microbubbles through the myocardium may not allow an estimation of MBF.

Another approach for the quantification of myocardial perfusion is the assessment of MBV as opposed to MBF. Most current imaging methods are unable to measure MBV because its primary requirement is that the tracer remain entirely within the vascular space. In other imaging modalities the tracer is either extracted by myocytes such as agents used for single photon (Kaul 1989; Maddahi *et al.* 1993)and positron emission imaging (Hutchins *et al.* 1993; Schelbert *et al.* 1993))or like radio opaque dyes enters the extra vascular space (Eigler *et al.* 1991; Wu *et al.* 1992)). Microbubbles remain entirely within the intravascular space (Skyba, Camarano et al. 1996) and therefore the concentration of microbubbles per unit of myocardium allows the estimation of MBV. Often, especially in this model with normal arteries, MBF and MBV are closely coupled. In the case of inotropic stimulation, there is a close coupling between increase in MBV, myocardial oxygen demand, and MBF.

2.5.2 Findings of the Present Study

In this study it was chosen to increase MBV by increasing myocardial oxygen demand using epinephrine. A close correlation between myocardial peak videointensity (essentially MBV) and coronary flow rate was found.

It was necessary to define the relation between microbubble concentration and videointensity both in-vivo and in-vitro to determine an optimum dose of MRX-115 capable of adequately opacifying the myocardium at low coronary flow rates and minimising attenuation and echo system saturation problems at higher flows. From these experiments a dose of 0.1 ml of MRX-115 was chosen which was then used in all the animals.

As the dogs in this study have essentially similar coronary flows, weights and heart rates, it has been possible to group them together. In addition, in this setting with normal coronary arteries nutrient flow (MBF) will rise in proportion to coronary flow with inotrope administration.

Figure 2.3 shows the linear relation between coronary flow and videointensity from the anterior myocardium. It also demonstrates that the linear portion of the curve is restricted to below flows of 160 mL/min. Had a smaller dose of MRX-115 been chosen, it may have been possible to extend this linear relation to encompass all flows but this would have been at the cost of reduced sensitivity at the lower flows. Figure 2.4 (adapted from Skyba *et al* 1994) illustrates the reasons behind the change in videointensity with increasing coronary flow. At the two flows of 40 and 160 ml/min the concentration profiles of microbubbles arriving at the ostium of the left main coronary artery are essentially the same if the administered dose is the same. However, as MBF and MBV are closely coupled in this setting, the increase in videointensity is due to a higher volume of microbubble containing blood per unit volume of myocardium in the latter compared to that in the former.

2.5.3 Criticisms

It would have been desirable to measure MBF with an independent method such as radiolabeled microspheres and correlate that to peak videointensity. Indeed if an assessment of myocardial blood volume is to be made in a future study in the presence of coronary stenoses from intravenous injection of contrast, it will be imperative to administer radiolabeled microspheres.

In this study it is assumed that there is a linear relation between MBV and microbubble concentration within the myocardial volume interrogated by ultrasound. It is well known that haematocrit within the microcirculation is lower than that within large vessels and is (Klitzman *et al.* 1979; Crystal *et al.* 1981) inversely related to the size of the blood vessels. If the increase in MBV is due to recruitment of vessels similar in size to those already present, then the haematocrit effect should be negligible. On the other hand, if the recruitment is principally of vessels that are significantly different in size to those already present, then the haematocrit effect needs to be considered. The correlation demonstrated between flow and peak videointensity argues against the importance of the haematocrit.

2.6 Conclusions

This study follows on from previous work using using left atrial injections of contrast to quantify myocardial perfusion. This study demonstrates that it is possible to opacify the myocardium from very low doses of contrast administered intravenously and that peak background subtracted videointensity (essentially myocardial blood volume) correlates closely with epicardial coronary flow rate.

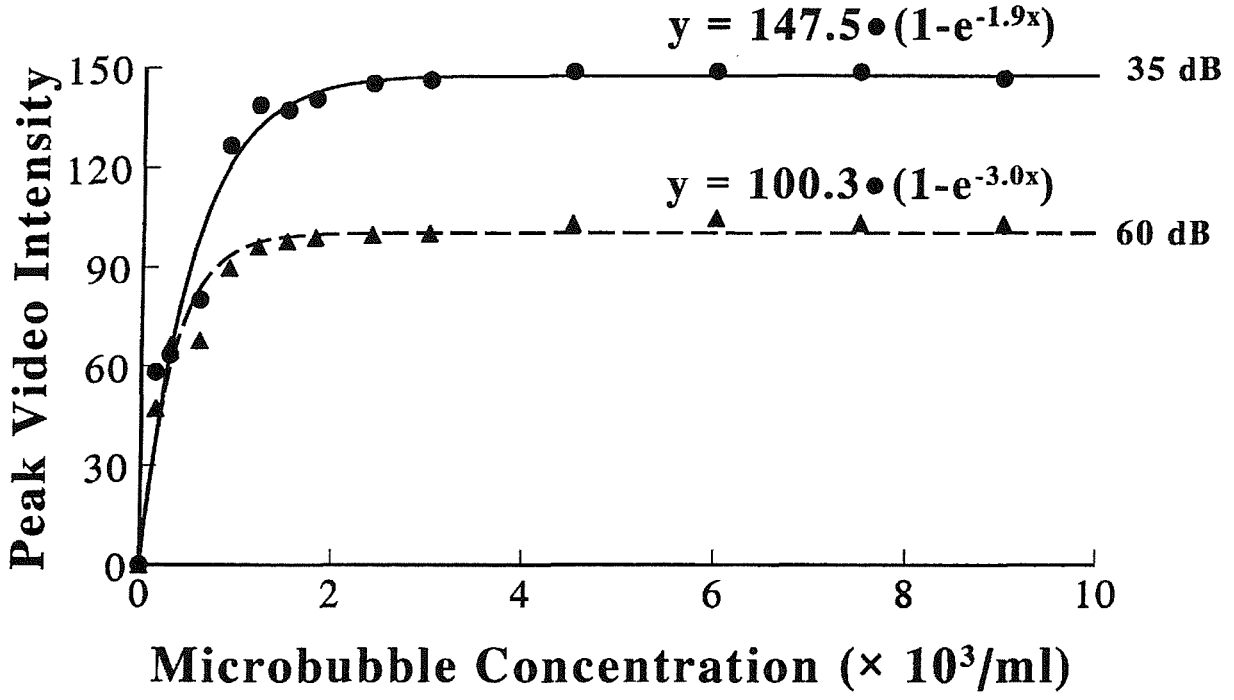
y = 147.5•(1-e^-1.9x)
35 dB
y = 100.3•(1-e^-3.0x)
60 dB
Peak Video Intensity
150
120
90
60
30
0
0
2
4
6
8
10
Microbubble Concentration (× 10³/ml)

Figure 2.1

Figure 2.1

This figure depicts the relation between videointensity (y-axis) and microbubble concentration (x-axis) at two compression settings (35 and 60 dB). The relation is exponential with a near linear portion over a small range of low concentrations of microbubble. Background subtracted videointensities are higher using the lower compression but this improved signal detection is limited to non-linear portions of the curve and therefore does not allow quantification of microbubble concentration. See text for details.

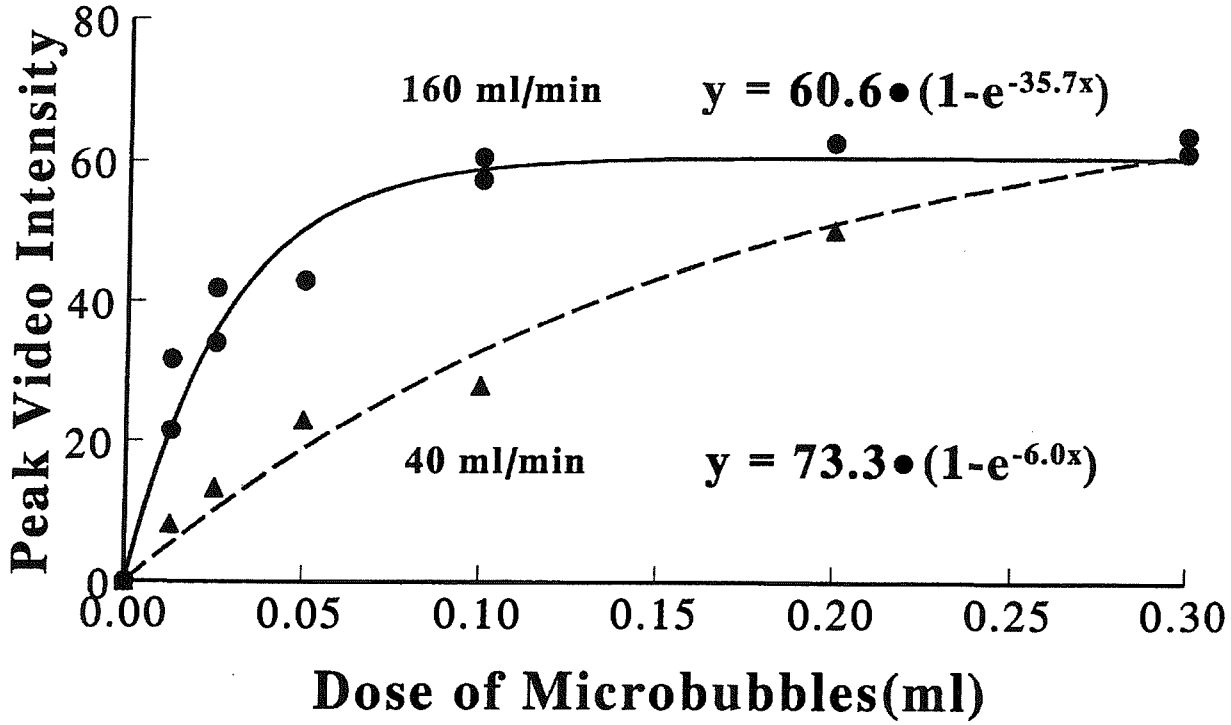
Peak Video Intensity
80
60
40
20
0
160 ml/min
y = 60.6•(1-e-35.7x)
40 ml/min
y = 73.3•(1-e-6.0x)
0.00
0.05
0.10
0.15
0.20
0.25
0.30
Dose of Microbubbles(ml)

Figure 2.2

Figure 2.2

This graph demonstrates the relation between the dose of administered microbubble (x-axis) and background subtracted videointensity (y-axis) at two coronary flow rates in one dog. At the lower flow rate, a near linear relation is found between microbubble dose and videointensity, whereas at the higher flow the linear portion of the relation is restricted to doses up to 0.1 mL of contrast agent. See text for details.

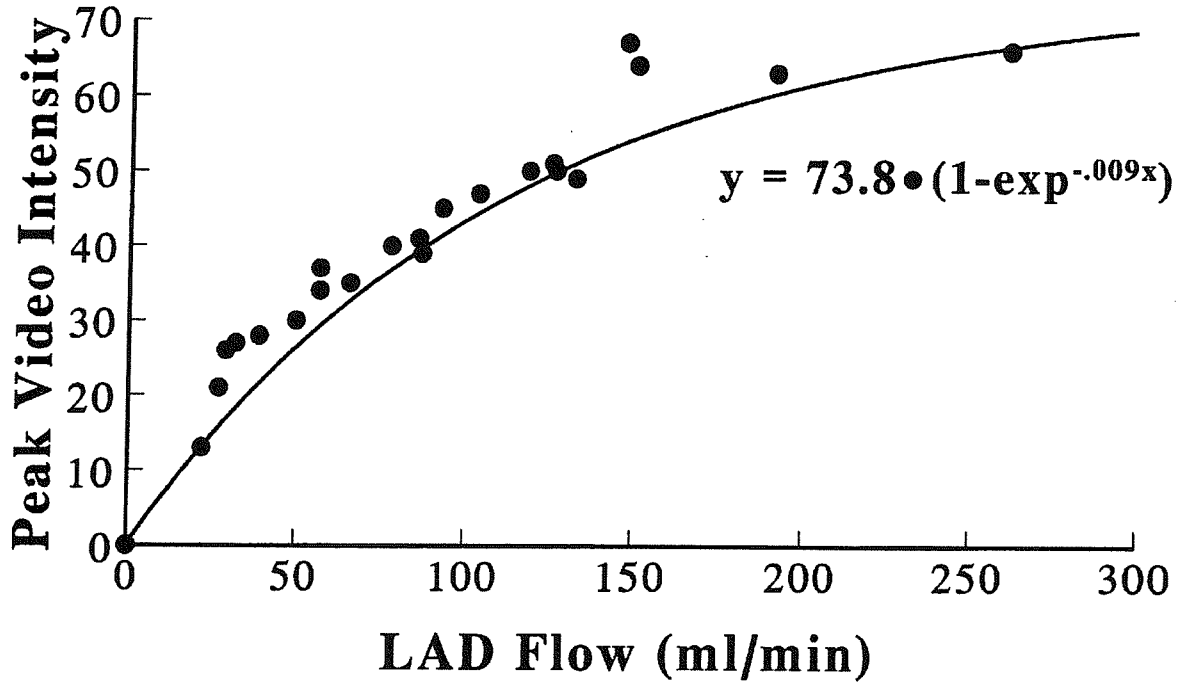
Peak Video Intensity
70
60
50
40
30
20
10
0
0
50
100
150
200
250
300
LAD Flow (ml/min)
y = 73.8•(1-exp-.009x)

Figure 2.3

Figure 2.3

This figure shows the correlation between LAD flow rate (x-axis, mL/min) and peak background subtracted videointensity (y-axis) during a 0.1 mL bolus injection of contrast. The near linear portion of this curve is restricted to flow rates below 160 mL/min. Above this flow, system saturation does not allow differentiation between higher flows using this dose of contrast. See text for details.

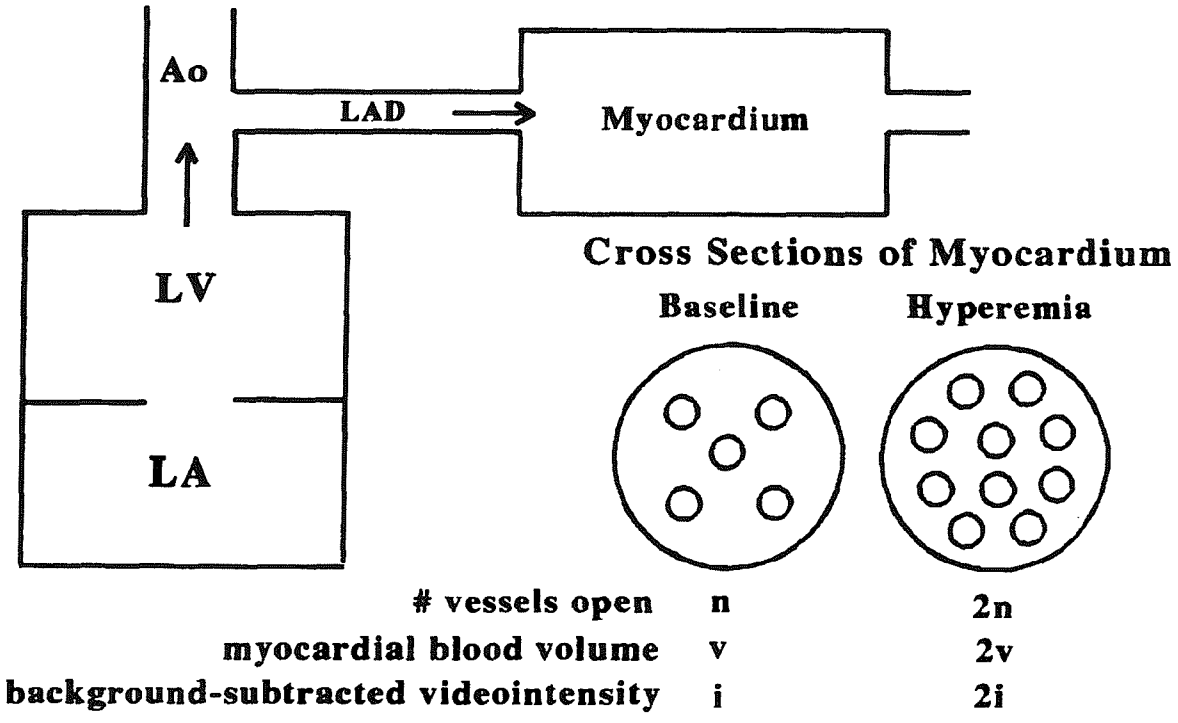
Ao
LAD
Myocardium
LV
LA
Cross Sections of Myocardium
Baseline
Hyperemia
vessels open n 2n
myocardial blood volume v 2v
background-subtracted videointensity i 2i

Figure2.4

Figure 2.4

When myocardial blood flow and myocardial blood volume are coupled with the administration of an inotrope, blood flow to the myocardial bed is increased by recruitment of capillary beds (here denoted by *n* to *2n*). As MCE images the capillary compartment, the concentration of contrast within the ultrasound beam increases leading to an increase in videointensity (*v* to *2v*). See text for details.

CHAPTER 3

QUANTIFICATION OF MYOCARDIAL BLOOD FLOW WITH MYOCARDIAL CONTRAST ECHOCARDIOGRAPHY DURING INFUSION OF CONTRAST

3.1 Introduction

It has previously been shown that the relation between myocardial blood flow (MBF) and total coronary blood volume (CBV) can be quantified with myocardial contrast echocardiography (MCE) (Jayaweera, Edwards *et al.* 1994; Lindner, Skyba *et al.* 1997). CBV includes the blood volume from epicardial arteries, arterioles, capillaries, venules and veins. When sonicated albumin microbubbles were injected into a coronary artery (Jayaweera, Edwards *et al.* 1994; Lindner, Skyba *et al.* 1997)., changes in their mean myocardial transit rates were found to reflect changes in the MBF/CBV relation. This finding was based on classic indicator dilution principles, which could be applied to the data, because these microbubbles have the same intravascular rheology as red blood cells, and therefore act as tracers of red cell kinetics (Jayaweera, Edwards et al. 1994). This approach is limited because the mean microbubble transit rate reflects relative, rather than absolute changes in MBF or CBV. Since changes in MBF and CBV are usually coupled, it is not possible to quantify one without knowing the other. Also, the need for intracoronary injection of contrast in this method, limit its potential application to the clinical setting. A number of advances have recently been made that make myocardial opacification possible from a venous injection of microbubbles. First,

microbubbles that contain high molecular weight gases are much more persistent in the circulation compared to air-filled microbubbles, and are likely to become the agents of choice for assessing myocardial perfusion with MCE. As the backscatter from a bubble is related to the sixth power of its radius (Albers 1960), prevention of any leakage of gas will be important in maintaining its echogenecity as it transits through the circulation. Advances in imaging techniques include harmonic and intermittent imaging (Porter *et al.* 1996). It has been previously shown that exposing microbubbles to ultrasound at or near their resonant frequency results in microbubble destruction (Wei *et al.* 1997). This effect could be related to the induction of non-linear oscillations in the microbubbles. Irrespective of the exact mechanism of ultrasound-induced microbubble destruction, the acoustic emissions from the development of non-linear oscillations contain harmonics (Schrope *et al.* 1992; deJong 1993). Selective reception of these harmonic signals results in an increased signal-to-noise ratio during MCE, since the acoustic signals from the microbubbles are much more likely to contain harmonics than those returning from tissue (Burns, Powers *et al.* 1996; Firschke, Lindner *et al.* 1997-2; Wei, Skyba *et al.* 1997; Lindner, Firschke *et al.* 1998). Harmonic imaging is therefore based on the transmission of ultrasound at one frequency (the fundamental or resonant frequency), but receiving the harmonic of that frequency.

Since microbubbles are destroyed by ultrasound, performing MCE at a high frame rate does not result in significant myocardial opacification despite the improved signal-to-noise ratio from harmonic imaging. This limitation can be overcome by decreasing the exposure of microbubbles to ultrasound by transmitting it intermittently rather than continuously. This has resulted in a significant increase in the contrast signal, and the combination of harmonic and intermittent imaging has led to successful

assessment of myocardial perfusion from a venous injection of microbubbles both in dogs and humans (Firschke, Lindner *et al.* 1997-2; Kaul *et al.* 1997; Wei *et al.* 1997-3; Lindner, Firschke *et al.* 1998).

3.2 Objectives

The aim of this study was to develop a method of measuring myocardial blood flow with myocardial contrast echocardiography during continuous infusion of contrast. If microbubbles are administered as a continuous infusion, then destroying them within the myocardium (with ultrasound) and measuring their myocardial rate of reappearance will provide a measure of mean myocardial microbubble velocity. Furthermore, if the microbubble concentration is allowed to plateau during long intervals between pulses of ultrasound, imaging during this phase will provide an assessment of the sum of cross-sectional areas of vessels within the sector. Knowing both the mean microbubble velocity and the cross-sectional area can then provide a measure of MBF. These hypotheses were tested using ex vivo, in vitro and in vivo experiments.

3.3 Methods

3.3.1 Model development

Let us assume that all the bubbles within the ultrasound field are destroyed in a single pulse. Also assume that the elevation (thickness) of the ultrasound beam '*E*' is uniform (Figure 3.1). If it is assumed that new bubbles enter this field with a flat profile at a velocity of v , then at time t microbubles would have travelled a distance d within the beam thickness given by the equation:

$$d=vt \qquad (1)$$

If all bubbles are destroyed with each ultrasound pulse, then the time available for bubbles to travel a distance d will be the pulsing interval of ultrasound. Because videointensity is proportional to microbubble concentration within the tickness of the beam, E, at any pulsing interval, videointensity within the beam will be proportional to $C \cdot (d/E)$, where C is the concentration of incoming bubbles. Substituting for d, from equation **(1)** it is seen that videointensity is proportional to $C \cdot vt/E$. At a constant v, videointensity increases with t until a specific pulsing interval T is reached where microbubbles have just enough time to fill the entire beam thickness E. Then,

$$E=vT \qquad \textbf{(2)}$$

When the pulsing interval t exceeds T videointensity will remain constant. This plateau phase will reflect the effective microbubble concentration within the myocardial microcirculation when ultrasound is no longer destroying microbubbles at a rate faster than their being replenished. The videointensities from different beds at the plateau phase will be proportional to the sum of cross sectional areas (a) of vessels within the beam.

In reality, neither the beam elevation E, nor the degree of microbubble destruction are uniform. The actual relation between videointensity and pulsing interval is, therefore, not likely to resemble that depicted in Figure 3.2A, but more likely to be curvilinear as shown in Figure 3.2B This can be described by the exponential function:

$$y=A(1-e^{-\beta t}) \qquad \textbf{(3)}$$

where y is videointensity at a pulsing interval t, A is the peak videointensity, and β is the rate constant that determines the rate of rise of videointensity. T is calculated by drawing tangents to the curve at its origin and its asymptote and determining the point of their intersection as shown in Figure3.2B.

It can analytically be demonstrated that:

$$T = 1/\beta \qquad (4)$$

Eliminating T between equations **(2)** and **(4)** results in:

$$v = E\beta \qquad (5)$$

Thus, for a given beam elevation (thickness at a given distance from the transducer E), the mean velocity of microbubbles is proportional to β. If flow f occurs through a cross-sectional area a, then:

$$f = av \qquad (6)$$

If E is constant, then a will be proportional to A. Therefore rearranging equation **(6)** and substituting for v from equation **(5)**, we get:

$$\beta = f/(AE) \quad (7) \qquad \text{or} \qquad f = A\beta E \quad (8)$$

Since E is constant:

$$f \propto A\beta$$

3.3.2 **Strategies to test the model**

Ex vivo experiments using explanted veins were initially used to evaluate the relation between pulsing interval and flow velocity as predicted in equations **(1)** and **(2)**. Due to the large cross-sectional area and low resistance of the ex vivo veins, the flow rates used were much higher than that seen physiologically. To evaluate flow rates similar to those in vivo, and to test the model in a system closer in size to the coronary microcirculation, in vitro experiments with small hollow fibre bundles were performed. The in vitro system was also used to derive the videointensity to pulsing interval relationship as shown in equation **(3)** at multiple different flow rates.

To test the model in vivo, an experimental setup where autoregulation was obliterated was used, but coronary flow rates could be altered. Subsequently, in the second group of dogs, an experimental preparation was used where changes in flow were secondary to changes in

intravascular volume. Finally the model was rested in a physiological coronary stenosis preparation.

3.3.3 Experimental preparations

Ex vivo studies: The aim of this experiment was to demonstrate that the use of an inappropriate pulsing interval undermines the ability to define differences in flow rate. Figure 3.3A illustrates the experimental setup. Two segments of external jugular vein obtained from dogs were attatched to tubing and immersed side-by-side within a water bath. Each vein had a diameter of approximately 0.8cm. The flow rate in the veins were controlled with separate flow pumps (model 2501-001, Harvard Apparatus, South Natick, MA, or model S10K,Sarns Inc, Ann Arbor, MI).

In vitro studies: The purpose of these experiments was to define the pulsing interval to videointensity relation at different flow rates as outlined in equation **(3)**. These experiments were performed using hollow haemodialysis fibre bundles (Spectra/Por® , Spectrum Microgon, Laguna Hills, CA). A single bundle consists of 352 fibres, each 200μm in diameter. Four bundles were attached to tubing and immersed in parallel in a 0.9% saline bath.The distance between the fibre bundles and the transducer was held constant for each experiment. A solution of microbubbles was continuously circulated through the hollow fibres using a flow pump (Model 2501-001, Harvard Apparatus).

In vivo studies: The study protocol was approved by the Animal Research Committee at the University of Virginia and conformed to the American Heart Association Guidelines for Use of Animals in Research. A total of 21 dogs were used for the experiments. They were divided into 3 separate groups and subjected to different protocols. The dogs were anesthetized with 30 $mg \cdot kg^{-1}$ sodium pentobarbital (Abbott Laboratories, IL), intubated and ventilated with a respirator pump (model 607, Harvard

Apparatus). Fluid was administered via 7F catheters placed in the femoral veins. A left lateral thoracotomy was performed and the heart was suspended in a pericardial cradle.

In group I dogs (n=7), the purpose of the experiments was to define the relation between absolute epicardial flow and ß in a setting where CBV remains constant. The proximal left anterior descending coronary artery (LAD) was dissected free from the surrounding tissues. A 12F cannula was inserted into the left carotid artery and connected to plastic tubing, the other end of which was connected to a custom-designed cannula (Figure 3.3B) After priming the tubing with blood from the carotid artery, the LAD was ligated. The cannula was inserted into the LAD via an incision made distal to the site of the ligation and was secured in place with silk ties . Flow through the tubing was controlled using an extracorporeal time-of-flight ultrasonic flow probe (series SC, Transonics) connected to a digital flow metre (model T206, Transonics).

In Group II dogs (n=5), MBF was altered using coronary vasodilators. Proximal segments of both the LAD and the left circumflex coronary artery (LCx) were dissected free from surrounding tissue. Time-of-flight extracorporeal ultrasonic flow probes were placed around both segments, and a side branch of the LAD was cannulated with with a 20g teflon catheter (Critikon, Tampa, FL) (Figure 3.4A). Coronary vasodilators were administered through this canula using a constant rate infusion pump (model 944, Harvard Apparatus)to change blood flow. Arterial pressure was monitored via a 7F catheter in the femoral artery.

The purpose of the third group of dogs was to evaluate microbubble velocity and volume changes in a coronary stenosis model. The 9 Group III dogs underwent coronary artery dissection similar to that in the Group II dogs, except that a branch of either the LAD or LCx was cannulated for measurement of distal coronary pressure (Figure 3.4B). A custom-

designed screw occluder was placed around the cannulated vessel to create coronary stenoses of various severities. A 7F catheter was placed in the ascending aorta and connected to a fluid-filled pressure transducer for measurement of aortic pressure. The severity of a coronary stenosis was judged by the pressure gradient between the central aortic and the distal coronary pressures.

All pressure transducers and the flow meter were connected to a multichannel recorder (model ES200, Gould Electronics, Valley View, OH). Repeated digital aquisitions of epicardial coronary arterial flows and all pressures were made at 200Hz using Labtech Notebook (Laboratory Technologies Corporation, Wilmington, MA).

3.3.4 Contrast Echocardiography: A prototype Sonos 2500 (Hewlett Packard Corporation, Andover, MA) with both harmonic and intermittent imaging capabilities was used for these experiments. All imaging was performed in harmonic mode, where ultrasound is transmitted at 2 MHz and received at 4 MHz. Ultrasound pulses were gated to either the electocardiogram signal or to an internal timer. Dual triggering, which allows ultrasound to be transmitted twice within an R-R interval, was used for the in vivo experiments. The rationale was to destroy microbubbles during the first ultrasound pulse and to image their reappearance with the second pulse. During an imaging sequence, the interval between these pulses was progressively prolonged to allow more bubble replenishment of the ultrasound beam elevation. The ultrasound transducer was fixed in position with a custom-designed clamp. The transmit power, focus, compression, overall gain and image depth were kept constant for all experiments. Data were recorded on 1.25cm video tape with a S-VHS recorder (Panasonic AG-MD830, Matsushita Electrical Co, Japan).

A second generation microbubble (MRX-115, ImaRx Pharmaceuticals, Tuscon, AZ) was used in this study. This agent was administered as a constant infusion in all experiments. These microbubbles have a mean size of 2.5μm and a concentration of $1.2x10^9 \cdot mL^{-1}$. They have an 8nm bilayer phospholipid shell and are filled with a mixture of air and perfluoropropane. These microbubbles have been shown to have no effect on systemic haemodynamics or pulmonary gas exchange.

Images were transferred from video tape to an off-line image analysis system (Mipron, Kontron Electronics, Eching Germany) in a 244x244x8 bit format and analysed. For the ex vivo and in vitro experiments, a large region of interest was defined in the centre of the vein or fibre bundles. For the in vivo experiments, frames set to the 'imaging' trigger were selected and aligned using computer cross-correlation. Large transmural regions of interest were defined over the anterior and lateral myocardium, with care taken to avoid the specular epicardial and endocardial borders. When video intensity from the LV cavity was analysed, a large region of interest measuring at least 600 pixels was defined. Video intensity measurements from 5 frames at each pulsing interval were averaged and subtracted from the average video intensity of pre-contrast frames.

3.3.5 Flow Measurements: The flow rate in the ex vivo, in vitro, and Gp I dogs was controlled with a peristaltic pump. The total conduit flow was measured using a time-of-flight ultrasonic flow probe attached to the tubing (Series C, Transonics).

In Group II and III dogs, tissue blood flow was measured using radiolabelled microspheres as a gold standard. Total nutrient MBF ($mL.min^{-1}g^{-1}$) was determined by injecting approximately $2x10^6$ 11 μm radiolabeled microspheres (Dupont Medical Products, Wilmington, DE) suspended in 4 ml 0.9% saline and 0.01% Tween 80 into the left atrium.

Duplicate reference samples were withdrawn from the femoral arteries over 130 seconds with a constant rate withdrawal pump (model 944, Harvard Apparatus, South Natick, MA). At the end of the experiment, the short-axis slice of the left ventricle corresponding to the echocardiographic image was cut into 16 wedge shaped pieces, excluding the papillary muscles, and each piece was further divided into epi-, mid-, and endocardial segments. The tissue and reference blood samples were counted in a well counter with a multichannel analyzer (model 1282, LKB Wallac, Washington D.C.). Corrections for activity spilling from one energy window to another were made using a custom-designed computer program.

Flow to each epi-, mid- and endocardial segment was calculated from the equation $Q_m = (C_m \times Q_r)/C_r$, where Qm is blood flow to the myocardial segment ($mL \cdot min^{-1}$), C_m is tissue counts, Q_r is rate of arterial sample withdrawal ($mL \cdot min^{-1}$) and C_r is arterial reference sample counts. Transmural MBF ($mL \cdot min^{-1}g^{-1}$) to each of the 16 wedge-shaped pieces was calculated as the quotient of the summed flows to the individual segments within that piece and their combined weight. The perfusion bed of either the LAD or LCx was determined using intracoronary injections of Albunex®, or monastral blue. The MBF to each bed was then calculated by averaging the transmural flows in the central 50 - 75% of the pieces in each bed.

3.3.6 Experimental Protocols

Ex vivo studies: The aim of this experiment was to demonstrate the importance of using an appropriate pulsing interval to define differences in flow rate from video intensity measurements. Each vein was connected to a separate piece of tubing and the same solution of MRX-115 (0.01 mL of MRX-115 in 560 mL of 0.9% saline) was continuously circulated through

both veins. This concentration of microbubbles resulted in adequate opacification in the veins without system saturation or attenuation. The flow in one vein was held constant at 52 mL • min^{-1} (control), while that in the other vein was increased from 52 mL • min^{-1} to 200 mL • min^{-1} in random order. This corresponds to flow velocities ranging from 1.7 cm • s^{-1} to 6.7 cm • s^{-1}. Imaging was performed with the ultrasound pulsing interval held constant at 33 ms, and then at 200 ms.

In vitro studies: The purpose of these experiments was to a) define the video intensity to pulsing interval relation for different flow rates as outlined in the model, and b) to define the effect of different microbubble concentrations on the determination of A and β at the same flow rate. Hollow fibre bundles were selected for these experiments because these fibres are closer in size to those of the coronary microcirculation. A solution of 0.2 mL of MRX-115 in 1 L of 0.9% saline was continuously circulated through the bundles using a peristaltic flow pump, and flow rates were varied from 10 to 50 mL • min^{-1}. The pulsing interval was varied from 200 to 3000 ms in order to construct video intensity versus pulsing interval curves. In one experiment, the concentration of microbubbles was varied while the flow was held constant at 30 mL • min^{-1} The concentrations of microbubbles in all these experiments did not result in system saturation or attenuation at any pulsing interval.

In vivo studies:

Group I dogs: Since microbubble flow velocity depends on both MBF and CBV, a preparation where total CBV remains constant was chosen to define the relation between the absolute epicardial flow and microbubble flow velocity. It has been previously shown that transection, ligation and cannulation of a coronary artery obliterates autoregulation, so CBV remains constant. Accordingly, after ligation and cannulation of the LAD,

the flow was set at 5 - 6 different levels, ranging from 6 to 66 mL/min, in random order in all dogs.

At each flow, microbubbles were administered as an infusion, and MCE was performed using a sequence of different pulsing intervals, as in the in vitro study.

Group II dogs: The purpose of these studies was to alter MBF through arteriolar vasodilation, and to assess the relation between flow velocity and myocardial blood flow as determined by radiolabeled microspheres. Adenosine was infused at both 2.5 $\mu g \cdot kg^{-1} \cdot min^{-1}$ (low dose) and 5.0 $\mu g \cdot kg^{-1} \cdot min^{-1}$ (high dose), and acetylcholine was infused at a rate of 0.3 $\mu g \cdot kg^{-1} \cdot min^{-1}$. During the administration of each drug, MCE was not started until the LAD flow reached a new level, and had stabilized for at least a minute. After MCE, the LAD flow was allowed to return to baseline for at least 5 minutes before the next dose/drug was administered.

Group III dogs: These experiments were performed to evaluate whether MCE derived flow velocity and peak video intensity can be used to quantify coronary stenosis severity, both at baseline, and in the presence of coronary hyperaemia. There were 3 stages in the protocol for these dogs. After baseline, 2 separate non-flow limiting stenoses were created using the screw occluder. At each stage, MCE was performed both before and during an infusion of WRC-0470, an adenosine A_{2a} receptor agonist. For the in vivo experiments, solutions consisting of 2 mL of MRX-115 in 25 mL 0.9% saline were infused. In Group I dogs, the infusion rate was determined by counting the drips in the drip chamber of the intravenous line, and calculated to equal 2 $mL \cdot min^{-1}$. Therefore, even though the infusion rate was constant for each stage, it may have varied slightly between stages. In Group II and III dogs, the microbubble solution was infused at a rate of 2 $mL \cdot min^{-1}$ using a volumetric pump (IVAC Corp., San Diego, CA) to attain more consistency between stages and different

dogs. All infusions were via the femoral vein. The infusion rate was noted to achieve myocardial opacification without system saturation or attenuation in all dogs. To confirm that the infusions were constant, background subtracted left ventricular and myocardial video intensity measurements were performed in 3 Group I dogs over a 5 min period, and in 1 Group II dog over a 12 min period using a pulsing interval that has been shown to cause negligible bubble destruction (>1000 ms). The concentration of microbubbles used for left ventricular video intensity determinations were lower than that used for the myocardium to ensure that the microbubble concentration to video intensity relationship was in the linear range.

As soon as a steady state from the infusion of microbubbles was achieved, an imaging protocol which consists of a sequence of different pulsing intervals was initiated. The 'imaging' trigger was set to the T-wave of the ECG signal (end-systole representing the smallest cavity size in the cardiac cycle), while the 'bubble destruction' trigger was set to different intervals prior to the 'imaging' trigger. Although both triggers resulted in the production of echocardiographic images, video intensity measurements were made only from images captured in end-systole. In 3 dogs, data were also collected with the 'imaging' trigger set to end-diastole (peak of the R-wave).

The relation between video intensity and microbubble concentration in both the LV cavity and myocardium was evaluated in 1 dog. The microbubble concentration was slowly increased by changing the infusion rate of the solution from 5 $mL \cdot hr^{-1}$ (0.08 $mL \cdot min^{-1}$) to 400 $mL \cdot hr^{-1}$ (6.7 $mL \cdot min^{-1}$) using small increments. To ensure that changes in microbubble concentration with each infusion rate were small, a dilute

solution of 4 mL MRX-115 in 96 mL 0.9% saline was used. Imaging was performed with gating to every eigth cardiac cycle (pulsing interval of 4.2 ± 0.3 s).

3.3.7 Statistical methods

Data were analysed using RS/1 (Bolt, Beranek and Newman, Cambridge, MA). Comparisons between more than 2 stages were performed using repeated measures ANOVA, while those between 2 stages were made using Student's t-test. All correlations were performed using least-squares linear regression analysis. Differences were considered significant at $p<0.05$ (2 sided).

3.4 Results

3.4.1 Ex vivo experiments

Figure 3.5 illustrates the influence of pulsing interval on the detection of differences in flow. In Panel A, imaging is being performed at a pulsing interval of 33 ms. The concentration of microbubbles in both veins is identical, but there is a 4-fold difference in the flow between the vein on the left (52 $mL \cdot min^{-1}$) and the one on the right (200 $mL \cdot min^{-1}$). At this pulsing interval, there is an obvious video intensity disparity between the 2 veins. The video intensity in the vein with faster flow is greater, because in the short time between pulses of ultrasound, there is more bubble replenishment of the beam elevation compared to the vein with slower flow. In Panel B, the pulsing interval has been increased to 200 ms. The video intensity between the 2 veins now appears equal. This phenomenon occurs because the entire beam elevation can be replenished even in the vein with slower flow at this pulsing interval.

3.4.2 In vitro experiments

Small hollow fiber bundles were used to simulate the microcirculation in these experiments. The video intensity to pulsing interval relationships for all flow rates are plotted in Figure 3.6A. It can be seen that video intensity increased more rapidly with faster flows, and plateaued at a shorter pulsing interval compared with slower flows. Figure 3.6Bshows an excellent linear relation between the value β from the fitted functions and flow in agreement with equation (7). It is also obvious that for any flow, several pulsing intervals are required to derive β.

Figure 3.7 depicts video intensity data using solutions with 3 different microbubble concentrations at a constant flow rate of 30 $mL \cdot min^{-1}$. Despite different values of A caused by the different microbubble concentrations, the pulsing interval at which the curves begin to plateau, as measured from the value of $1/\beta$ from the fitted functions, is the same. Thus, as long as the relation between microbubble concentration and video intensity remains within the linear range, β reflects velocity and is not affected by microbubble concentration. Since changing microbubble concentration is equivalent to changing microvessel density, these results also indicate that the value of A effectively reflects the cross-sectional area (a).

3.4.3 In vivo experiments

During constant infusions over 5 to 12 min in duration, both myocardial and left ventricular video intensities remained unchanged, using a pulsing interval greater than 1000 ms . There is an initial rapid rate of rise of video intensity in the LV cavity as microbubble concentration increases. The video intensity then plateaus as system saturation is reached. As the microbubble concentration continues to increase, attenuation of ultrasound transmission through the bubbles results in a decrease in the LV cavity

video intensity. The exponential function was fitted only to the initial points before attenuation developed. In the myocardium, there is initially no detectable contrast signal because of the system threshold. As the microbubble concentration was increased, there is again an initial linear rise in myocardial video intensity.

Group 1- Panels A to D in Figure 3.8 depict images obtained at a constant LAD flow of 65 $mL \cdot min^{-1}$ and pulsing intervals of 316, 536, 1608 and 5360 ms respectively. At the shortest pulsing interval, no contrast can be seen in either the LAD or LCx beds, indicating that the pulsing interval was too short to allow replenishment of detectable amounts of microbubbles in either bed. At higher pulsing intervals, the video intensity in the LAD bed increases progressively, and appears to plateau at an interval of 5360 ms. Initial opacification of the LCx bed is seen at a higher pulsing interval than the LAD bed, and its rate of rise is also slower, indicating a lower microbubble velocity in the LCx bed.

Figure 3.9A illustrates the video intensity to pulsing interval relationship, and the fitted functions from the LAD bed at 5 different flows in a single dog. As the LAD flow was increased, the rate of rise of the curve, and therefore the value of β also increased. Figure 3.9B shows the excellent relation between β and LAD flow in the same dog. Similar results were found in all other dogs with an average correlation between ß and mean flow of $r = 0.91$ (range $r = 0.77$ to 0.97). Figure 3.10 (A-F), illustrates individual correlations in the other 6 dogs.

These results pertain to imaging in end-systole. In the 3 dogs where imaging was also performed in end-diastole, no differences were found between the value of β derived from the end-systolic or end-diastolic video intensity to pulsing interval curves, or in the relation between the value of β and flow from either part of the cardiac cycle. This is because the time between the "bubble destruction" ultrasound pulse and the

"imaging" pulse may span more than 1 cardiac cycle, so the microbubble replenishment rate reflects an average of that from different phases of the cardiac cycle.

Group II - MBF was increased in these dogs with intracoronary infusion of vasodilators. Since both adenosine and acetylcholine increase MBF by vasodilation of the coronary microvasculature, the results from both drugs were analysed together (Table 3.1). These infusions were sufficient to cause increases in LAD flow, without any changes in LCX flow or mean arterial pressure. During peak hyperaemia, both epicardial flow probe flow and tissue flow determined from radiolabeled microspheres increased about 3-fold compared to baseline (28 ± 15.8 mL • min^{-1} to 77.4 ± 56.1 mL • min^{-1}, and 0.96 ± 0.69 mL • min^{-1} • g^{-1} to 2.46 ±1.15 mL • min^{-1} • g^{-1}, respectively). An excellent correlation was found in all dogs between the value of β and radiolabeled microsphere derived MBF (r = 0.88, P <0.001). Similar results were found between β and epicardial flow (r = 0.8, P < 0.001).

Both adenosine and acetylcholine cause vasodilation of microvessels larger than 200 μm in size, and changes in MBF are coupled to increases in CBV. Despite large increases in MBF, however, no significant changes in A (normalized to baseline peak video intensity) were found. The mean ratio of A from the LAD bed normalized to baseline or to the control LCx bed was 1.1 ± 0.1 and 0.8 ± 0.2, respectively, from all stages. Subsequently, as Figure 3.11A shows, since A remained constant, the relation between MBF and $A\beta$ was also found to be excellent (r =0.96, P <0.001).

Group III - The protocol could not be completed in 1 dog due to hemodynamic instability, and the distal coronary cannula resulted in a myocardial infarct in another dog, so the data from the remaining 7 dogs are presented in Table 3.2.

Page 67
missing from
this Thesis

3.5 Discussion

When microbubbles are injected as a discrete bolus directly into a coronary artery, their mean myocardial transit rate reflects the MBF/CBV relation (Jayaweera, Edwards *et al.* 1994; Lindner, Skyba *et al.* 1997). When microbubbles are injected intravenously, however, classic tracer kinetic principles cannot be applied to quantify MBF for a number of reasons. Firstly, the concentration of microbubbles must exceed a certain level before they can be detected in the myocardium, due to the "threshold" effect of echocardiographic systems (Skyba *et al.* 1994). Since the concentration of microbubbles in the myocardium is much lower than that of the left ventricular (LV) cavity, the width of the myocardial time intensity curve is also significantly narrower than that in the LV. The input function from the LV cannot, therefore, be derived from the myocardial curve. The threshold effect also precludes analyses of changes in the shape of the "tail" of the myocardial time intensity curve, which would theoretically be altered as the bolus passed through the myocardium. The transit rate of microbubbles through the myocardium invariably reflects the dispersion of the bubbles in the large central circulation. The much smaller effect caused by myocardial dispersion is not measurable. Furthermore, the number of microbubbles entering the coronary circulation is only a small proportion of those in the LV cavity. To produce adequate myocardial opacification, therefore, the concentration of microbubbles in the LV cavity must be so high that it is no longer within the linear range of the microbubble concentration versus video intensity relation. Thus, using the ratio of the areas under the myocardial and LV time intensity curves to derive myocardial blood volume fraction is not possible.

Using the ability of ultrasound to destroy bubbles in an image slice, and then measuring the reappearance rate of the bubbles into that slice is a novel approach that overcomes many of the above limitations. In this study, using both in vitro and in vivo models, excellent correlations have been shown between the rate constant "β" and absolute epicardial flow probe flow, or radiolabeled microsphere derived myocardial blood flow. A further advantage of this technique is that the peak video intensity during the plateau phase of the video intensity to pulsing interval relation, A, reflects the blood volume fraction of tissue, as shown in equation **(8)**. Even though similar intravascular tracers are used with both the current technique and intracoronary injections of contrast, and even though both approaches quantify myocardial perfusion by assessing the "transit rate" of the tracer, important differences exist between them. The most significant difference is that the former technique measures the transit of a tracer through the microcirculatory myocardial blood volume (MBV), whereas the latter measures transit through the total coronary blood volume (CBV). In the pig, the entire coronary system (epicardial conduit arteries, arterioles, capillaries, venules and veins) contains approximately 12 mL of blood per 100 g of LV mass. The blood present in the myocardial microcirculation, or MBV, measures approximately 4 mL per 100 g of LV mass. Furthermore, the MBV resides in vessels <200 μm in size, of which about 90% is in the capillaries (Kassab *et al.* 1994). The MBV, therefore, constitutes only a fraction of CBV, and imaging this compartment gives information related to changes in capillary flow and volume. Using these data and presuming that the sizes of the region of interest and the thickness of the beam are known, it is possible to attempt the measurement of absolute regional myocardial blood flow. The velocity of a tracer through a compartment is dependent on both the MBF and the cross sectional area of that compartment. The volume of a vessel is equal

to the product of the cross sectional area and length, which is the beam elevation in a sector of ultrasound. Since the beam elevation at any depth is fixed, the cross sectional area will be proportional to the volume. Since MCE evaluates the myocardial capillary compartment, the velocity of microbubbles will depend on the MBF/MBV relation. In Group I dogs, a preparation was used where autoregulation was obliterated. Since CBV, and therefore MBV, is fixed, changes in absolute epicardial flow were reflected by changes in the rate constant β, as predicted in equation **(6)**. In Group II dogs, flow was increased by infusion of intracoronary vasodilators. Crystal et al also evaluated changes in CBV and MBV after intracoronary infusions of adenosine. When radiolabeled red blood cells were administered as an intracoronary bolus, the mean transit rate of the red blood cells decreased in the presence of adenosine. This finding was due to a 35% increase in total CBV. There were, however, no changes found in MBV during adenosine administration. The changes in CBV, therefore, were presumably related to dilation of macroscopic vessels of the coronary bed. Such macroscopic vessels form a very small proportion of the myocardial blood volume interrogated by the ultrasound beam and changes in them are not detectable using this method. Similar results were reported by Eliasen et al(Eliasen *et al.* 1984). In this study, the value of A from the video intensity-pulsing interval relation also reflects changes in MBV. No changes in the peak video intensity were seen despite large changes in MBF induced by either adenosine or acetylcholine, which supports the findings of Crystal and Eliasen (Crystal, Downey et al. 1981; Eliasen and Amtrop 1984). Subsequently, the excellent linear relation found between ß and flow can again be explained by the fixed MBV. Further evidence that MBV was constant in Group II dogs is that the slope of the relation between B and absolute epicardial flow in these dogs was similar to that of Group I dogs. There are other potential explanations for

the lack of change seen in peak video intensity after intracoronary administration of vasodilators. It is known that the red cell hematocrit of small vessels is reduced compared to large vessels - a phenomenon explained by the Fahraeus effect. Since microbubbles have the same intravascular rheology as red blood cells, it follows that microbubble concentrations will also be lower in the microcirculation compared to larger vessels. With increasing flow, the red cell hematocrit has been found to decrease further. Other phenomena which are more flow-dependent, such as plasma skimming or red cell screening, may also play a role. Reductions in microvascular microbubble concentration, especially during high flow, may interfere with the ability to detect changes in volume. It is also possible that small changes in microbubble concentration that accompany changes in blood volume may not be detectable with current echocardiographic systems. In the future, the ability to directly sample radiofrequency data, with expanded dynamic range and less need for compression may improve sensitivity.

In the presence of mild or moderate coronary stenoses (< 85% luminal diameter narrowing), MBF is maintained by vasodilation of microvessels distal to the stenosis. Techniques that can assess changes in total CBV, such as intracoronary bolus injections of microbubbles, have shown that the degree of change of CBV is related to the severity of the stenosis. In Group III dogs, using a continuous infusion of microbubbles, no increase in myocardial peak video intensity *(A)* was seen with coronary stenoses compared to baseline. This suggests that changes in blood volume from autoregulation do not occur at the capillary level. In the presence of non-flow limiting stenoses, and normal resting flow, no changes in the value of β were found. This provides further evidence suggesting that MBV did

not increase, since microbubble velocity depends on the MBF/MBV relation.

With the addition of exogenous hyperaemia in Group III dogs, both the estimate of MBV (the peak video intensity A at the plateau phase), and blood flow velocity (β) were found to decrease in the stenosed bed when compared to the control bed. This supports previous studies using ultrafast cine-CT (Wang *et al.* 1989) and MCE that showed decreases in both myocardial blood volume and flow during exogenous hyperaemia distal to a stenosis. This study extends those observations by suggesting that the site of volume change may be the capillaries, or possibly a post-capillary compartment (venules). Other studies have shown that the size of coronary microvessels is both flow and pressure dependent. At rest MBF across non-flow limiting stenoses is maintained by vasodilation of distal microvessels. The same stenosis, however, markedly attenuates the increase in blood flow that should occur in the presence of coronary hyperaemia. The transtenotic gradient increases, leading to decreases in distal pressure which can lead to capillary collapse, and therefore, a reduction in myocardial blood volume. This hypothesis is in part supported by the observation that the value of A (a measure of CSA) tends to fall with more severe stenoses during hyperaemia. Venules may also be affected by flow and pressure changes, and this may also be important during pharmacologically induced hyperaemia.

Limitations

The ultrasound beam elevation (thickness or E) is heterogeneous at different depths from the transducer. The elevation is also likely to be different between various commercially available echocardiographic systems. One reason the correlation between velocity and flow was often worse when all dogs were grouped together is that the anterior

myocardium of all dogs could not be placed at exactly the same distance from the transducer. In order to precisely quantify microbubble velocity, it is essential to have the correct value of"E" at all image depths. This can be achieved by calibrating E at different depths using an invitro system where both the flow and cross sectional area are known. It may also be possible to "defocus" the beam or alter its profile so that E becomes uniform at all depths.

The determination of beam width by industry standards may also be different from that derived from bubble destruction. The threshold power needed to destroy bubbles results in a "functional" beam width as determined by MCE which may be narrower or wider than the industry definition. There may be further differences in the bubble destruction threshold for various contrast agents, transducers and echocardiographic systems.

Cardiac translation, caused by the base to apex systolic shortening and by respiration, results in different planes of the heart being imaged at different times in the cardiac cycle. If imaging were performed using apical views, there is also counterclockwise rotation of the heart during systole. Thus, the plane where microbubble destruction occurs may not be precisely the same as where imaging occurs. In this study, the heart was suspended in a pericardial cradle, which lessens translation. The respirator was also turned off during data acquisition, abolishing respiration-induced cardiac motion. Finally, all video intensity measurements were made from anterior and anteroseptal regions of interest, where less translation occurs compared to the inferoposterior wall. Cardiac translation is less problematic if imaging is always peformed in the same phase of the cardiac cycle.

In this study, analyses were only performed using transmural flows. It would be interesting to extend these observations to evaluate whether

microbubble velocity from subendocardial or subepicardial layers of the myocardium correlate to the corresponding flows, in the presence of coronary stenoses. It is likely that phasic changes in microbubble velocity can also be measured if the 'imaging' trigger is set to different parts of the cardiac cycle.

3.6 Conclusions

A novel method for measuring microbubble velocity based on bubble destruction by ultrasound is described. Measuring this velocity provides a quantitative assessment of myocardial perfusion using a venous injection of microbubbles - a technique that is likely to become clinically feasible in the near future. Although these data were derived from the myocardium, this method can be applied to any tissue accessible to ultrasound, and therefore has potential for quantifying perfusion in many organ systems. Furthermore, this approach is likely to be a cost effective method for the quantification of perfusion, and utilizes technology that would only require minimal hardware and software modifications.

Table 3.1

	Baseline	Mild Hyperemia	Moderate Hyperemia
Heart rate, bpm	124±23	119±24	118±21
Mean aortic pressure, mm Hg*	100±10	97±13	94±7
Mean LAD flow, mL · min^{-1}†	28.0±15.8	59.0±49.2	77.4±56.1
Mean LAD MBF, mL · min^{-1} · g^{-1}†	0.96±0.69	1.75±0.75	2.46±1.15
β†	0.62±0.13	1.32±0.51	1.66±0.86
A*‡	1.0±0.0	1.12±0.14	1.19±0.13
$A\beta$†‡	0.64±0.50	0.97±0.14	2.50±0.74

* No interstage differences noted.

† $P<.01$ between stages.

Table 3.2.

	No Stenosis	Mild Stenosis	Severe Stenosis	*P*
	Before hyperemia			
Mean aortic pressure, mm Hg*	104±12	103±16	92±12	NS
Mean heart rate, bpm*	113±16	109±15	97±12	NS
Mean gradient, mm Hg†	2.0±3.2	10.8±2.6	21.8±14.9	.02
Mean MBF, mL · min^{-1} · g^{-1}†‡	1.0±0.2	1.0±0.2	0.9±0.3	NS
A†‡	1.1±0.2	1.0±0.2	0.9±0.3	NS
β†‡	1.1±0.2	1.0±0.2	0.8±0.3	NS
A · β†‡	1.2±0.4	1.1±0.4	0.7±0.4	NS
	During hyperemia			
Mean aortic pressure, mm Hg*	93±16	91±21	86±13	NS
Mean heart rate, bpm*	121±10	109±15	105±14	NS
Mean gradient, mm Hg†	3.8±3.8	21.2±7.0	33.1±9.7	<.001
Mean MBF, mL · min^{-1} · g^{-1}*‡	0.87±0.13	0.61±0.26	0.34±0.15	<.001
A†‡	1.00±0.22	0.96±0.25	0.71±0.19	.05
β†‡	1.05±0.12	0.58±0.17	0.43±0.17	<.001
A · β†‡	1.06±0.30	0.54±0.24	0.30±0.13	<.001

* No changes before or during hyperemia at any stage.
† Significant differences before and during hyperemia for at least one stage.
‡ Normalized to nonstenotic bed.

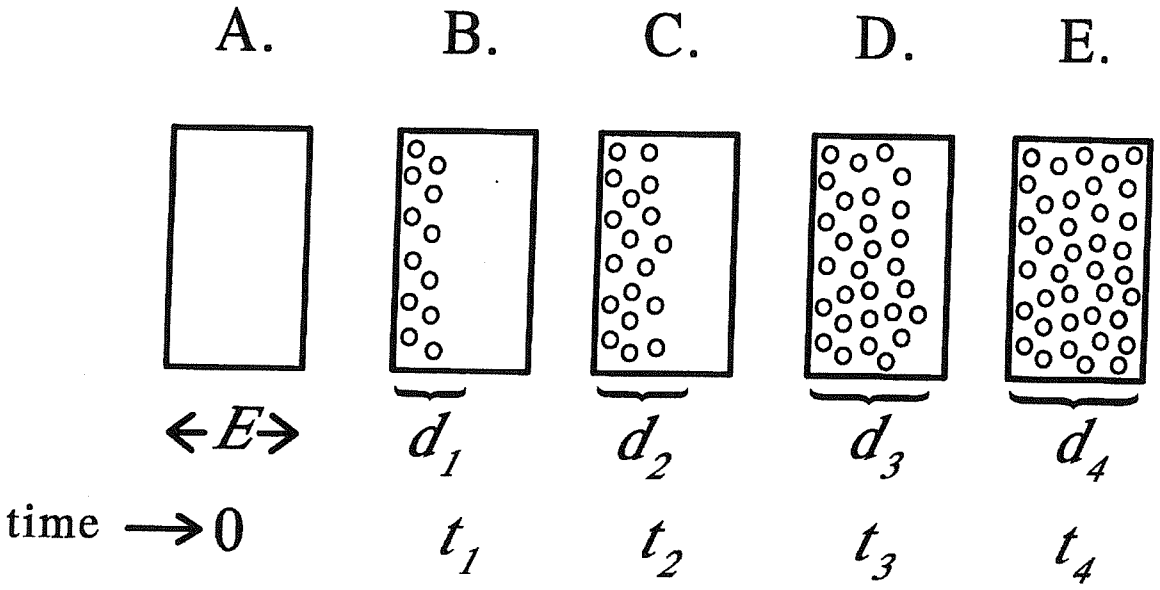

Figure 3.1

Figure 3.1

The elevation (thickness) of the ultrasound beam is represented as E (**A**). If it is assumed that all microbubbles (open circles) are destroyed by a single pulse of ultrasound at t_0, then replenishment of the beam elevation (d_1 through d_4, **B** through **E**) will depend upon the velocity of microbubbles and the time allowed for replenishment or pulsing interval (PI, t_1 through t_4). See text for details.

A.

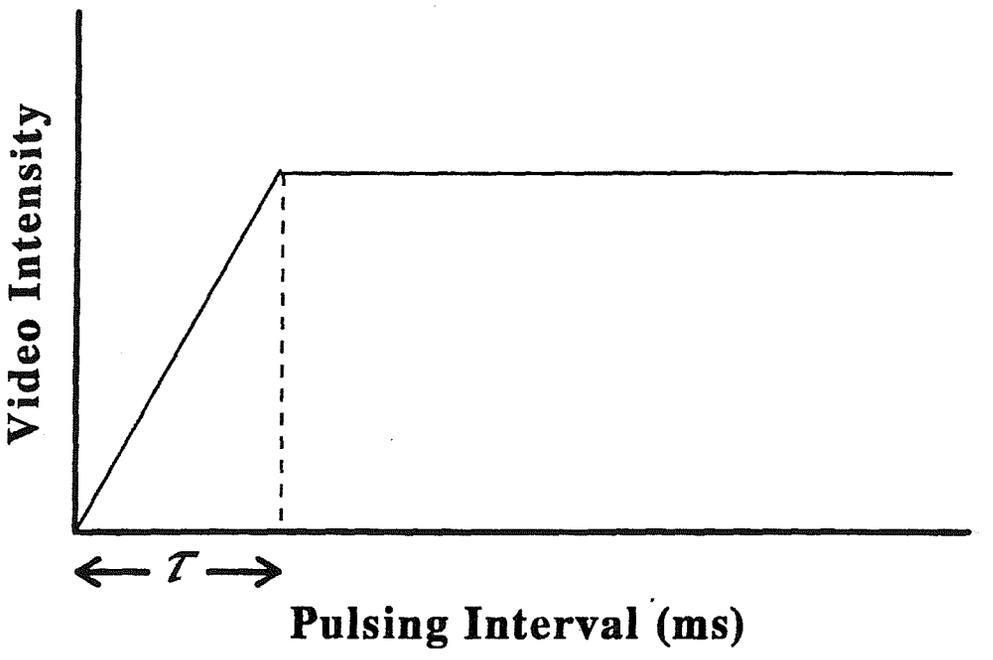
Video Intensity
τ
Pulsing Interval (ms)

B.

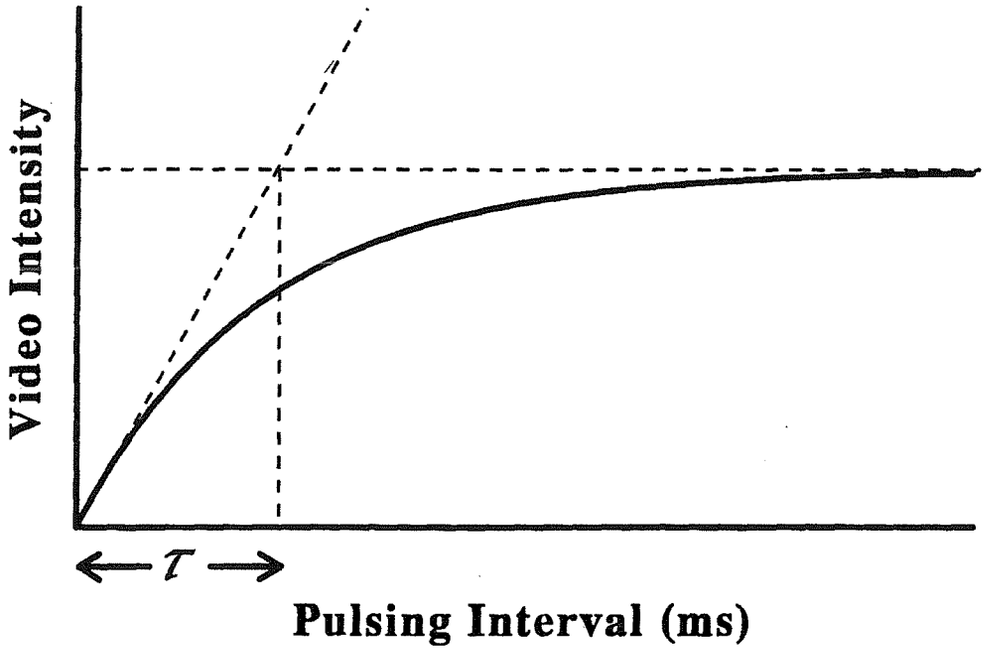
Video Intensity
τ
Pulsing Interval (ms)

Figure 3.2

Figure 3.2

The PI (x-axis) versus VI (y-axis) relation as predicted by the model (**A**) and observed experimentally (**B**). The function is used to derive parameters A and ß. See text for details.

A.

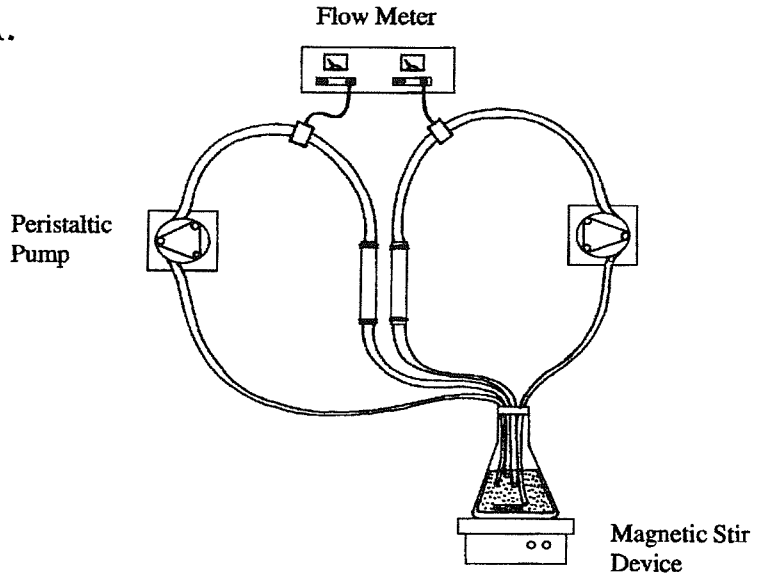

Figure 3.3A

B.

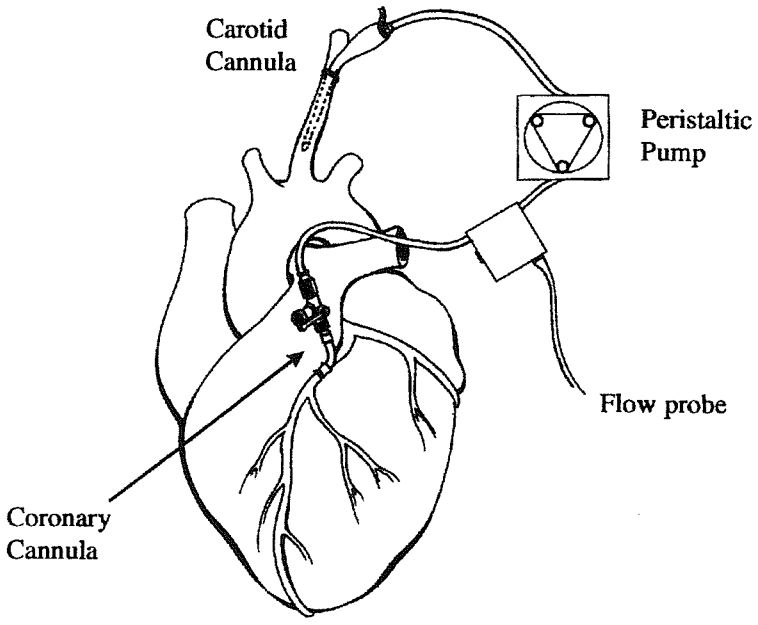

Figure 3.3B

Figure 3.3

A) Ex vivo experimental set up. **B**) Animal preparation for Group I dogs. See text for details.

A.

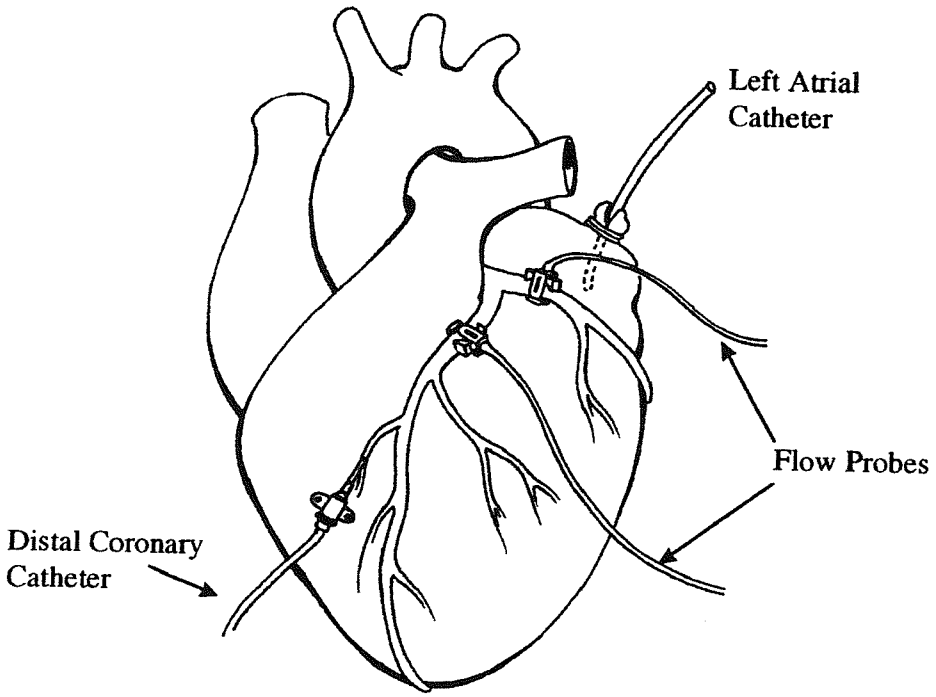

Figure 3.4A

B.

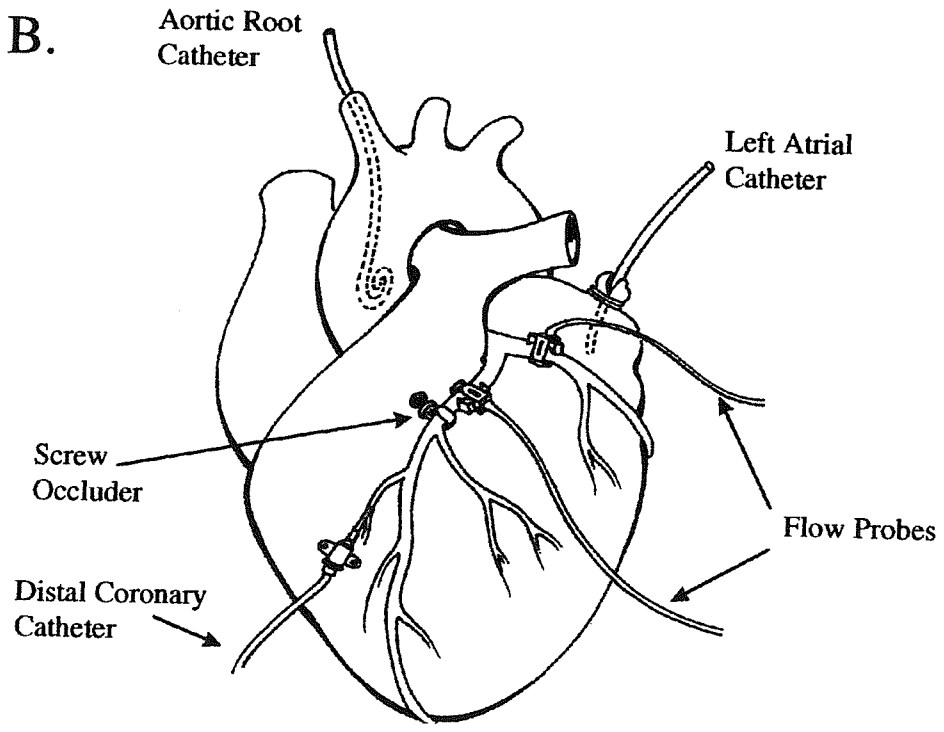

Figure 3.4B

Figure 3.4

A) Animal preparation used for Group II dogs. **B**) Animal preparation used for Group III dogs. See text for details.

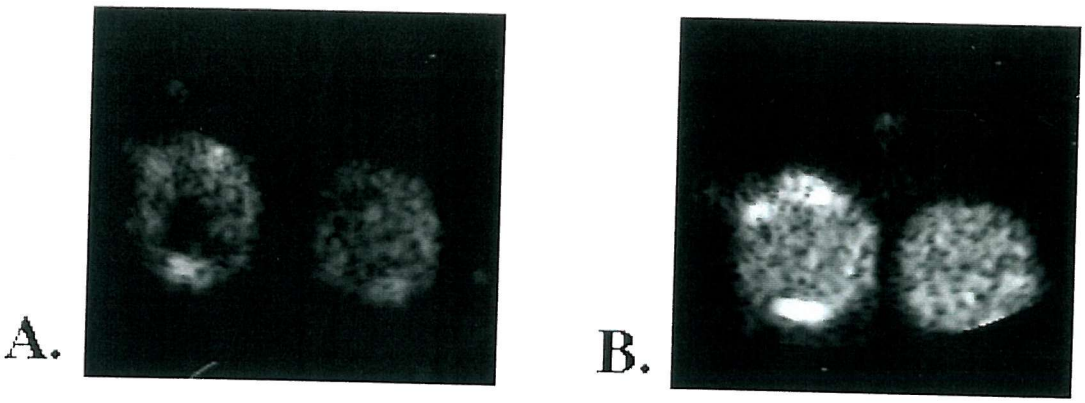

Figure 3.5

Figure 3.5

The effect of pulsing interval (PI) on VI in the ex vivo experiment. The vein on the left in each panel has a quarter of the flow in the vein on the right. Microbubble concentration is identical in the two veins. In panel A, the PI is short such that in this interval the elevation interrogating the left vein has not been replenished, hence the brighter signal from the vein with faster flow. In panel B, the PI has been lenghthened leading to full rplenishment of the beam interrogating both veins. As the elevation is fully replenished and microbubble concentration is identical in both veins, no disparity is seen in the VI despite the difference in flow. The timing of the PI is critical to distinguish between flow velocities. See text for details.

A.

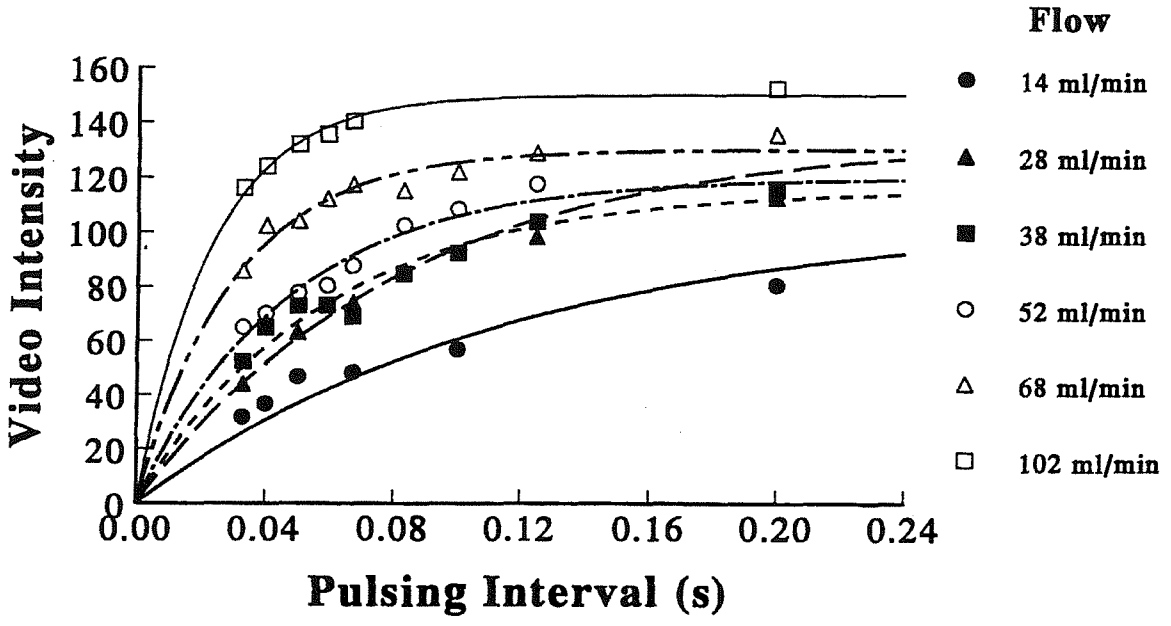
Flow
14 ml/min
28 ml/min
38 ml/min
52 ml/min
68 ml/min
102 ml/min
Video Intensity
160
140
120
100
80
60
40
20
0
0.00
0.04
0.08
0.12
0.16
0.20
0.24
Pulsing Interval (s)

B.

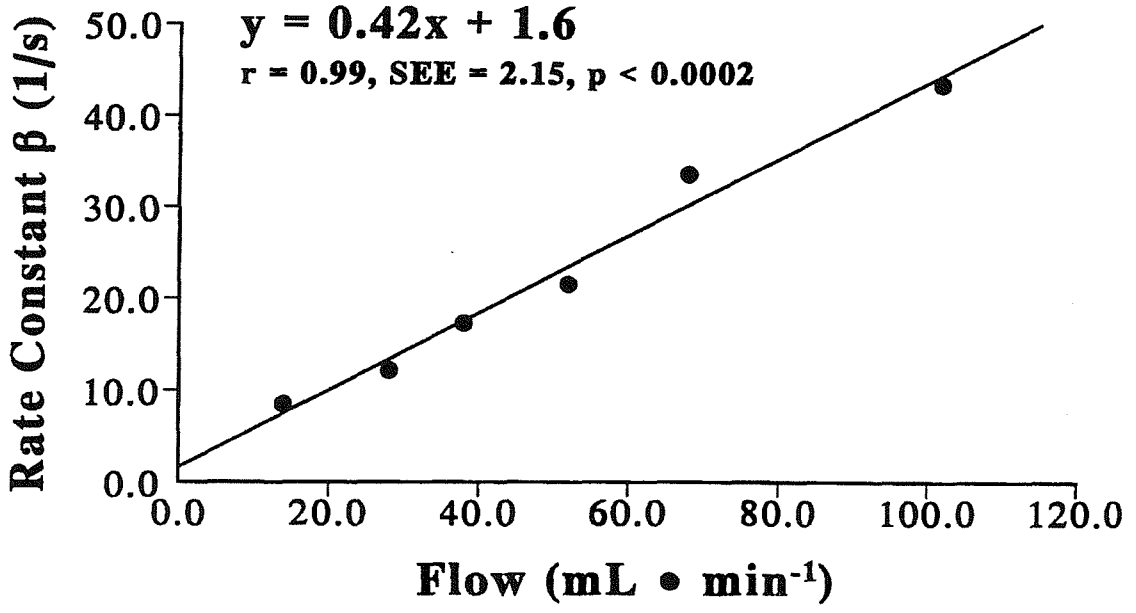
y = 0.42x + 1.6
r = 0.99, SEE = 2.15, p < 0.0002
Rate Constant β (1/s)
50.0
40.0
30.0
20.0
10.0
0.0
0.0
20.0
40.0
60.0
80.0
100.0
120.0
Flow (mL • min-1)

Figure 3.6

Figure 3.6

In panel **A** the PI (x-axis) is plotted against VI (y-axis) at six different flow rates in the hollow fibre in vitro experiments. In panel **B**, the relation between absolute flow (x-axis) and the rate constant ß from each of the fitted functions in **A** is shown. See text for details.

fig 3.7

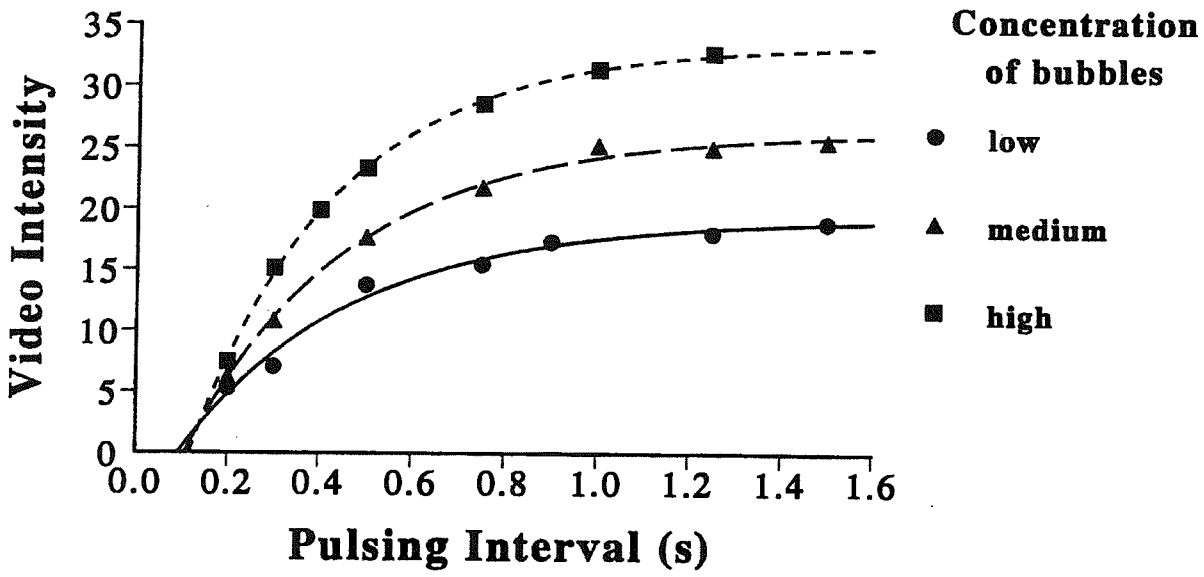

Figure 3.7

Figure 3.7

Effect of microbubble concentration on the rate constant ß and the plateau videointensity A at a constant flow. The plateau increases with increasing microbubble concentration but the rate constant ß remains unchanged. See text for details.

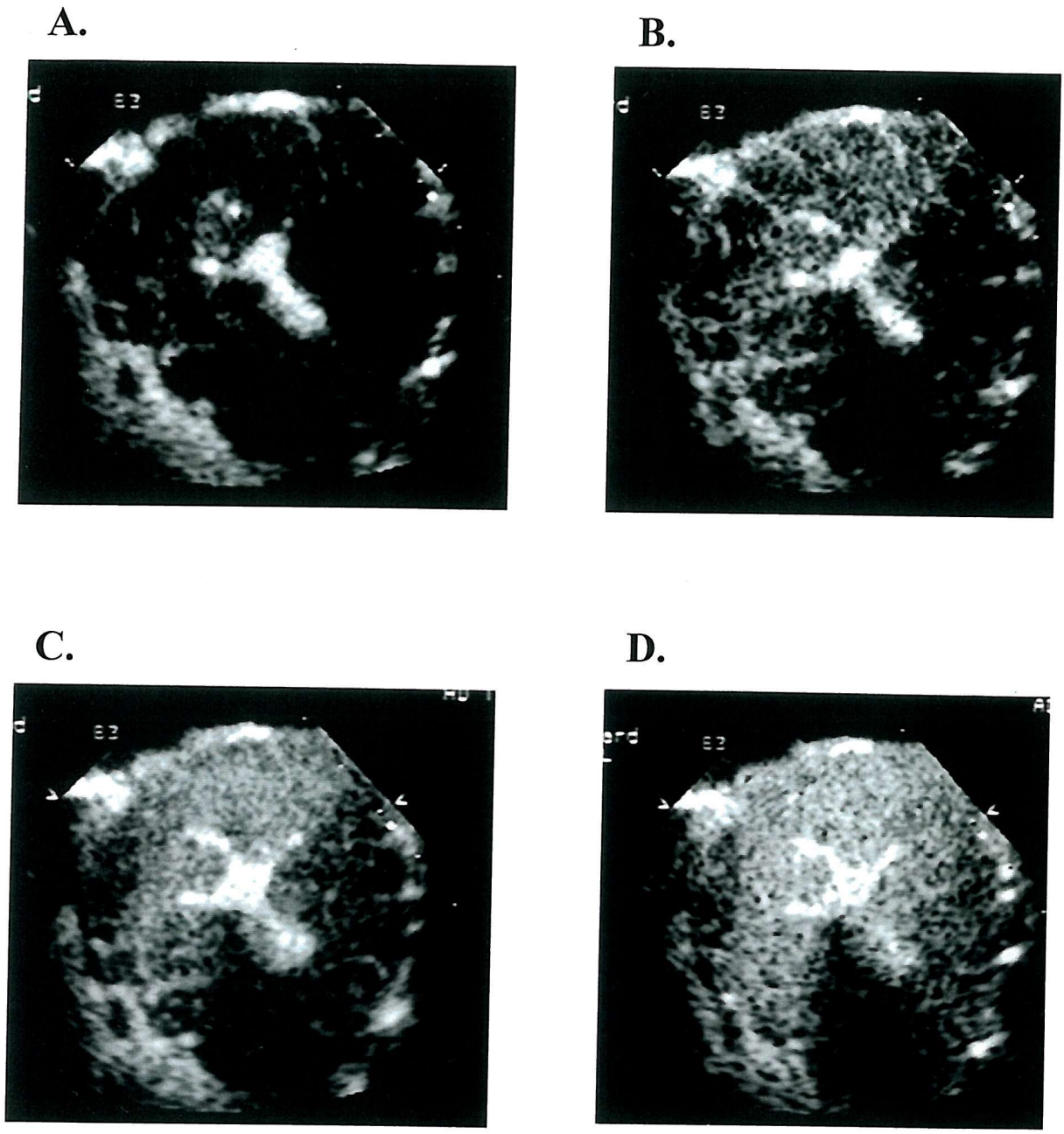

Figure 3.8

Figure 3.8

End-systolic short axis views at mid-papillary level with a constant LAD flow of 65mL/min at four different PIs (316, 536, 1608 and 5360 ms in **A** through **D** respectively) in one Group I dog. At the shortest PI, no contrast enhancement is seen in either the LAD or LCx beds because the time interval is too short to result in any measurable replenishment of the beam elevation. As the PI is prolonged, the VI is seen to increase until it plateaus at an interval of 5360ms. See text for details.

A.

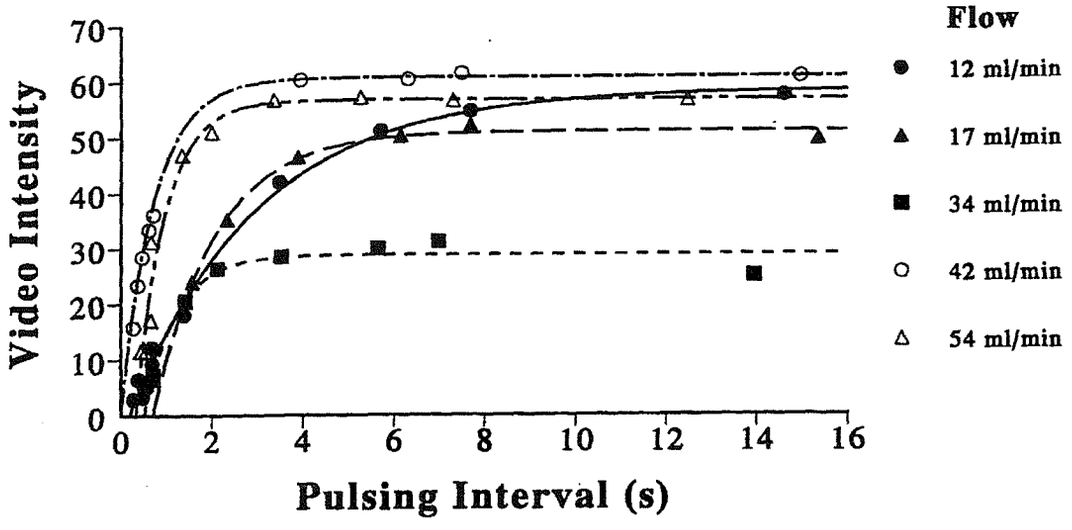
Video Intensity
70
60
50
40
30
20
10
0
0
2
4
6
8
10
12
14
16
Pulsing Interval (s)
Flow
12 ml/min
17 ml/min
34 ml/min
42 ml/min
54 ml/min

B.

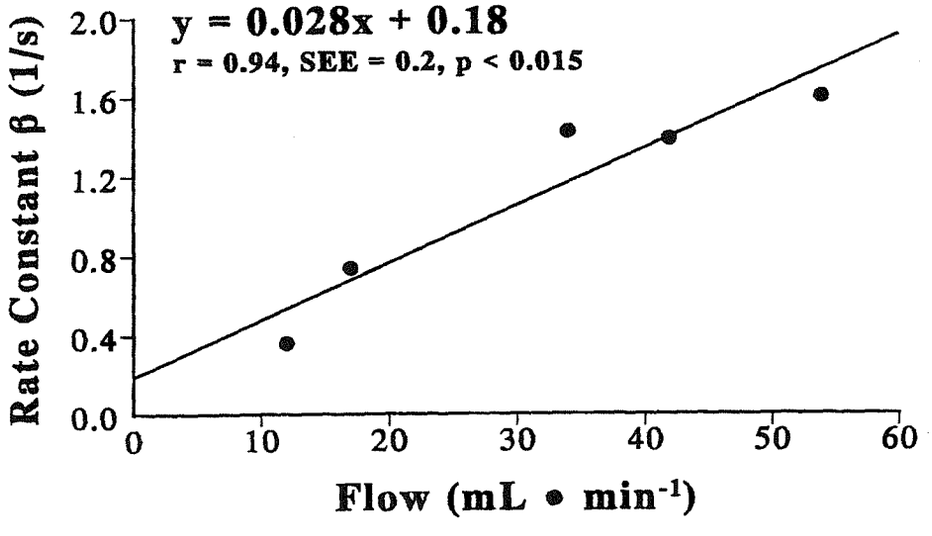
y = 0.028x + 0.18
r = 0.94, SEE = 0.2, p < 0.015
Rate Constant β (1/s)
2.0
1.6
1.2
0.8
0.4
0.0
0
10
20
30
40
50
60
Flow (mL • min-1)

Figure 3.9

Figure 3.9

A) Relation between PI (x-axis) and VI (y-axis) at five different LAD flow rates in one Group I dog. **B**) Relation between the epicardial LAD flow rate (x-axis) and the rate constant ß derived from the fitted functions (y-axis) in **A** for the same dog. See text for details.

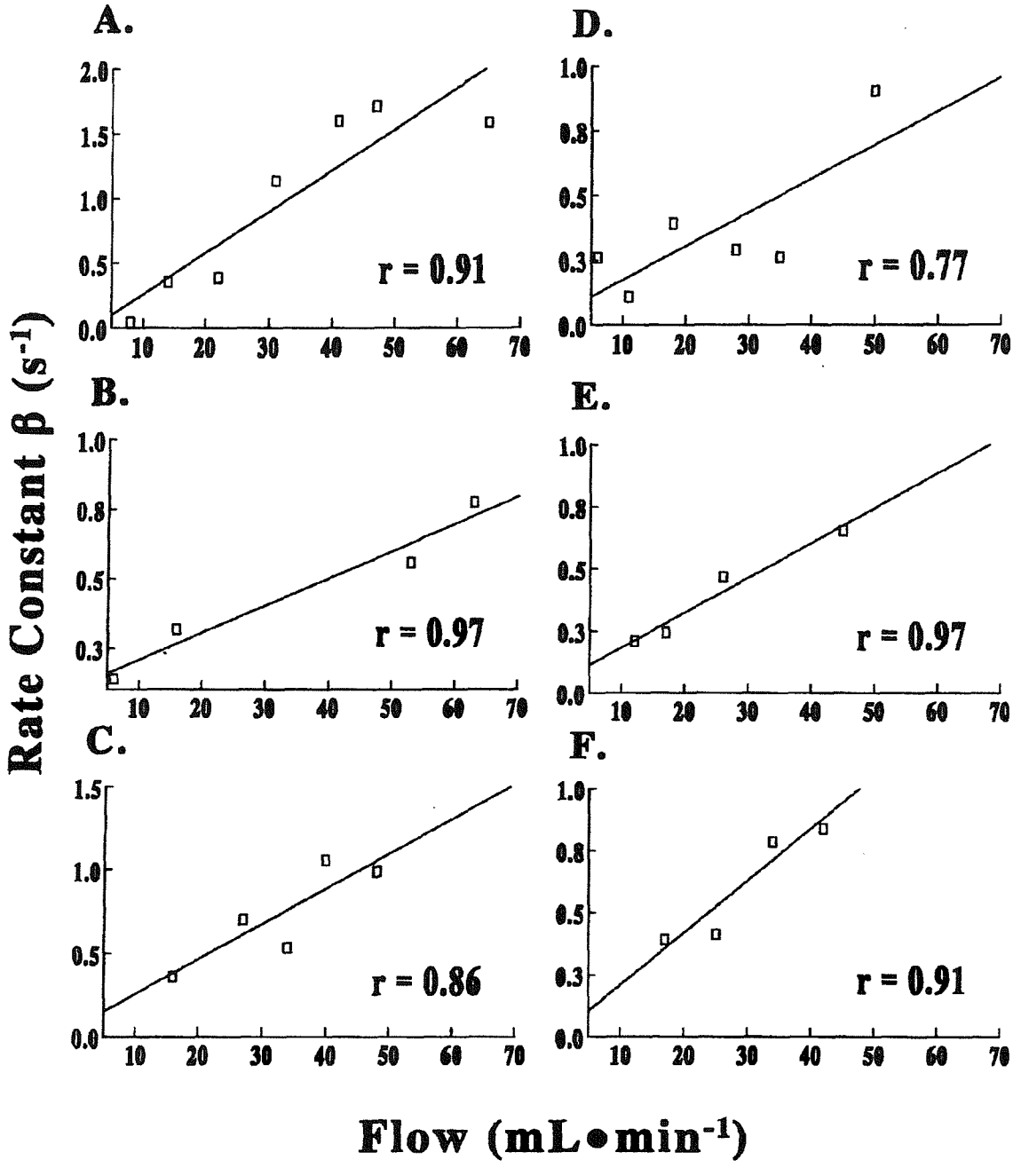
A.
D.
B.
E.
C.
F.
r = 0.91
r = 0.77
r = 0.97
r = 0.97
r = 0.86
r = 0.91
Rate Constant β (s-1)
Flow (mL•min-1)

Figure 3.10

Figure 3.10

Relation between absolute epicardial flow rate (x-axis) and ß (y-axis) for the other six dogs in Group I (**A** through **F**). The average correlation for all seven dogs was r=0.91. See text for details.

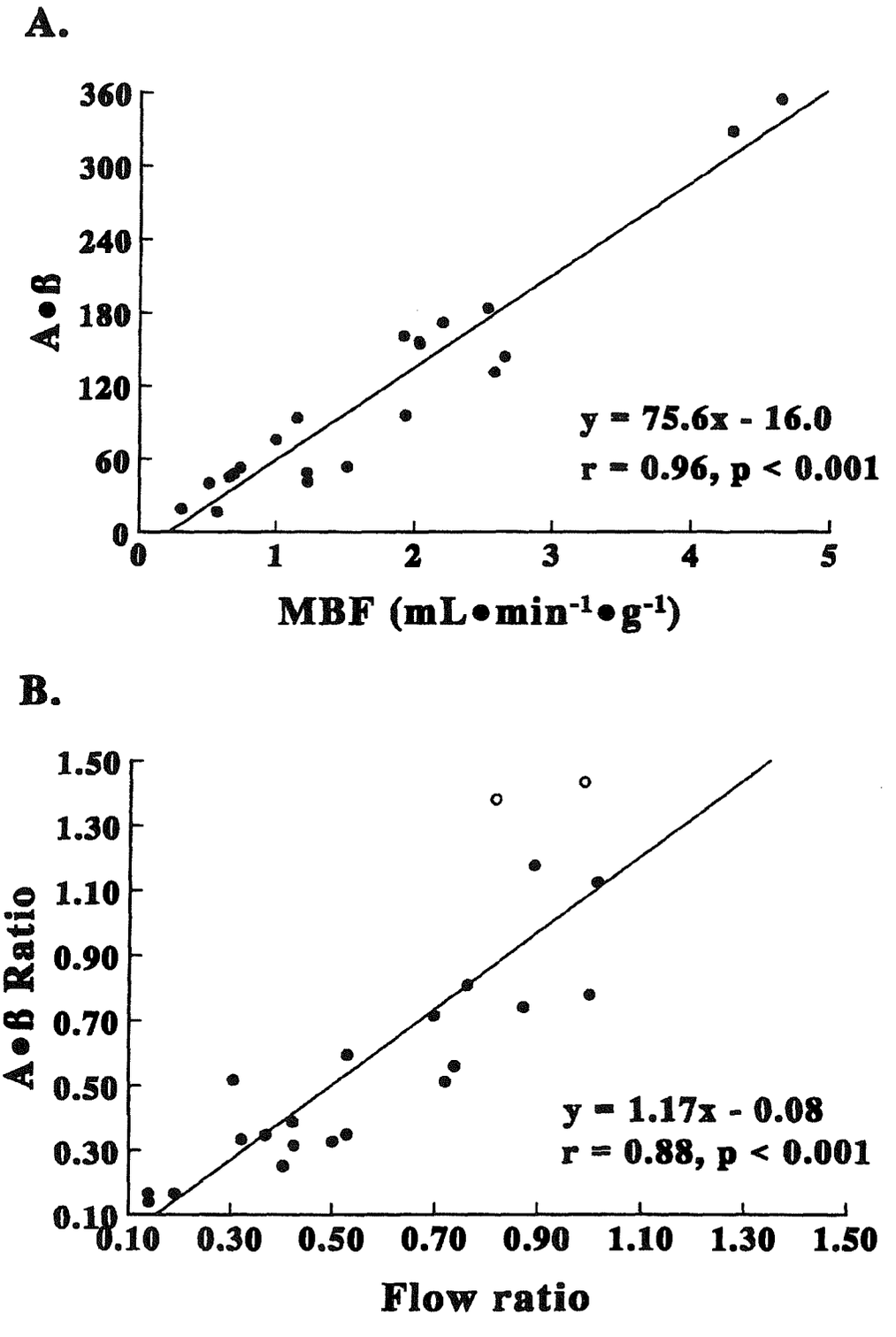
A.
360
300
240
180
120
60
0
A•ß
0
1
2
3
4
5
MBF (mL•min-1•g-1)
y = 75.6x - 16.0
r = 0.96, p < 0.001
B.
1.50
1.30
1.10
0.90
0.70
0.50
0.30
0.10
A•ß Ratio
0.10
0.30
0.50
0.70
0.90
1.10
1.30
1.50
Flow ratio
y = 1.17x - 0.08
r = 0.88, p < 0.001

Figure 3.11

Figure 3.11

A) Relation between radiolabeled microsphere-derived myocardial blood flow (x-axis) and $A\beta$ derived from MCE data (y-axis) in Group II dogs. **B)** relation between the ratio of radiolabeled microsphere-derived myocardial blood flow from the stenosed bed and normal beds (x-axis) and the $A\beta$ ratio derived using MCE data from the two beds (y-axis) in Group III dogs. See text for details.

CHAPTER 4

THE BASIS FOR STENOSIS DETECTION USING VENOUS ADMINISTRATION OF MICROBUBBLES

4.1 Introduction

Localizing coronary stenoses and estimating their severity is the most frequent indication for myocardial perfusion imaging (Lindner *et al.*). MCE is a method of assessing myocardial perfusion where microbubbles are injected into the vascular system and their presence in the myocardium is detected with ultrasound (Lindner and Kaul). Microbubbles capable of opacifying the myocardium from a venous injection have recently become available (Porter and Xie 1995; Mulvagh *et al.* 1996; Firschke, Lindner et al. 1997; Lindner, Firschke et al. 1998). When combined with intermittent harmonic imaging, they result in adequate myocardial opacification (Porter and Xie 1995; Mulvagh, Foley et al. 1996; Firschke, Lindner et al. 1997; Lindner, Firschke et al. 1998)..

It has been shown that during exogenously induced coronary hyperaemia the relative back-ground subtracted VI from different myocardial beds during a bolus intravenous injection of microbubbles reflects the relative MBF to these regions (Firschke, Lindner et al. 1997). It was postulated that the ability of VI to reflect relative MBF resulted from the closely coupled changes in MBF and MBV during hyperaemia (Firschke, Lindner et al. 1997). As described in the previous chapter, MBF can be quantified

quantified during a continuous intravenous infusion of microbubbles by measuring changes in mean myocardial microbubble velocity and microvascular CSA (or MBV) (Wei *et al.* 1998) . The purpose of this study was to determine the basis of stenosis detection using venous administration of microbubbles during MCE and the relative merits and drawbacks of continuous infusion versus bolus injections.

4.2 Objectives

The aim of this study was to determine the physiological basis of stenosis detection by myocardial contrast echocardiography using venous administration of microbubbles and to define the relative merits of bolus versus continuous infusion.

4.3 Methods

4.3.1 Animal Preparation

The study protocol was approved by the Animal Research Committee at the University of Virginia and conformed to the American Heart Association Guidelines for Use of Animals in Research.. A total of 18 dogs were used for the experiments. They were anaesthetised with 30 $mg \cdot kg^{-1}$sodium pentobarbital (Abbott) intubated, and ventilated with a respirator pump (model 607 Harvard Apparatus). Catheters (7F) were placed in both femoral arteries for the withdrawal of reference samples during radiolabeled microsphere injections and both femoral veins for administration of fluids, drugs, and microbubbles, respectively. The tip of a 7F pulmonary arterial balloon tipped flotation catheter (Model MPA-372T, Millar Instruments) was positioned in the main pulmonary artery for measurement of cardiac output.

A left lateral thoracotomy was performed and the heart was suspended in a pericardial cradle. A 7F catheter was placed in the left atrium for pressure measurements and the injection of radiolabeled microspheres. A similar catheter was placed in the ascending aorta for the measurement of aortic pressure. Ultrasonic time-of-flight flow probes (series SB, Transonics) were placed around the proximal portions of the LAD and LCx and were connected to a digital flow meter (model T206, Transonics). A 20 g teflon catheter (Critikon) was introduced into one of the arteries via a side branch and a custom-designed screw occluder was placed around the vessel in order to produce coronary stenoses of varying severity.

4.3.2 Haemodynamics:

All catheters were connected to fluid-filled pressure transducers which. like the flow meter were connected to a multichannel recorder (model ES 2000, Gould Electronics). CBF and pressures were acquired digitally at 200 Hz into a personal computer. The signals were displayed on-line using Labtech Notebook (Laboratory Technologies). The severity of the stenosis was judged by the mean pressure gradient between the aorta and the distal coronary artery. Coronary driving pressure was calculated by subtracting the mean right atrial pressure from the mean distal coronary pressure.

4.3.3 Myocardial Contrast Echocardiography

Imaging was performed in harmonic mode (transmit 2 MHz and receive 4 MHz) using a prototype Sonos 2500 system (Hewlett Packard) (Wei, Jayaweera et al. 1998). The ultrasound transducer was fixed in position with a custom-designed clamp and a saline bath served as an acoustic interface between the transducer and the heart. The maximal dynamic

range (60 dB) was used. The transmit power, focus, overall gain, and image depth were held constant for each experiment.

A second-generation microbubble *ImagentUS* (AFO 150, Alliance Pharmaceuticals) was used which consists of surfactant-coated microbubbles containing perfluorohexane and nitrogen. These microbubbles have a mean diameter of 5 μm and a mean concentration of $5 \cdot 10^8 \cdot mL^{-1}$. For the bolus injections, a single trigger was used to acquire one end-systolic image from each cardiac cycle . For continuous infusions, dual triggering was used. The first trigger was used for microbubble destruction and the second one to acquire images in end-systole . The interval between these triggers (PI) was increased from 150 ms to 12 s in order to allow progressively greater bubble replenishment of the ultrasound beam elevation (Wei, Jayaweera et al. 1998). Up to 8 end-systolic images were acquired at each PI.

MCE images were analysed off-line as previously described (Jayaweera *et al.* 1994). For the bolus injections, end-systolic images from just before contrast injection until its disappearance from the myocardium were aligned. For continuous infusions, 5 images acquired at baseline and at each PI were selected and aligned. Large transmural regions-of-interest were defined over the LAD and LCx beds in any one image and VI was automatically measured from the same regions in all images.

Average VI from 4-5 frames prior to the appearance of microbubbles in the myocardium was considered to represent background. For bolus injections, time-intensity plots were generated from the background-subtracted VI and fit to a gamma-variate function: $y = Ate^{-at}$, where A is a scaling factor, t is time, and a is proportional to the transit rate of the

tracer. Peak VI was calculated from the equation A/ae (Jayaweera, Sklenar et al. 1994). For continuous infusions, background-subtracted P1 versus VI plots were generated, which were fitted to an exponential function: $y=A(1-e^{-\beta t})$, where y is VI at a pulsing interval t, A is the plateau VI representing microvascular CSA (or MBV), and β is the rate constant reflecting the rate of rise of VI (or the mean microbubble velocity) (Wei, Firoozan et al. 1997). In addition to the above analyses, colour-coding was also performed in order to visually enhance the presence of perfusion mismatch (Jayaweera, Sklenar et al. 1994). Shades of red progressing to hues of orange, yellow and then white represent incremental myocardial opacification. The LV cavity was masked out.

4.3.4 Radiolabeled microsphere MBF measurement

MBF was measured using left atrial injections of approximately $2 \cdot 10^6$ 11μm radiolabeled microspheres (Dupont Medical Products) suspended in 4.0 mL 0.9% saline and 0.01% Tween-80 (Heymann *et al.* 1977) Arterial reference blood samples were collected using a constant rate withdrawal pump (model 944 Harvard Apparatus). At the end of the experiment, the short-axis slice of the left ventricle corresponding to the MCE image was cut into 16 wedge shaped pieces and each piece was further divided into epi-, mid-, and endocardial segments. The tissue and blood samples were counted in a well counter with a multichannel analyser (model 1282, LKB Wallac). Corrections were made for activity spilling from one energy window to another.

MBF to each epi-, mid- and endocardial segment was calculated from the equation $Qm = (Cm \cdot Qr)/Cr$ where Qm is blood flow to the myocardial segment ($mL \cdot min^{-1}$), Cm is tissue counts Qr is rate of arterial sample withdrawal ($mL \cdot min^{-1}$) and Cr is arterial reference sample counts.

Transmural MBF ($mL \cdot min^{-1} \cdot g^{-1}$) to each of the 16 wedge-shaped pieces was calculated as the quotient of the summed flows to the individual segments within that piece and their combined weight. MBF to each bed (defined by monastral blue dye injection, see below) was then calculated by averaging the transmural MBF in the central 50-75% of the pieces in each bed.

4.3.5 Experimental Protocol

In Group I dogs (n=l0), a baseline stage and up to 5 separate stenosis stages were performed. These stenoses were non-flow limiting at rest and their severity was judged by the pressure gradient across them. At each stage, haemodynamic data were acquired and MCE was performed at baseline by injecting 0.2-0.8 mL of AFOl5O (mean 0.5±0.2) into the femoral vein followed by a 5 mL 0.9% NaCl flush. The dose was determined at the beginning of each experiment and was adjusted to produce mild myocardial opacification with minimal posterior wall attenuation. It was then held constant for the duration of the study. MCE and injection of radiolabeled microspheres were performed only during hyperaemia prior to and after placement of each stenosis. Hyperaemia was induced by venous infusion of 0.4 $mg^{-1} \cdot kg^{-1} \cdot min^{-1}$ of WRC-0470 (Discovery Therapeutics), a selective adenosine A_{2a} receptor agonist .

In Group II dogs (n=8), haemodyanamic, radiolabeled microsphere, and MCE data were obtained prior to and after placement of 2 non-flow limiting stenoses of varying severity. All data were obtained at baseline and during hyperaemia. Microbubbles were administered at each stage both as an intravenous bolus and as a continuous infusion. For continuous infusions, a solution consisting of 4 mL of AFO15O in 50 mL of 0.9% saline was administered via the femoral vein at a rate of 2 $mL \cdot min^{-1}$

which allowed adequate myocardial opacification and no posterior wall attenuation.

At the end of the experiment, the artery undergoing the stenoses was occluded at the site of the screw occluder and monastral blue dye (Sigma Chemical) was injected into it via the distal catheter. This procedure allowed delineation of the LAD or LCx bed at the short-axis MCE imaging plane. The dog was then killed with an overdose of pentobarbital and the heart was removed from the chest cavity. It was cut into 5 short-axis slices and the slice corresponding to the MCE imaging plane was processed for the radiolabeled microsphere analysis.

4.3.6 Statistical Methods

Comparisons between more than two values were made using two-way repeated measures ANOVA and group interactions between levels of stenosis and presence or absence of hyperaemia were ascertained. When ANOVA showed significance ($p<0.05$. two-tailed) multiple comparisons between groups was performed using paired Student's t-test with Bonferroni correction. Linear regression analysis (least squares fit) was performed for deriving correlations.

4.4 Results

4.4.1 Group I dogs

Table 4.1A depicts data from the stenosed bed at baseline in the 10 Group I dogs. The severity of each stenosis was defined by the pressure gradient across it: 2±2 mm Hg (none), 10±3 mm Hg (mild), and 23±6 mm Hg (moderate). The epicardial CBF remained unchanged at different levels of stenosis, indicating that all stenoses were non-flow limiting at baseline. No differences were noted in the normalised background-subtracted peak

VI. Table 4.lB depicts data from the stenosed bed during hyperaemia in the Group I dogs. The mean trans-stenotic gradient increased, while the epicardial CBF and radiolabeled microsphere-derived MBF decreased with increasing levels of stenosis. These values were significantly different from baseline. The normalised peak VI was significantly lower with increasing levels of stenosis, and for moderate stenosis was significantly less compared to baseline.

Figure 4.1 illustrates colour-coded images and their corresponding time-intensity curves obtained prior to stenosis placement and in the presence of LAD stenoses of different severity during hyperaemia. In all images, some attenuation of the posterior wall is seen because of the presence of microbubbles in the LV cavity. Nonetheless, much of the LCx bed is visible in the lateral portion of the myocardium. Prior to stenosis placement, the degree of contrast enhancement (and therefore the colour) is similar in the two beds. After stenosis placement, the colour of the LAD bed takes on more hues of orange and red, denoting lesser degrees of contrast enhancement compared to the LCx, which still retains hues of yellow and white. A good correlation was found between the background subtracted peak VI and radiolabeled microsphere derived MBF ratios from the stenosed versus normal bed during hyperaemia when data from all 10 dogs were pooled (Figure 4.2).

4.4.2 Group II dogs

Table 4.2A depicts data from the stenosed bed at baseline in the 8 Group II dogs, where stenosis severity was classified in the same manner as in the Group I dogs. No changes were noted in epicardial CBF, radiolabeled microsphere-derived MBF, background-subtracted plateau VI *(A),* mean

microbubble velocity (β), or MCE-derived MBF ($A \bullet \beta$) with increasing levels of stenosis which, as stated earlier, were not flow-limiting at rest.

Table 4.2B depicts data from the stenosed bed during hyperaemia in the Group II dogs. The trans-stenotic gradient increased significantly with increasing degrees of stenosis during hyperaemia, while the mean epicardial CBF decreased. The values for no stenosis and mild stenosis were significantly different from baseline. Radiolabeled microsphere-derived MBF decreased progressively with increasing levels of stenosis, but was always higher compared to baseline. The value of A, β, and $A \bullet \beta$ also decreased with increasing levels of stenosis during hyperaemia, and the two latter values were significantly lower than at baseline. No significant interactions were noted between the level of stenosis and presence or absence of hyperaemia.

The top panels in Figure 4.3 illustrates colour-coded images and corresponding time-intensity curves from bolus injections during hyperaemia in the absence and presence of a LAD stenosis. It is evident that peak VI in the LAD bed decreases during hyperaemia in the presence of a stenosis. The top panels in Figure 4.4 illustrate data in the same dog during continuous infusions. Similar to Figure 4.3, the severity and extent of relative hypoperfusion in the stenosed bed during hyperaemia is clearly seen. There is however, no posterior wall attenuation. Similar to bolus injections (Figure 4.3), the VI during continuous infusion (Figure 4.4) is lower during stenosis. Furthermore, the mean microbubble velocity (β) and MCE-derived MBF ($A \bullet \beta$) are also less.

Figure 4.5A illustrates a linear relation between the $A \bullet \beta$ and radiolabeled microsphere derived MBF ratios from the stenosed versus the normal bed.

The relation is linear with a slope close to the line of identity. A linear relation was also noted between the peak and plateau VI ratios from the stenosed versus normal beds during bolus injections and continuous infusions, respectively (Figure 4.5B). Thus, similar information on MBV was afforded by both methods of microbubble administration.

The PI at which the greatest disparity in VI between the two beds is seen during continuous infusions can also be selected from the PI versus VI plots (Figure 4.6). Panels A to C in this figure depict three contrast-enhanced colour-coded images obtained at different PI during continuous infusion in a dog with a very mild stenosis. Panel D in the same image illustrates the PI at which these images were selected. Only in panel B is the VI disparity most clearly seen. This image can be selected from the sequence of images in order to optimize the display of both the severity of stenosis and the extent of relative hypoperfusion.

4.4.3 Haemodynamic Results

No effects were noted on left atrial, right atrial, and aortic pressures, or on cardiac output during repeated injections of AFOl5O in the Group I and II dogs (Table 4.3), who received a total dose of approximately 20 mL and 35 mL, respectively.

4.5 Discussion

4.5.1 Basis for Stenosis Detection During Venous Administration of Microbubbles

The entire coronary system (epicardial conduit arteries, arterioles, capillaries, venules, and veins) contains approximately 12 mL of blood 100 gm^{-1} of LV mass (total CBV), one-third of which is in the capillaries

(Kassab, Lin et al. 1994). The blood present in the LV myocardial vessels is the MBV and measures approximately 4.5 $mL \cdot 100g^{-1}$. When a mild to moderate stenosis (<85% luminal diameter narrowing) is present on an epicardial coronary artery, baseline MBF is maintained at normal levels by vasodilation of arterioles distal to the stenosis (Gould and Lipscombe 1974). The magnitude of this response is related to the severity of the stenosis. It follows therefore, that the measurement of CBV at rest can provide an estimate of stenosis severity. It has been previously shown that CBV increases with increasing levels of stenosis (Wu *et al.* ; Lindner, Skyba et al. 1997). These results were obtained from the measurement of mean transit rates after direct bolus injections of microbubbles into the coronary artery, which reflect changes in the entire CBV (Kaul *et al.* 1997).

In the present study, no change in myocardial VI at baseline was noticed despite the placement of mild to moderate stenoses, which indicates that in the presence of non-flow limiting stenoses at rest, MBV remains constant despite increases in total CBV. This phenomenon occurs because autoregulation does not principally involve the vessels within the myocardium, the majority of which (> 90%) are capillaries (Kassab, Lin et al. 1994). In comparison to the situation at rest, a decrease in MBV was noted for increasing levels of stenosis during hyperaemia.

Based on previous work using bolus injections of contrast, it had been postulated that MBV may actually decrease distal to the stenosis during hyperaemia (Ismail, Jayaweera et al. 1996; Firschke, Lindner et al. 1997-2). With bolus injections, however, it could not be determined whether the lower VI in the stenosed bed was due to an absolute decrease in MBV distal to the stenosis, or simply relative to a greater MBV increase in the

normal bed. In the present study, since the concentration of microbubbles in blood remained constant during continuous infusions. a decline in myocardial VI distal to a stenosis indicates an actual decline in MBV in the stenosed bed during hyperaemia. The mechanism for the decrease in MBV is not known, but indicates a reduction in capillary density distal to the stenosis in the presence of hyperaemia. This finding forms the basis for the detection and determination of the physiological relevance of a coronary stenosis with MCE, irrespective of the method of contrast injection.

4.5.2 Bolus or Continuous Infusion?

In order to produce myocardial opacification from a venous injection, initially large doses of microbubbles were used which resulted in severe attenuation of the posterior half of the heart . It was therefore necessary to wait for the microbubble concentration in the LV cavity to decrease before VI measurements in the LAD or LCx beds could be made (Firschke, Lindner *et al.* 1997-2; Lindner, Skyba *et al.* 1997). Consequently, measurements were not necessarily performed when maximal VI disparity was noted between the two beds. In this study, the doses for bolus injections were adjusted to levels where adequate myocardial opacification could be produced with minimal posterior wall attenuation. As can be appreciated from Figures 4.1 and 4.3, myocardial VI measurements could be made simultaneously from both beds during peak contrast effect, despite the presence of posterior wall attenuation.

The difference between bolus and continuous infusion is that in the former, the concentration of microbubbles in blood changes with time, while in the latter, it remains stable after equilibration is reached. In either case, the relative VI between two myocardial beds reflects the relative MBV

fractions of those beds (Firschke, Lindner *et al.* 1997-2), provided the microbubble concentration is low enough to be in the linear range of its relation with VI (Jayaweera *et al.* 1994). The obvious advantages of bolus injections are that they can be performed in a rapid manner and can provide an immediate qualitative assessment of stenosis severity during hyperaemia. However, continuous infusion is a better approach for stenosis detection for several reasons.

During continuous infusions. the dose of microbubbles can be customized to individual patients. There is great variability in the degree of tissue attenuation in different patients. and an individualized dose is more appropriate in order to provide meaningful results. Second. posterior wall attenuation can be largely abolished with continuous infusions by titrating the rate of infusion, something almost impossible to achieve consistently with a bolus injection. Shadowing of the posterior wall has so far precluded the use of parasternal views during bolus injections. These views are important for the comprehensive evaluation of patients with coronary artery disease. Third, a constant infusion provides time and leisure to interrogate each myocardial segment in detail, using even unorthodox views, without having to worry about missing a segment because of the limited duration of myocardial opacification afforded by a bolus injection. Fourth, the same person can start the infusion, adjust the rate of administration, and perform the entire examination. Another person is not required for repeated microbubble administration, as is needed with bolus injections. Finally, both microbubble velocity and MBV can be assessed with this approach. If myocardial VI can be calibrated to left ventricular VI, and if the beam elevation is known, then the product of microbubble velocity and MBV can provide a quantitative assessment of MBF (Wei, Firoozan et al. 1997-2).

4.6 Conclusion

The choice of bolus vs continuous administration of microbubbles for the assessment of myocardial microvascular blood flow depends entirely upon the question being asked. In the setting of total coronary occlusion where risk area size measurement is of interest, bolus administration of contrast may be more appropriate. In this situation the spatial resolution is very good. However, if measurements of flow velocity and videointensity ratios between beds are required, it is best to use the more robust continuous infusion method.

As echo systems develop, it is possible that this method of assessing myocardial microvascular blood supply will complement, or in some cases replace, nuclear methods.

Table 4.1

Hemodynamic, MBF and MCE data from the stenosed bed of Group I dogs

Variable	No Stenosis (n = 9)	Mild Stenosis (n = 15)	Moderate Stenosis (n = 13)	p-value
A. Baseline				
Mean Transtenotic Gradient (mmHg)	2 ± 2	10 ± 3	23 ± 6	< 0.001
Mean CBF ($mL \cdot min^{-1}$)	37 ± 14	35 ± 17	34 ± 16	0.59
Peak VI¶	1.3 ± 0.4	0.8 ± 0.3	0.9 ± 0.3	0.51
B. Hyperemia				
Mean Transtenotic Gradient (mmHg)	5 ± 4*	18 ± 7*	33 ± 10*	< 0.001
Mean CBF ($mL \cdot min^{-1}$)	97 ± 46*	57 ± 20*	51 ± 21*	0.002
Mean MBF ($mL \cdot min^{-1} \cdot g^{-1}$)†	1.9 ± 0.5	1.4 ± 0.5	1.3 ± 0.3	0.03
Peak VI¶	0.9 ± 0.2*	0.7 ± 0.3	0.6 ± 0.2*	0.001

¶ = Normalized to the non-stenosed bed
* $p < 0.001$ compared to baseline
† Data not obtained during baseline

Table 4.2

Hemodynamic, MBF and MCE data from the stenosed bed of 8 Group II dogs

Variable	No Stenosis	Mild Stenosis	Moderate Stenosis	p-value
A. Baseline				
Mean Transtenotic Gradient (mmHg)	2 ± 2	12 ± 3	21 ± 6	< 0.001
Mean CBF ($mL \bullet min^{-1}$)	39 ± 24	32 ± 21	31 ± 11	0.90
Mean MBF ($mL \bullet min^{-1} \bullet g^{-1}$)	1.1 ± 0.4	0.9 ± 0.3	1.0 ± 0.1	0.60
$A^{\P}$	1.1 ± 0.2	0.9 ± 0.3	0.9 ± 0.2	0.30
$\beta^{\P}$	1.1 ± 0.2	1.0 ± 0.2	0.9 ± 0.1	0.10
$A \bullet \beta^{\P}$	1.2 ± 0.4	1.0 ± 0.4	0.8 ± 0.2	0.10
B. Hyperemia				
Mean Transtenotic Gradient (mmHg)	3 ± 2	22 ± 6*	25 ± 6	< 0.001
Mean CBF ($mL \bullet min^{-1}$)	89 ± 48†	47 ± 27*	38 ± 13*	0.03
Mean MBF ($mL \bullet min^{-1} \bullet g^{-1}$)	2.7 ± 1.3†	1.4 ± 0.6†	1.5 ± 0.5†	0.03
$A^{\P}$	1.1 ± 0.2	0.9 ± 0.2	0.7 ± 0.3	0.005
$\beta^{\P}$	1.1 ± 0.3	0.5 ± 0.3†	0.6 ± 0.2†	0.001
$A \bullet \beta^{\P}$	1.2 ± 0.3	0.4 ± 0.2†	0.3 ± 0.1†	< 0.001

A = Plateau VI representing microvascular CSA (or MBV), β = rate constant reflecting rate of rise of VI, ¶ = normalized to non-stenotic bed, * p = 0.002 compared to baseline† p = 0.001 compared to baseline

Table 4.3

Hemodynamic effects of AFO150 in Group I (n=10), and Group II (n=8) dogs¶

	RAP (mmHg)	LAP (mmHg)	AoP (mmHg)	CO ($L(min^{-1})$)
A. Group I dogs				
Baseline	8 ± 6	12 ± 3	87 ± 12	3 ± 1
Injection 1	8 ± 4	15 ± 4	86 ± 9	3 ± 1
Injection 2	8 ± 5	15 ± 2	77 ± 7	3 ± 1
Injection 3	7 ± 3	15 ± 5	79 ± 10	4 ± 1
Injection 4	8 ± 2	16 ± 3	77 ± 8	3 ± 1
B. Group II dogs				
Baseline	7 ± 1	13 ± 3	102 ± 12	-
Infusion 1	7 ± 1	14 ± 3	96 ± 10	-
Infusion 2	7 ± 1	13 ± 2	90 ± 16	-

RAP = right atrial pressure, LAP = left atrial pressure, AoP = mean aortic pressure, CO = cardiac output, ¶ = no interstage differences noted

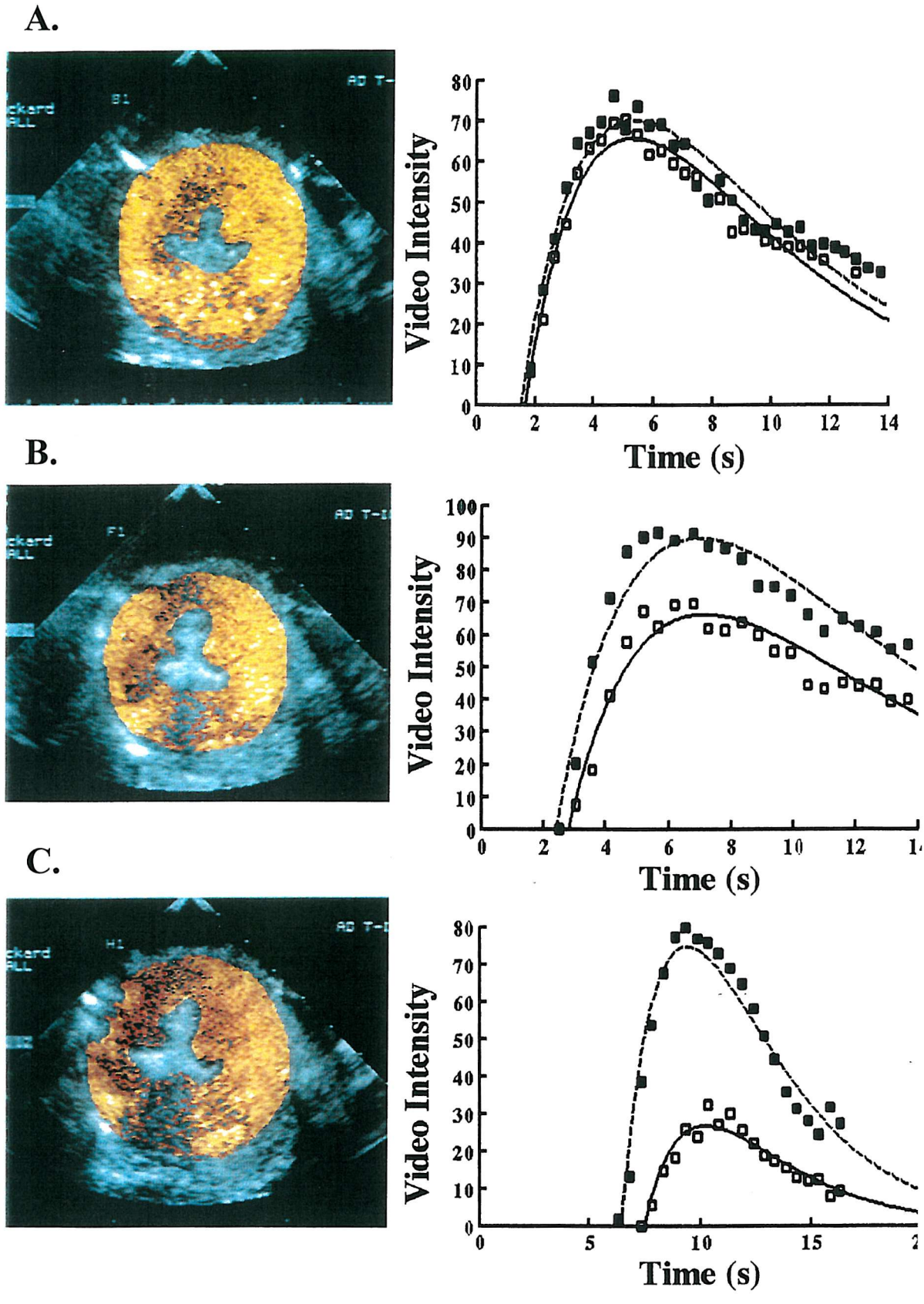
A.
B.
C.
Video Intensity
Time (s)
Video Intensity
Time (s)
Video Intensity
Time (s)

Figure 4.1

Figure 4.1

Colour-coded images and corresponding time-intensity curves (fitted to gamma-variate function) in one of the group I dogs during hyperaemia. At baseline (panel A), there is no difference in the VI between the LAD and LCx beds. In the presence of a mild LAD stenosis, VI in the LAD bed decreased compared to the LCx bed (panel B). The decrease was even greater (panel C) in the presence of a moderate stenosis. Open squares = LAD bed, closed squares = LCx bed. See text for details.

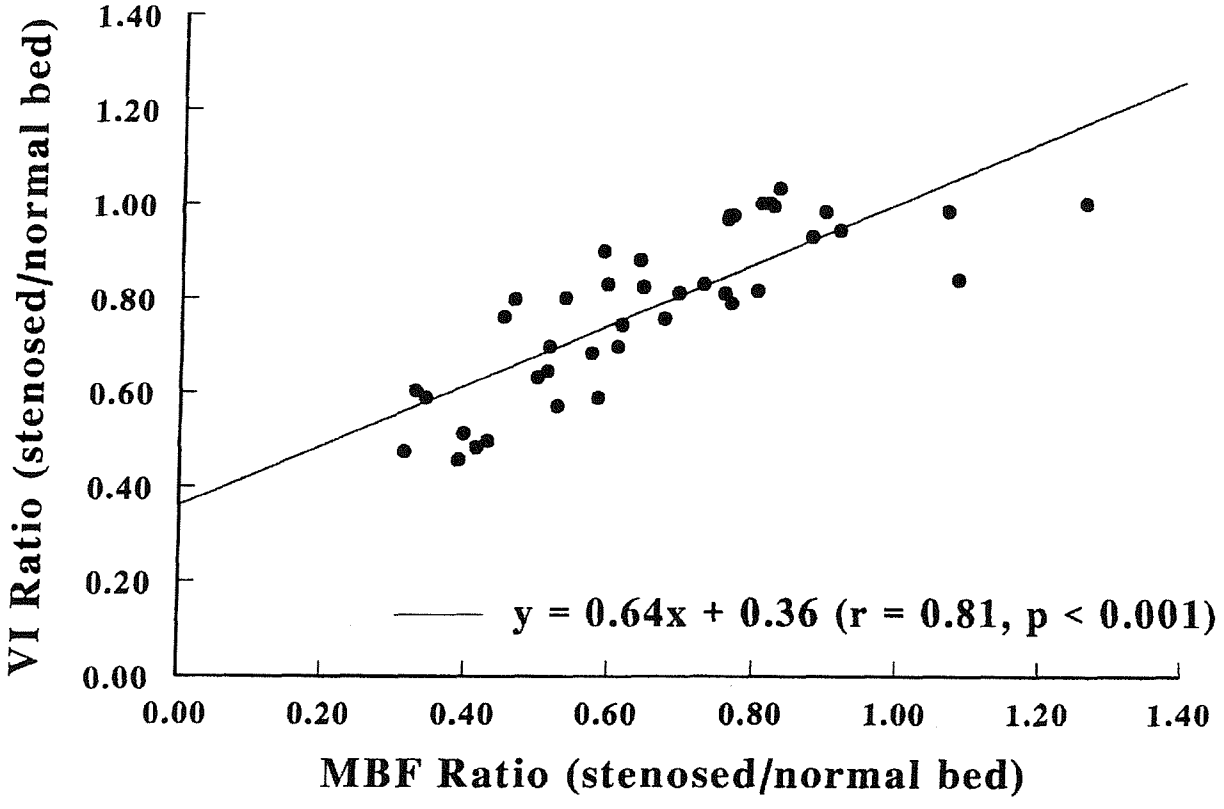
VI Ratio (stenosed/normal bed)
1.40
1.20
1.00
0.80
0.60
0.40
0.20
0.00
0.00
0.20
0.40
0.60
0.80
1.00
1.20
1.40
MBF Ratio (stenosed/normal bed)
y = 0.64x + 0.36 (r = 0.81, p < 0.001)

Figure 4.2

Figure 4.2

Relation between MBF ratio (x-axis) and VI ratio (y-axis) obtained from the stenosed versus the normal bed in Group I dogs during hyperaemia. See text for details.

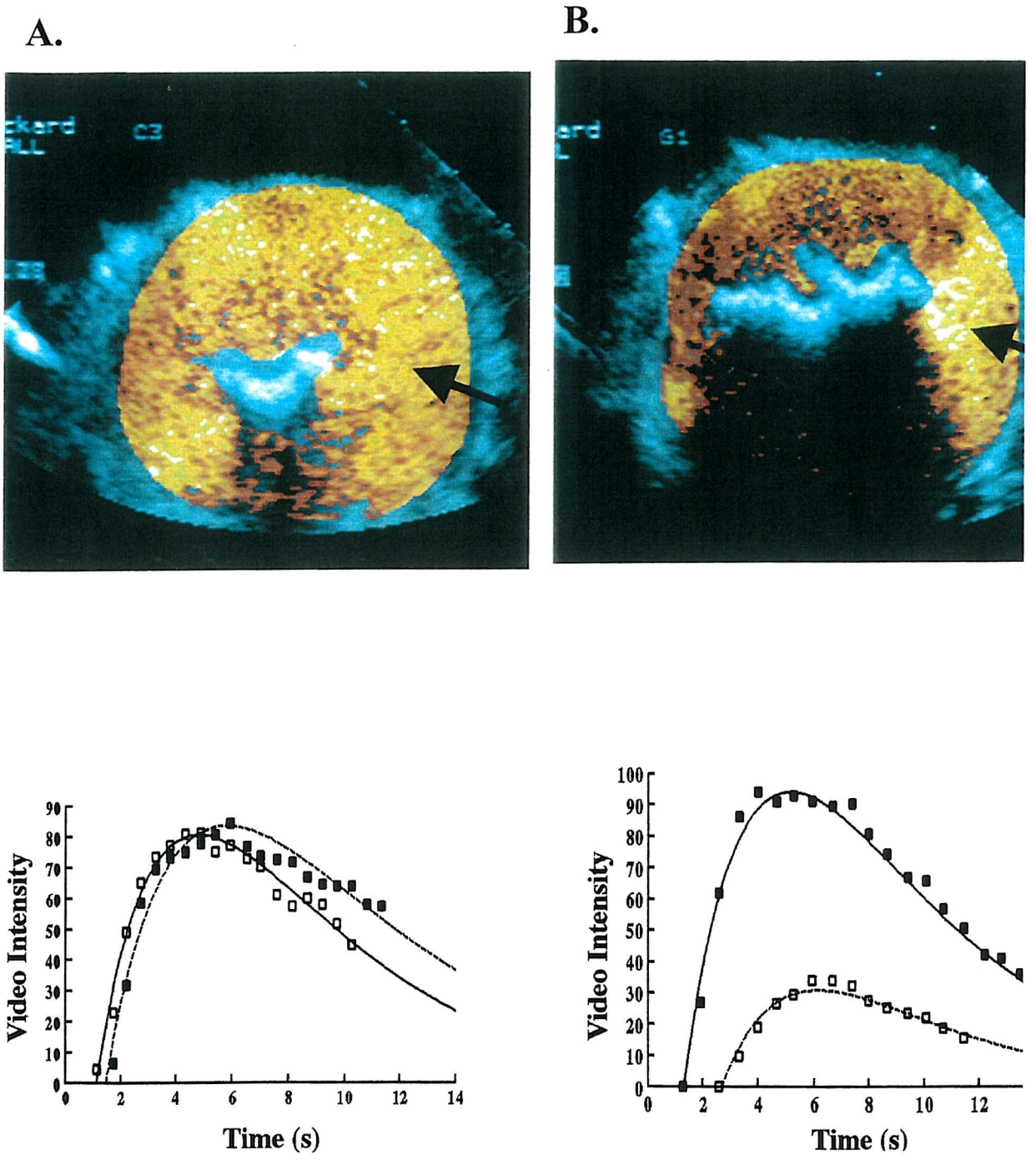

Figure 4.3

Figure 4.3

Colour-coded images and corresponding time-intensity plots (fitted to a gamma-variate function) from a Group II dog during hyperaemia. At baseline (panel **A**), there is no difference in the VI between the LAD and LCx beds. In the presence of a mild stenosis, VI in the LAD bed is less compared to the LCx bed (panel **B**). The arrows indicate the region in the LCx bed from which time-intensity data were generated. Open squares = LAD bed, closed squares = LCx bed. See text for details.

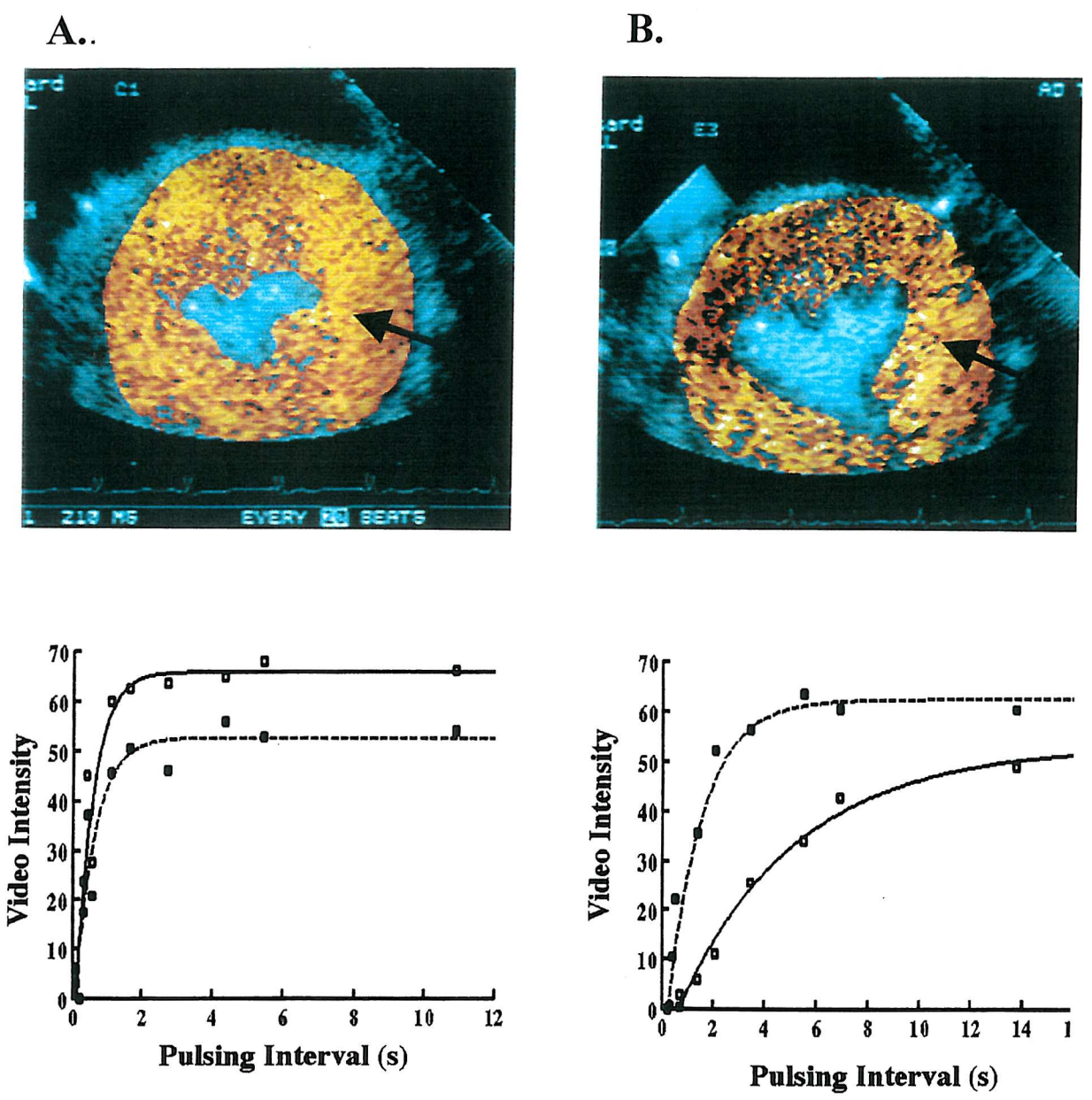
A..
B.
Video Intensity
Pulsing Interval (s)
Video Intensity
Pulsing Interval (s)

Figure 4.4

Figure 4.4

Colour-coded images and their corresponding VI vs PI curves at baseline (panel **A**) and in the presence of an LAD stenosis (panel **B**) during a continuous infusion of contrast in the Group II dog whose images during bolus injection are shown in Figure 4.3. The images correspond to the point in the curves where maximal contrast disparity between stenosed and normal beds were seen. The arrows indicate the region in the LCx bed from which time-intensity data were generated. Open squares = LAD bed, closed squares = LCx bed. See text for details.

A.

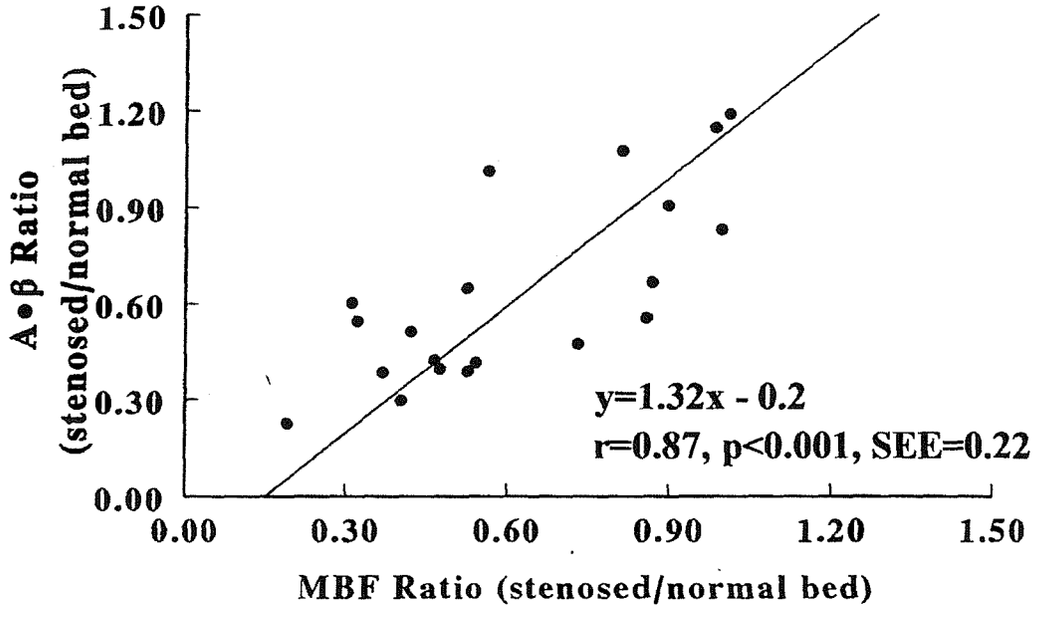
1.50
1.20
0.90
0.60
0.30
0.00
A•β Ratio
(stenosed/normal bed)
y=1.32x - 0.2
r=0.87, p<0.001, SEE=0.22
0.00
0.30
0.60
0.90
1.20
1.50
MBF Ratio (stenosed/normal bed)

B.

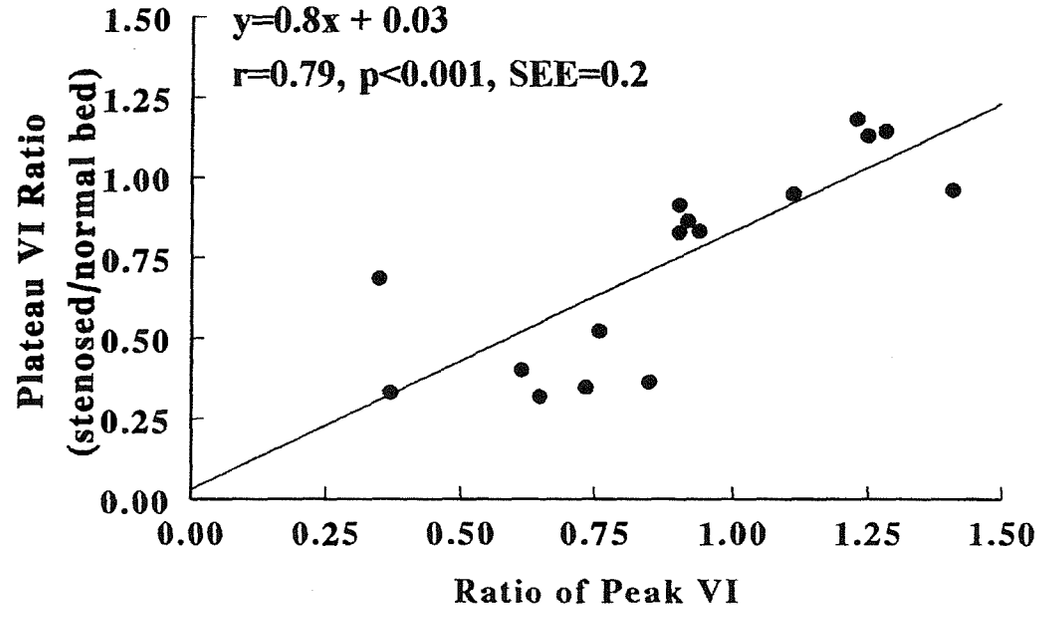
y=0.8x + 0.03
r=0.79, p<0.001, SEE=0.2
1.50
1.25
1.00
0.75
0.50
0.25
0.00
Plateau VI Ratio
(stenosed/normal bed)
0.00
0.25
0.50
0.75
1.00
1.25
1.50
Ratio of Peak VI

Figure 4.5

Figure 4.5

A) Relation between radiolabeled microsphere-derived MBF ratio (x-axis) and the $A \bullet \beta$ ratio from the stenosed versus normal bed in all group II dogs during hyperaemia (y-axis). **B**) Relation between peak VI ratio during bolus injection (x-axis) and plateau VI ratio during continuous infusion (y-axis) from the stenosed versus normal bed in all Group II dogs. See text for details.

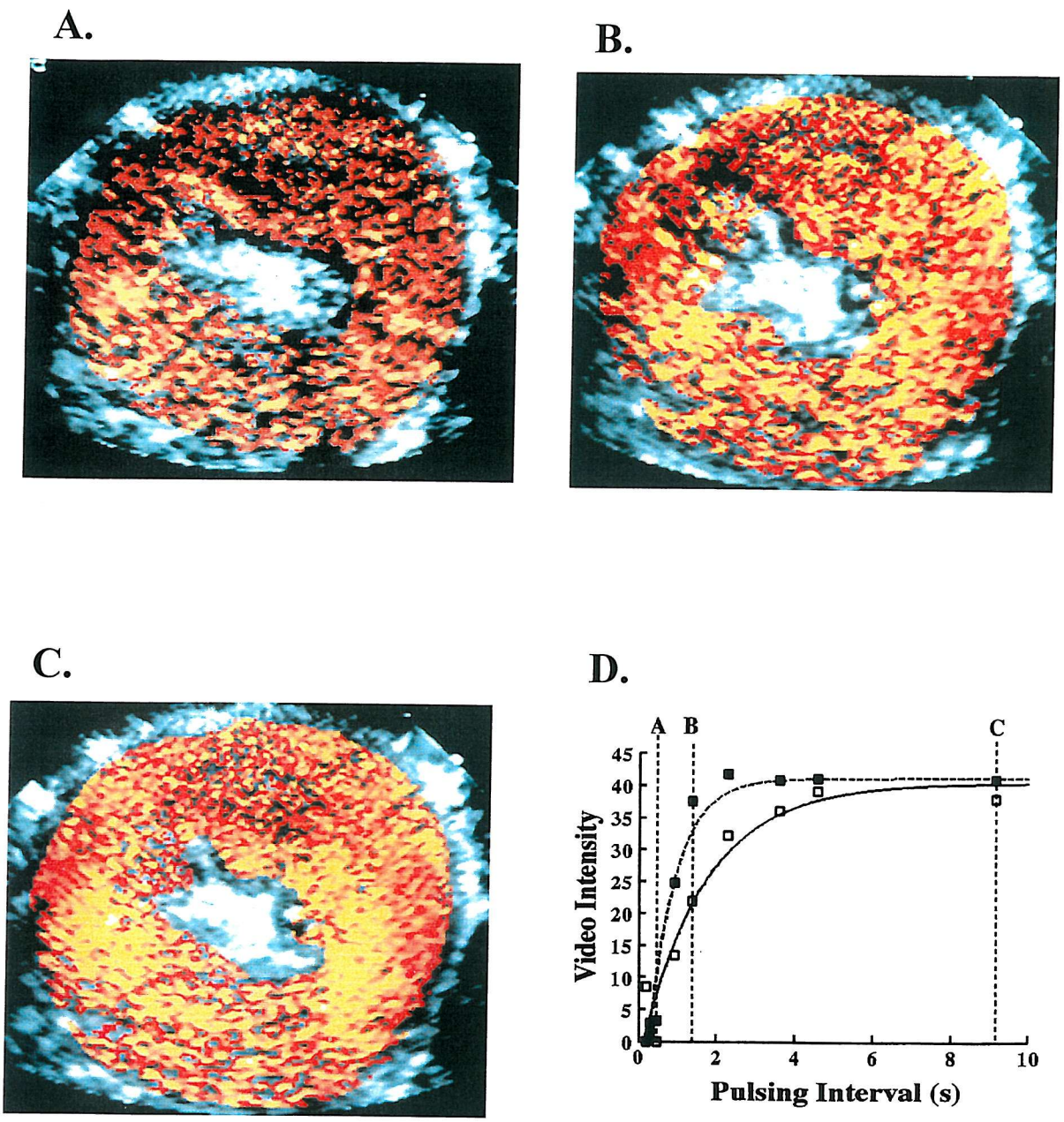
A.
B.
C.
D.
A
B
C
Video Intensity
Pulsing Interval (s)
0
5
10
15
20
25
30
35
40
45
0
2
4
6
8
10

Figure 4.6

Figure 4.6

Colour-coded images during a continuous infusion in a Group II dog (panels **A-C**) with a mild LAD stenosis at 3 different pulsing intervals (PI). The image showing the maximal VI disparity between the stenosed (LAD) and normal (LCx) beds (panel **B**) was selected from the VI vs PI curve in panel **D**. This image best represents the presence and the severity of stenosis. See text for details.

CHAPTER 5

QUANTIFICATION OF MYOCARDIAL BLOOD FLOW AND FUNCTION IN A CHRONIC MODEL OF PROGRESSIVE ISCHAEMIC LEFT VENTRICULAR DYSFUNCTION

5.1 Introduction

Of the patients in the Western Hemisphere with known congestive heart failure, anywhere from one-half to three-fourths have ischaemic cardiomyopathy(Gheorghiade *et al.* 1998). Many others with severe CAD but without overt congestive heart failure also have ischaemic cardiomyopathy (Passamani *et al.* 1985; Varnauskas 1988) .
If untreated, the prognosis of this condition is very poor (Passamani, Davis et al. 1985; Varnauskas 1988; DiCarli *et al.* 1995; Pagley *et al.* 1997; Gheorghiade and Bonow 1998). Coronary revascularization can improve symptoms and enhance longevity, if sufficient viable tissue is present (Varnauskas 1988; DiCarli, Asgarzadie et al. 1995; Pagley, Beller et al. 1997; Gheorghiade and Bonow 1998).

There is considerable debate and controversy regarding the pathophysiology of chronic LV dysfunction in patients with severe CAD not associated with myocardial infarction (Braunwald *et al.* 1986; Rahimtoola 1996; Vanoverschelde *et al.* 1997). Unlike post-ischaemic dysfunction seen in the setting of acute myocardial infarction and reperfusion, where the pathophysiology has been clearly defined in animal

models (Braunwald *et al.* 1982; Ross 1986), no animal model currently exists for evaluating the pathophysiology of chronic ischaemic LV dysfunction.

Whilst attempts have been made at developing animal models of chronic ischaemia, these have largely been limited to brief periods of a low-flow state (Schulz *et al.* 1993; Arai *et al.* 1995; Berman *et al.* 1996; Chen *et al.* 1996; Sherman *et al.* 1997) . The major limitations of such an approach are that the entire basis of chronic ischaemic LV dysfunction is presumed to be related to a persistent low-flow state, and that an acute experiment can resemble the state seen in patients with chronic ischaemic dysfunction who have reduction in resting MBF.

Chronic animal models developed so far have been limited to stenosis involving only a single artery (Bolukoglu *et al.* 1992; Mills *et al.* 1994; Shen and Vatner 1995; Fallavolita *et al.* 1997). A major limitation of this approach is that the model does not resemble the coronary anatomy of most patients with chronic ischaemic LV dysfunction who have multivessel CAD. Additionally, in the canine model of single vessel stenosis, the decrease in regional LV function is transient, and reverses upon development of collaterals to the stenosed bed (Shen and Vatner 1995).

Given these limitations, we sought to develop a model of chronic ischaemic LV dysfunction that more closely mimics the condition seen in humans. In this chapter the time course of deterioration of global LV systolic function and the histopathology of this model will be described. The main emphasis, however, is the characterization of regional flow-function relations, which provide unique mechanistic insights into the

pathophysiology of ischaemic dysfunction in the setting of multivessel coronary stenosis.

5.2 Objectives

The study of the pathophysiology of ischaemic myocardium has been made more difficult because of the lack of a suitable animal model of this condition. The main objectives of this study were the development of an animal model of multivessel coronary artery disease and the description of myocardial blood flow/function relations in it.

5.3 Methods

5.3.1 Animal Preparation

The study was approved by the Animal Research Committee at the University of Virginia and conformed to the American Heart Association Guidelines for the Use of Animals in Research. Twenty-two large adult dogs (weight = 30-35 kg) were instrumented to create chronic ischaemic cardiomyopathy by placing ameroid constrictors over proximal portions of the LAD and LCx arteries and their major branches (Litvak *et al.* 1957). They were pre-treated with 75 mg of aspirin daily for 3 days prior to surgery and were maintained on this dose until euthanasia.

Surgery was performed in a fully-equipped operating suite under sterile conditions. Anaesthesia was induced with 20 $\mu g \cdot kg^{-1}$ of fentanyl (Abbott Laboratories, Chicago, Illinois), 400 $\mu g \cdot kg^{-1}$ of etomidate (Bedford Laboratories, Bedford, Ohio), and 300 $\mu g \cdot kg^{-1}$ (Elkins-Sinn Inc., Cherry Hill, NJ) of diazepam administered intravenously. One gram of cefazolin sodium (Apothecon Corp., Princeton, NJ) was administered intravenously

prior to surgery and continued twice daily for 5 days after surgery. An injection of 80 mg of gentamycin (Fujisawa Corp., Deerfield, IL) was also administered intravenously prior to surgery.

The animal was intubated and anaesthesia was maintained with a mixture of 1-1.5% isofluorane, oxygen, and air given through a respirator (Model 607, Harvard Apparatus, South Natick, MA). The minute volume was set between 5.5 and 6.5 $L \cdot min^{-1}$ to maintain a physiologic P_{CO_2}. Heart rate and electrocardiogram were monitored throughout the operation. A small incision was made in the right groin and a 6F indwelling catheter (Cook Instruments, Bloomington, IN) was inserted into the femoral artery and secured in place with silk ties. The catheter was flushed with a dilute solution of heparin (Sololak Laboratories, Elk Grove Village, IL) and capped off with a rubber injection port. It was then tunnelled beneath the skin in the groin area to allow subsequent transcutaneous access for arterial pressure monitoring, as well as withdrawal of samples for blood gas and radiolabeled microsphere-derived MBF analysis. The groin incision was then closed in layers.

After skin preparation and draping, 300 $\mu g \cdot kg^{-1}$ of atracurium was administered to induce muscle paralysis (Burroughs Wellcome Co., Research Triangle Park, NC). A left lateral thoracotomy was performed in the fourth intercostal space. The heart was suspended in a pericardial cradle and proximal sections of the LAD and LCx were dissected free of surrounding tissues. Any large proximal branches of these arteries were similarly dissected. Up to 4 appropriately sized (1-3.5 mm) ameroid constrictors (Medical Research & Manufacturing, Corvallis, OR) were placed around these arteries. LV function was assessed by 2DE after placement of each ameroid constrictor to ensure that there had been no

deterioration in regional function. Direct epicardial imaging was performed with the transducer placed in a sterile plastic sleeve.

A 6F indwelling catheter was inserted in the left atrium and secured in placed with prolene sutures. After flushing with a dilute heparin solution, its end was capped off with a rubber injection port. The catheter was then tunnelled beneath the abdominal skin to allow subsequent transcutaneous injection of radiolabeled microspheres. The chest was then closed in layers, and the animal was revived and transferred to an observation area in the vivarium. The animals were examined twice a day and treated for heart failure or infection, if required.

5.3.2 Two-dimensional Echocardiography

2DE was performed with a phased-array digital system (HDI 3000, Advanced Technology Laboratories, Bothell, WA) using a 2.3 MHz probe. Apart from the intraoperative 2DE described above, all subsequent examinations were performed with the dog lying on its left side with imaging from the right thorax. At least 3 short-axis views were obtained at each examination, with care taken to obtain the same views every time in an individual dog. The images were recorded on 1.25 cm super-VHS tape using a high-fidelity recorder (Panasonic AG-7350, Matsushita Electrical Co. Secaucus, NJ).

For each animal, the short-axis view displaying the maximal degree of global or regional LV dysfunction at any time during follow-up was identified. All measurements were then made from this single view. An entire systolic contraction sequence (from end-diastole to end-systole) was selected from each examination and the images were transferred to a custom-designed off-line image analysis system. End-diastolic and end-systolic areas were measured (Kaul *et al.* 1991) from these images and

regional percentage wall thickening (%WT) (Sklenar *et al.* 1992), and end systolic wall stress (ESWS) were calculated (Hood *et al.* 1968).

The method for measuring regional %WT has been previously described (Sklenar, Jayaweera et al. 1992). A number of both epicardial and endocardial targets are defined by the observer in each frame from end-diastole to end-systole. In order to correct for cardiac systolic rotation, the junction of the posterior LV free wall and the right ventricular free wall is defined over the epicardium in each frame. These points are then automatically connected using cubic-spline interpolation to derive the epicardial and endocardial contours . The computer then generates 100 equidistant chords between the two contours starting at the junction of the posterior LV free wall and the right ventricular free wall. Each chord represents the shortest distance between the epicardial and endocardial contours. The observer then identifies the regions of the myocardium where the chord lengths are averaged in each frame (Figure 5.1). Regions in both the LAD and LCx territories with no evidence of infarction on post-mortem tissue staining were identified. Plots of %WT over the entire systolic contraction sequence in these regions were then generated. In order to normalize for inter-stage differences in heart rate, each sequence was divided into deciles. Information was, therefore, available not only for end-systolic %WT, but also for the rate of %WT over systole. All sequences were analyzed by two blinded observers. ESWS (10^3dynes $\bullet$ cm^{-2}) was calculated for both the LAD and LCx regions using the equation $(p \bullet r)/(2 \bullet t)$ where p (mmHg) is aortic systolic pressure, and r and t are LV radius and myocardial wall thickness (cm), respectively at end-systole (Hood, Rackley et al. 1968).

5.3.3 Haemodynamic data

For pressure measurements, tubing primed with normal saline was connected at one end to a pressure transducer (model 1295A, Hewlett Packard) and at the other end transcutaneously to the arterial catheter. This transducer and the electrocardiographic port were connected to a multichannel recorder (model 4568C, Hewlett-Packard), which in turn was connected to a 80386-based personal computer via an 8-channel analogue-to-digital converter (Metrabyte Corp., Taunton, MA). The signals were displayed on-line using Labtech Notebook (Laboratory Technologies Corp., Wilmington, MA) and were digitally acquired at 200 Hz for future analysis.

5.3.4 Myocardial Blood Flow:

Up to 6 radiolabeled microspheres were used in each animal to determine regional MBF (Heymann, Payne et al. 1977). Approximately $2 \cdot 10^6$ 11μm radiolabeled microspheres (Dupont Medical Products, Wilmington, DE) were suspended in 4 mL of normal saline-0.01% tween 80 solution and injected into the left atrium at each stage. Reference samples were withdrawn from the femoral artery over 130s with a constant rate withdrawal pump (Harvard Apparatus, Model 944, South Natick, MA). Three of the post-mortem heart slices corresponding to the 2DE short-axis images were cut into 16 wedge-shaped pieces. Each piece was further divided into epicardial, mid-myocardial and endocardial portions. The tissue and arterial reference samples were counted in a well counter with a multichannel analyzer (Model 1282, LKB Wallac, Washington DC). Corrections were made for activity spill-over from one window to the next. MBF to each sample was calculated by the equation $Q=(C_m \cdot Q_r)/C_r$ where Q=flow ($mL \cdot min^{-1}$), C_m = tissue counts, Q_r = rate of arterial blood withdrawal ($mL \cdot min^{-1}$) and C_r = counts in the reference sample.

Transmural MBF ($mL \cdot min^{-1} \cdot g^{-1}$) to each segment was derived by dividing the sum of MBF to individual segments by their combined weight. Mean transmural MBF in each bed was calculated by averaging the transmural MBF in the segments within that bed. Average endocardial and epicardial MBF were similarly calculated.

5.3.5 Histopathology

The two heart slices that were not used for radiolabeled microsphere MBF analysis were processed for histopathology. They were immersed in a solution of 1.3% 2,3,5 triphenyl tetrazolium chloride (Sigma Corp., St Louis, MO) and 0.2M Sorensen's buffer (KH_2PO_4 and K_2HPO_4 in distilled water, pH 7.4) at 37°C for 20 min. Using this method areas of viable myocardium stain brick red whereas infarcted areas do not take up the stain. The presence or absence of gross infarction was assessed in this manner.

Samples from each wall of the heart (anterior, lateral, posterior and septal) showing no infarction on tissue staining were taken for histologic analysis after fixation of the slices in 10% formalin solution. These samples were placed in cassettes and dehydrated in serial exchanges of ethyl alcohol (from 70% to absolute ethyl alcohol) over 8 hours. The tissue was cleared in xylene solution for 2 hr and placed in molten paraffin maintained at 60°C in a water bath for an additional 2 hr. The paraffin-impregnated tissue was transferred to vinyl base moulds and left overnight to harden. They were thin-sectioned and stained with haematoxylin-eosin for interpretation by a cardiac pathologist for evidence of ischaemic insult.

5.3.6 Study Protocol

After a minimum period of 48 hr for recovery after surgery, the dogs were lightly sedated with fentanyl (20μg kg^{-1}) and etomidate (300 mg kg^{-1}). They were placed on their left side on the examination table and paralysed with 10 mg of atracurium, intubated, and ventilated on room air using a respirator pump (Model 607, Harvard Apparatus, South Natick, MA). After recording baseline LV function on 2DE, the first radiolabeled microsphere was administered. This procedure was repeated in all dogs just before killing the animals, the timing of which was judged by the development of severe of global LV dysfunction on 2DE, which was performed twice a week. In 6 dogs, both 2DE and radiolabeled microsphere administration was repeated at various intervals throughout the study as LV function progressively deteriorated. At the end of the study, the dogs were euthanised with an overdose of pentobarbital and KCl. Post-mortem coronary angiography was performed in half of them to determine the status of the coronary arteries at the site of ameroid constrictor placement. The heart was then sliced at 5 short-axis levels and prepared for MBF analysis and histopathology .

5.3.7 Statistical methods

Unless otherwise stated, data are expressed as mean ± SE. Inter-stage comparisons were made using ANOVA. When significance was found by ANOVA, individual comparisons between two stages were performed-using student's t test with Bonferroni correction. Differences between stages were considered significant at $p<0.05$ (two-sided).

5.4 Results

Of the 22 dogs, 10 died suddenly before a complete follow-up examination (both 2DE and radiolabeled microsphere injection) could be performed. No evidence of infarction was seen in these animals on post-mortem tissue staining. In the surviving 12 dogs, %WT, MBF analysis, and histopathology were performed in both LAD and LCx beds. Infarction was detected by post-mortem tissue staining in 4 dogs, but never involved the entire bed distal to the ameroid constrictor. Only the area within each bed not showing necrosis was analyzed. Nine dogs had evidence of heart failure: 5 required long-term, and an additional 4 needed incidental drug treatment with frusemide and/or digoxin.

No dog was euthanised before the development of global LV dysfunction. Both LAD and LCx beds showed significant regional dysfunction in all but one dog which had dysfunction only in the LCx bed. In the 6 dogs undergoing post-mortem coronary angiography, sub-total or total occlusion of the coronary artery was seen at the sites of ameroid constrictor placement. Extensive epicardial collateral arteries were seen connecting the portion of the LAD proximal to the ameroid constrictor to branches of the LAD distal to the constrictor. LAD to LCx collateral connections were not seen as often.

5.4.1 Global Function:

There were no changes in mean aortic blood pressure and heart rate over the course of the study (Table 5.1). The time-variance data are grouped according to the mean time at which observations were made post-operatively. The number of observations made at each mean time point are shown in Table 5.1.

Figure 5.2 illustrates end-diastolic and end-systolic images at baseline (A and B) and on postoperative day 65 (panels C and D) from one dog in the study. LV end-diastolic and end-systolic areas are greater and LV wall is thinner on post-operative day 65 compared to baseline. Change in LV area and wall thickness from end-diastole to end-systole are also significantly reduced at post-operative day 65 compared to baseline.

Figure 5.3 depicts changes in LV end-diastolic and end-systolic short-axis areas (Figure 5.3A) and the percent change in area from end-diastole to end-systole (Figure 5.3B) over the observation period in all 12 dogs. Both end-diastolic and end-systolic areas progressively enlarged, with the end-systolic area almost doubling by the time the dogs were euthanised. Likewise, the percent change in LV area from end-diastole to end-systole (a measure of global LV systolic function) also decreased over time, becoming half of that at baseline.

5.4.2 Regional function:

Figure 5.4 illustrates %WT over the course of an entire systolic contraction sequence when data from both the LAD and LCx beds in all 12 dogs were combined. The upper curve depicts data at baseline where virtually equal increments in %WT were noted in all deciles from end-diastole to end-systole. In contrast, as depicted in the lower curve, just before the dogs were euthanised, not only was the final degree of %WT reduced, but the pattern of thickening was also abnormal. There was almost no thickening in the first 3 deciles, followed by a slow rate of thickening in latter part of systole (tardokinesia).

Figures 5.5A and 5.6A illustrate the changes in %WT and ESWS in the LAD and LCX beds, respectively. In the LAD bed (Fig 5A), final %WT deteriorated to one-third of that at baseline, while ESWS more than doubled. The decrease in %WT and increase in ESWS were greater in the LCx (Fig 6A) compared to the LAD bed ($P<0.03$ for both).

5.4.3 Myocardial Blood Flow:

Figures 5.5B and 5.6B illustrate changes in MBF over time in the LAD and LCx beds, respectively. Although there is a small initial drop in transmural MBF in the LAD bed at day 5, followed by a return to baseline by day 13, this change is not statistically significant. In comparison, transmural MBF did not change in the LCx bed until day 13. A significant ($P<0.01$) decrease in transmural MBF was noted in both beds between days 13 and 21. While transmural MBF in the LCx bed declined further at day 42, that in the LAD returned to just below baseline levels. MBF was, therefore, significantly different ($P<0.01$) between the two beds at the time the dogs were euthanised.

Even when transmural MBF was normal, the endocardial/epicardial MBF ratio reversed by day 5 in both beds. Endocardial MBF was disproportionately reduced compared to epicardial MBF by day 28 ($P<0.01$). Data from Figures 5.5 and 5.6 indicate that a decrease in %WT preceded a decrease in transmural MBF in the LCx bed. In the LAD bed, however, a decrease in %WT was not associated with a decrease in transmural MBF except on day 21.

5.4.4 Flow-function relations

To establish the relation between MBF and %WT, the 24 myocardial segments in the 12 dogs were divided into 2 groups - one in which transmural MBF was reduced at day 42 (n=11), and the other in which it

was not reduced (n=13). The former involved the LCx bed in 8 dogs and the LAD bed in 3, while the latter involved the LCx bed in 4 dogs and the LAD bed in 9. The relation between %WT and transmural, endocardial and epicardial MBF were examined in both groups.

In regions that showed an ultimate reduction in transmural MBF, a mildly curvilinear relation was noted between %WT and MBF (Figure 5.7 A-C) at all myocardial depths, with %WT progressively decreasing with decrease in MBF below normal. There were no significant differences between the slopes and intercepts of the relations between %WT and MBF at any myocardial depth , although endocardial MBF was consistently lower than epicardial MBF when %WT was moderately (10-20%) or severely (<10%) reduced (0.68±0.46 vs 0.90±0.42 $ml \cdot min^{-1} \cdot g^{-1}$.and 0.56±0.40 vs 0.76±0.38 $ml \cdot min^{-1} \cdot g^{-1}$.,respectively).

In regions that did not show an ultimate reduction in MBF, there was no relation between %WT and transmural, endocardial, or epicardial MBF (Figure 5.8 A-C). There were no significant differences between the slopes and intercepts of the relations between %WT and MBF at any myocardial depth. Except in the setting of moderate reduction in %WT, endocardial MBF was not significantly lower than epicardial MBF in the presence of reduced %WT.

5.4.5 Histopathology:

Histopathology was performed in 11 of the 12 dogs. Regions showing no infarction on post-mortem tissue straining from both the LAD and LCx beds distal to the placement of the ameroid constrictors were examined. The majority of the regions (14 of 22) showed no evidence of acute or chronic ischaemic insult or fibrosis. Of the 8 regions showing abnormalities, small, focal areas of coagulative necrosis and fibrosis were seen in 6. More extensive subendocardial necrosis with granulation tissue

was seen in only 2 areas, both of which were located in segments which showed ultimate reduction in transmural MBF, but did not involve more than 5-10% of the myocardial thickness .

5.5 Discussion

This is the first description of a large animal model of chronic ischaemic LV dysfunction which mimics the condition in humans. The general characteristics of the model are progressive LV dilatation and decrease in global and regional LV systolic function associated in most cases with transient or persistent congestive heart failure. While most myocardial regions do not show histopathologic changes under light microscopy, about one-third show focal areas of chronic ischaemic damage and fibrosis. The decrease in regional LV systolic function may or may not be associated with reduction in MBF. These findings have important pathophysiological and clinical implications.

5.5.1 Flow-function relations

The new information from this study is that in the presence of multivessel disease, different myocardial beds behave differently, which may be related to the extent of collateral MBF. The ameroid constrictor was placed distal to the first septal perforator on the LAD, since in dogs this artery frequently comes off directly from the left main artery or from a very proximal and inaccessible portion of the LAD. The region supplied by the LAD that was susceptible to ischaemia was therefore usually smaller than that supplied by the LCx. Following a transient decrease in transmural MBF, the LAD bed showed normal transmural MBF during most of the observation period. This pattern of change in MBF probably represents development of collaterals to the LAD bed, which was

confirmed on post-mortem angiography. Extensive collateral development has previously been documented in a chronic model of single vessel stenosis. Despite normal resting MBF, however, function in the LAD bed was markedly reduced by the third week after ameroid constrictor placement, when stenosis severity had likely become critical. The magnitude of reduction in function in the LAD bed was similar to that in the LCx bed where MBF was actually decreased.

In contrast to the LAD bed, on average, both transmural MBFand %WT progressively decreased in the LCx bed. All segments that exhibited an ultimate reduction in transmural MBF always showed reduction %WT before a decline in transmural MBF. In these segments a relation was noted between %WT and transmural, endocardial, and epicardial MBF in that decreases in regional function were associated with proportionate decreases in MBF at all myocardial depths with endocardial MBF being lower than epicardial MBF.

There is debate as to whether regional dysfunction in chronic ischaemic heart disease is associated with normal or reduced MBF (Braunwald and Rutherford 1986; Rahimtoola 1996; Vanoverschelde, Wijns et al. 1997). It has been argued that despite normal resting MBF, a critical stenosis can result in repeated episodes of ischaemia during periods of increased myocardial oxygen demand (walking, etc.), so that the myocardium is in a perpetual state of post-ischaemic dysfunction ('stunning') (Vanoverschelde *et al.* 1993; Shen and Vatner 1995; Gerber *et al.* 1996; Marinho *et al.* 1996; Vanoverschelde, Wijns et al. 1997). On the other hand it has also been shown that MBF is actually reduced in chronic ischaemic dysfunction. In either case, recovery in function would be expected from

revascularization in the absence of significant scarring or muscle damage (DiCarli, Asgarzadie et al. 1995; Pagley, Beller et al. 1997).
The proponents of perpetual stunning have based their argument on animal and human studies of single vessel occlusion with or without infarction where MBF is normal or only mildly reduced because of increased collateral flow (Sabia *et al.* 1992; Vanoverschelde, Wijns et al. 1993; Shen and Vatner 1995; Gerber *et al.* 1996; Marinho, Keogh et al. 1996; Vanoverschelde, Wijns et al. 1997). The results from the LAD bed in this study support the presence of perpetual stunning in at least some myocardial beds, which seem to have increased collateral flow that develops over time. These findings also support an earlier postulate that stunning may also be seen before MBF is eventually reduced, as evidenced from the LCx bed in these dogs (Kaul 1995-1). Segments that demonstrated ultimate reduction in resting transmural MBF, demonstrated severe regional dysfunction even when MBF was normal.

These results also support an earlier postulate (Kaul 1995-2) that in the natural course of coronary stenosis development, regional dysfunction will be first seen when the stenosis is severe enough to limit increase in MBF (>50% luminal diameter stenosis). This dysfunction will initially be transient and will occur only at high levels of stress (such as during stress 2DE) (Homans *et al.* 1986; Kloner *et al.* 1991). As the stenosis severity increases, regional dysfunction will be seen at lower levels of stress. Perpetual dysfunction will be seen with normal resting MBF when the stenosis is critical and ischaemia occurs with minimal effort. This same phenomenon can also be seen when the artery is totally occluded but resting MBF is maintained through collaterals (Sabia, Powers et al. 1992; Vanoverschelde, Wijns et al. 1993; Shen and Vatner 1995; Gerber,

Pages 144-145
missing from
this Thesis

normal and the LV dysfunction could be related to repeated episodes of post-ischaemic dysfunction (stunning). Based on results of PET studies, there is a tendency now to label all patients with chronic ischaemic LV dysfunction as having normal MBF (Vanoverschelde, Wijns *et al.* 1997). It has been suggested that the perfusion defects seen using flow tracers are due to the partial volume effect. The findings of this study disagree with this stance and the results support the notion that MBF is reduced in many segments showing decreased %WT in the setting of chronic ischaemic LV dysfunction.

Although the partial volume effect can lead to underestimation of perfusion as stated previously, particularly in a non-contracting compared to a contracting segment, the underestimation should be no more than 30%. In most instances, the presence of viability is not an an issue when the magnitude of a defect is only 30% (Ragosta *et al.* 1993). The results from the recent PET studies showing normal MBF in dysfunctional segments (Vanoverschelde, Wijns *et al.* 1993; Gerber, Vanoverschelde *et al.* 1996; Marinho, Keogh *et al.* 1996)could be related to patient selection, such as the inclusion of those with single-vessel disease and uncompromised collaterals and those with small infarctions. These results show that segments that ultimately show reduction in MBF will first show severe dysfunction in the presence of normal MBF. The timing of the study may also, therefore, influence the results.

Another technique often used to assess myocardial viability is dobutamine 2DE (Cigarroa *et al.* 1993; LaCanna *et al.* 1994; Senior *et al.* 1995; Kaul 1996; Sklenar *et al.* 1996). It is apparent from these results that this technique should be able to identify viability in segments with normal resting MBF. The stunned myocardium will respond to small to moderate doses of dobutamine before becoming ischaemic at higher doses where

the stenosis becomes flow-limiting (biphasic response) (Senior, Glenville et al. 1995; Kaul 1996; Sklenar, Camarano et al. 1996). In segments with reduced MBF, %WT would not be expected to increase with dobutamine if only the flow-function relation was taken into consideration.

Previous work has led to the postulate that because of down-regulation of function during hibernation, the flow-function relation would be shifted to the right, which would allow some contractile reserve to exist (Kaul 1995). The present study shows a rightward shift of the relation in the range of MBF from 0.4 to 1.2 $ml \cdot min^{-1} \cdot g^{-1}$. In this range of MBF, dobutamine would be expected to increase %WT to the level represented in the solid line in Figure 5.9. The dose of dobutamine to achieve this effect before worsening of %WT occurs would have to be very finely titrated. The increase in %WT would also not require an increase in MBF if no other changes occur that can also affect myocardial bioenergetics. These data also imply, however, that %WT is unlikely to increase with any dose of dobutamine when MBF <0.4 $mL\ mL \cdot min^{-1} \cdot g^{-1}$ even though viable tissue is present.

There are two other potential mechanisms that could also cause an increase in %WT despite reduced resting MBF. The first is the peripheral vasodilator effect of dobutamine which causes reduction in LV size and may reduce ESWS (Meyer *et al.* 1976). The reduction in ESWS may allow an increase in %WT for the same MBF. A transient improvement in %WT has been shown with dobutamine in a model of short-term hibernation without a concomitant increase in MBF (Arai, Grauer et al. 1995). The second mechanism is the presence of MBF reserve distal to a stenosis despite reduction in resting MBF (Canty *et al.* 1985; Versano *et*

al. 1985). Dobutamine may exploit this reserve allowing increase in %WT, although a concomitant increase in MBF would have to occur.

The discrepancy between the results of dobutamine 2DE and myocardial perfusion imaging in patients with chronic ischaemic LV dysfunction may in part be related to the mix of pathophysiologic substrate in the population being studied. Unlike dobutamine 2DE which depends on unmasking the contractile reserve, myocardial perfusion imaging at rest depends upon the presence of intact microvessels and myocytes. Even when MBF is reduced, perfusion is present, albeit at lower levels, which may be sufficient to maintain the the integrity of the microvasculature and myocytes. These myocytes are unlikely to respond to dobutamine in the presence of reduced MBF, but may ultimately recover their function if revascularized. Recovery in such regions may take longer than in those with normal resting MBF.

5.6 Conclusions:

In this Chapter, a canine model of chronic ischaemic LV dysfunction has been described which closely resembles the condition seen in patients with CAD and reduced LV function. The heterogeneity of regional flow-function relations which provide important insights into the pathophysiology of this condition have been identified. This model may be ideal to further understand the molecular mechanisms responsible for these structural and functional manifestations in chronic ischaemic LV dysfunction. It may also be suitable for studying the effects of interventions on this condition.

Table 5.1

Haemodynamic Data ¶

Mean Post Operative Day	Number of Dogs	Aortic Pressure (mmHg)	Heart rate (bpm)
2	12	85 ± 12	85 ± 19
5	11	88 ± 13	97 ± 37
13	4	91 ± 8	86 ± 18
21	6	89 ± 12	91 ± 25
28	3	83 ± 15	96 ± 31
42	12	88 ± 14	86 ± 29

¶ = No significant interstage differences found
bpm = beats/minute

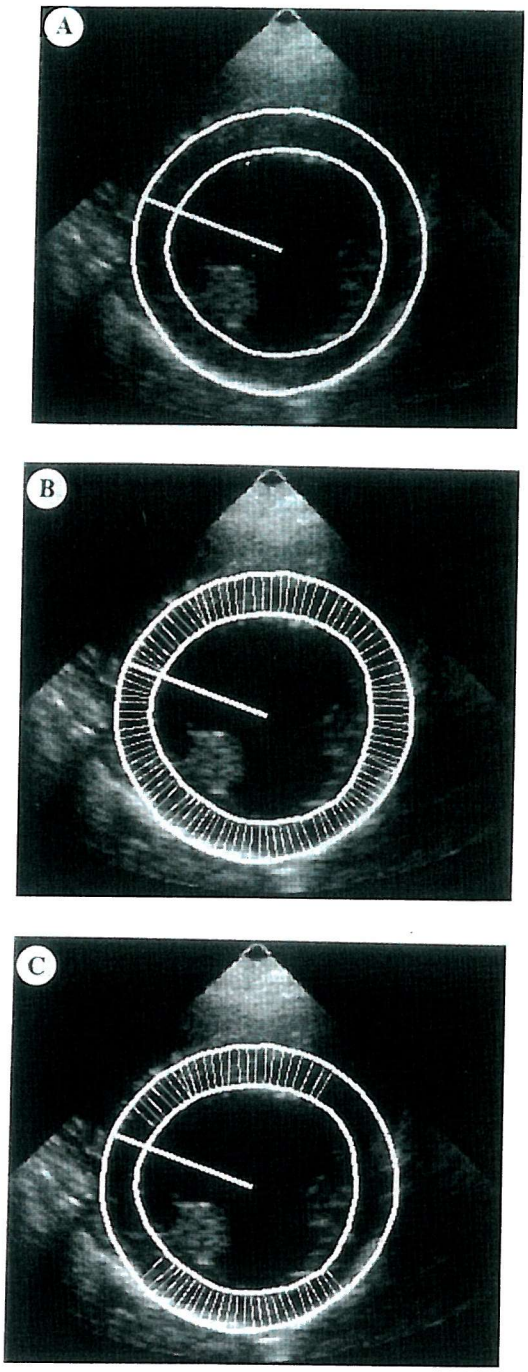

Figure 5.1

Figure 5.1

Method of wall thickening (WT) analysis. **A.** The epicardial and endocardial borders are derived from cubic spline interpolation of points placed on them. **B.** 100 equidistant chords are automatically generated. **C.** Regions of interest are identified. See text for details.

A.

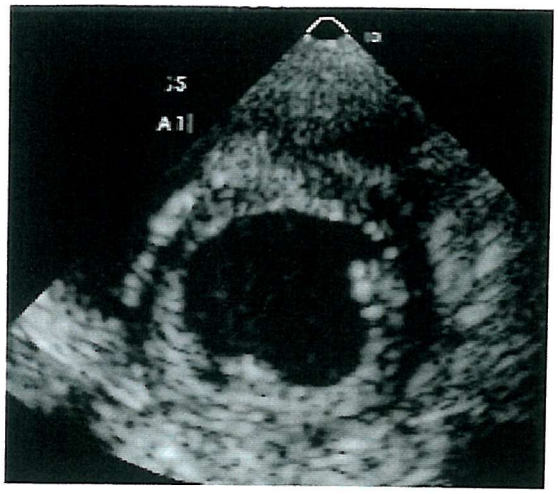

B.

C.

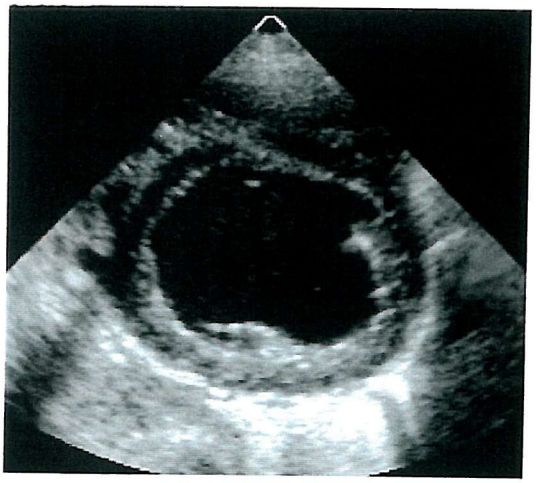

D.

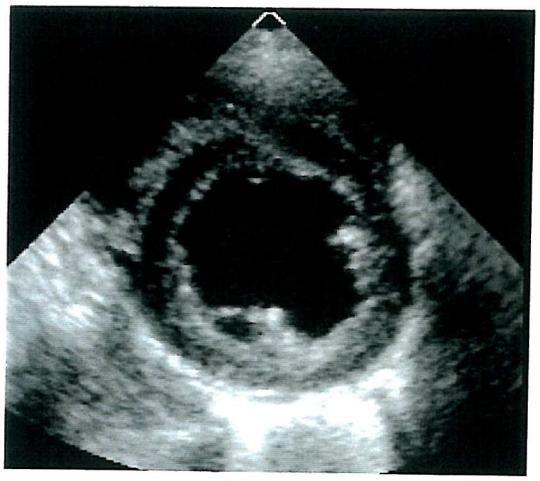

Figure 5.2

Figure 5.2

End diastolic and end systolic short axis views at baseline (**A** and **B**) and at the end of the study (**C** and **D**) in one dog showing wall thinning, reduced systolic function and left ventricular dilatation. See text for details.

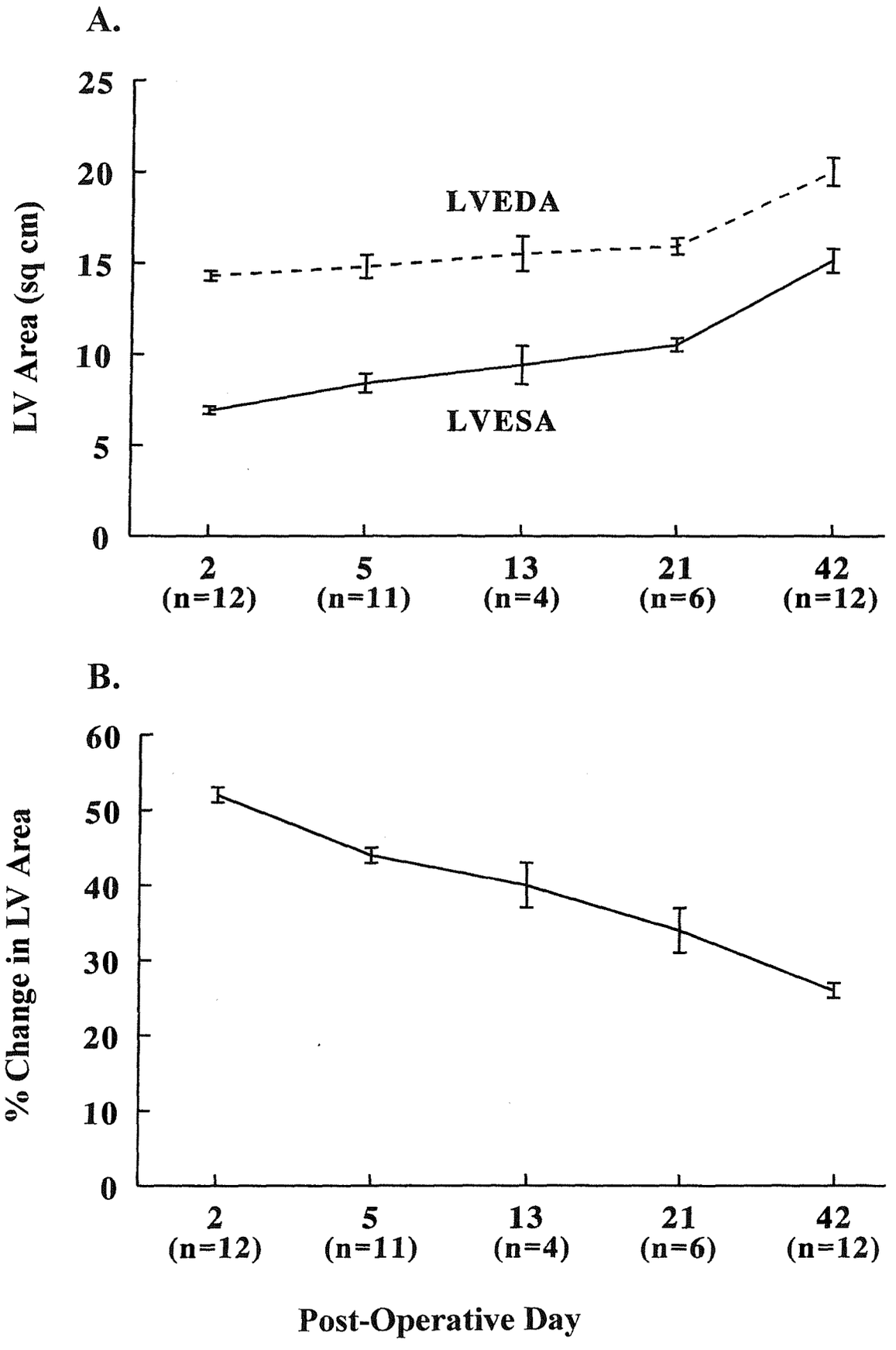
A.
25
20
15
10
5
0
LV Area (sq cm)
LVEDA
LVESA
2 (n=12)
5 (n=11)
13 (n=4)
21 (n=6)
42 (n=12)
B.
60
50
40
30
20
10
0
% Change in LV Area
2 (n=12)
5 (n=11)
13 (n=4)
21 (n=6)
42 (n=12)
Post-Operative Day

Figure 5.3

Figure 5.3

Changes in left ventricular (LV) end-diastolic (LVEDA) and end-systolic (LVESA) area during the course of the study (**A**) and percent change in area from end diastole to end systole (**B**). '*n*' represents the number of observations at that point in time. See text for details.

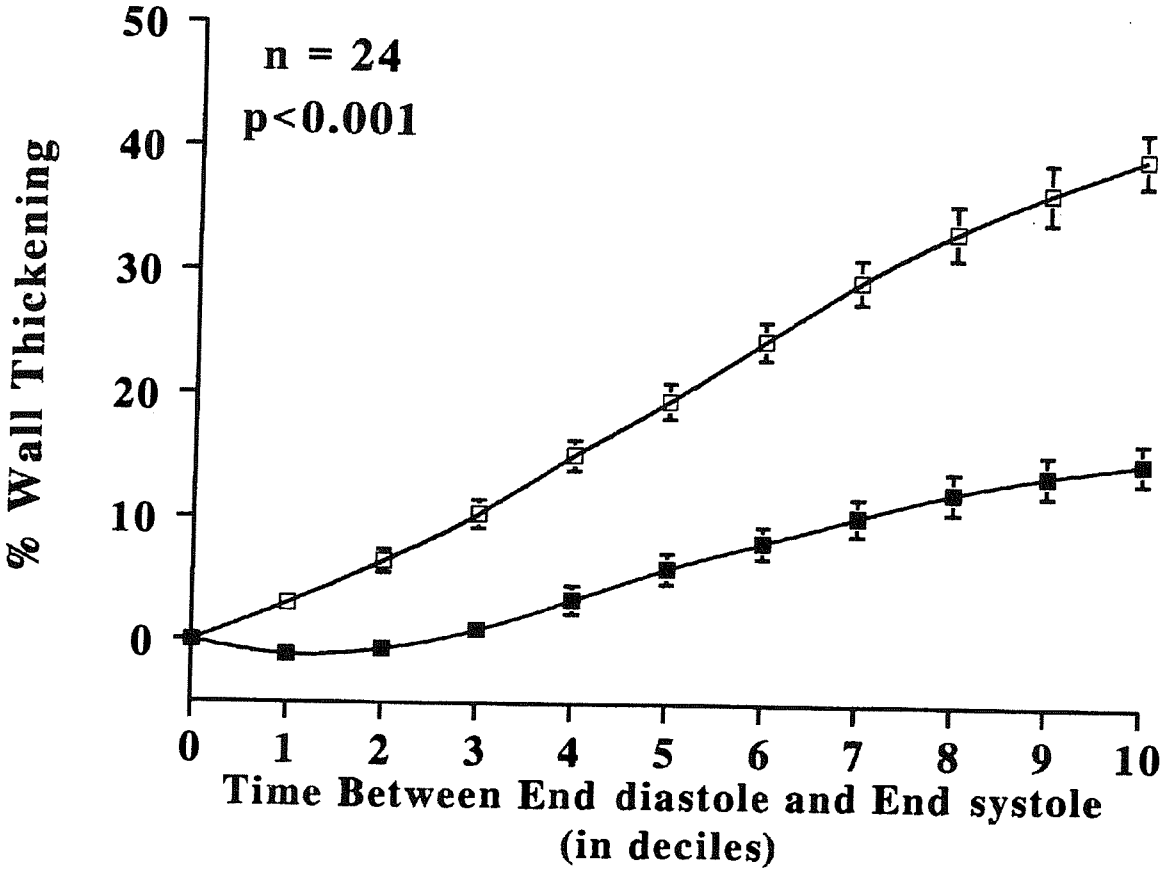
n = 24
p<0.001
% Wall Thickening
50
40
30
20
10
0
0 1 2 3 4 5 6 7 8 9 10
Time Between End diastole and End systole
(in deciles)

Figure 5.4

Figure 5.4

% WT over the entire systolic contraction period from all 24 myocardial beds studied at baseline (*top graph*) and before euthanasia (*bottom graph*) Error bars are mean ± SE. See text for details.

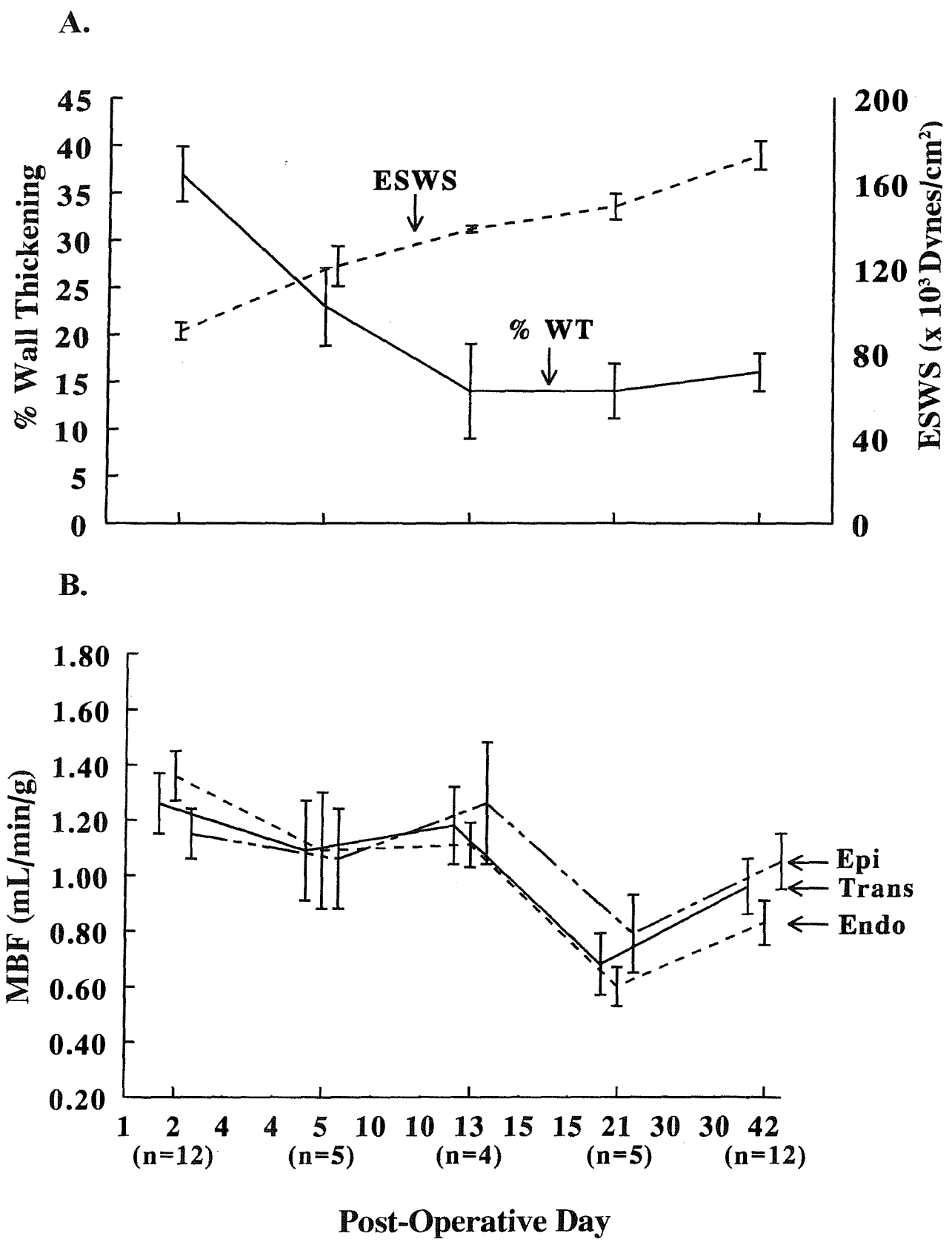
A.
% Wall Thickening
ESWS (x 10³ Dynes/cm²)
ESWS
% WT
45
40
35
30
25
20
15
10
5
0
200
160
120
80
40
0
B.
MBF (mL/min/g)
1.80
1.60
1.40
1.20
1.00
0.80
0.60
0.40
0.20
Epi
Trans
Endo
1 2 4 4 5 10 10 13 15 15 21 30 30 42
(n=12) (n=5) (n=4) (n=5) (n=12)
Post-Operative Day

Figure 5.5

Figure 5.5

Changes in %WT (**A**; left axis), end-systolic wall stress (**A**; right axis) and in regional myocardial blood flow (MBF) in the left anterior descending coronary artery bed (**B**) over time (y-axis) after placement of ameroid constrictors. Error bars are mean ± SE. Epi, epicardial; Trans, transmural; Endo, endocardial. See text for details.

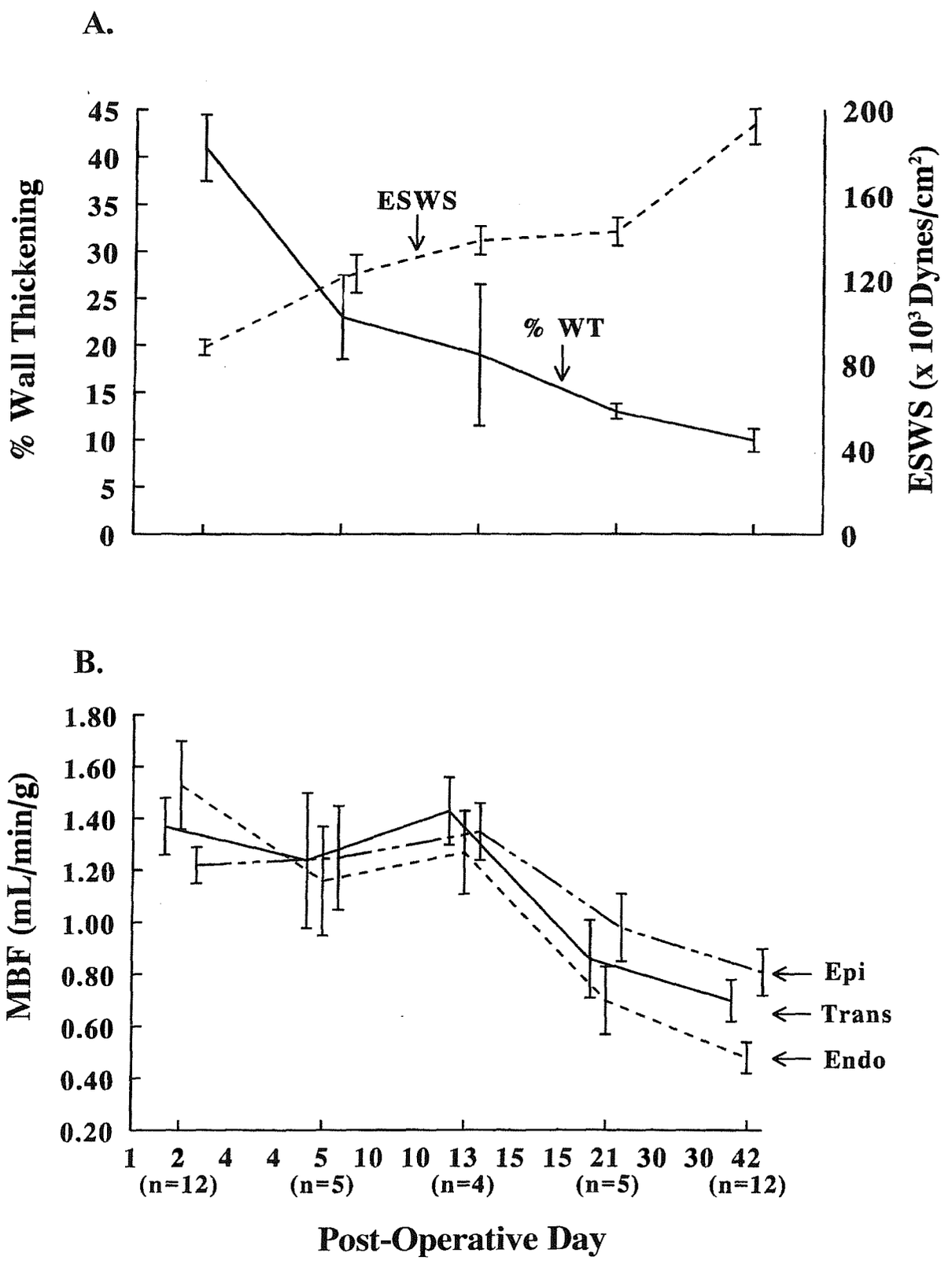
A.
% Wall Thickening
ESWS (x 10³ Dynes/cm²)
ESWS
% WT
45
40
35
30
25
20
15
10
5
0
200
160
120
80
40
0
B.
MBF (mL/min/g)
1.80
1.60
1.40
1.20
1.00
0.80
0.60
0.40
0.20
Epi
Trans
Endo
1 2 4 4 5 10 10 13 15 15 21 30 30 42
(n=12) (n=5) (n=4) (n=5) (n=12)
Post-Operative Day

Figure 5.6

Figure 5.6

Changes in %WT (**A**; left axis), end-systolic wall stress (**A**; right axis) and in regional myocardial blood flow (MBF) in the left circumflex coronary artery bed (**B**) over time (*y*-axis) after placement of ameroid constrictors. Error bars are mean ± SE. Epi, epicardial; Trans, transmural; Endo, endocardial. See text for details.

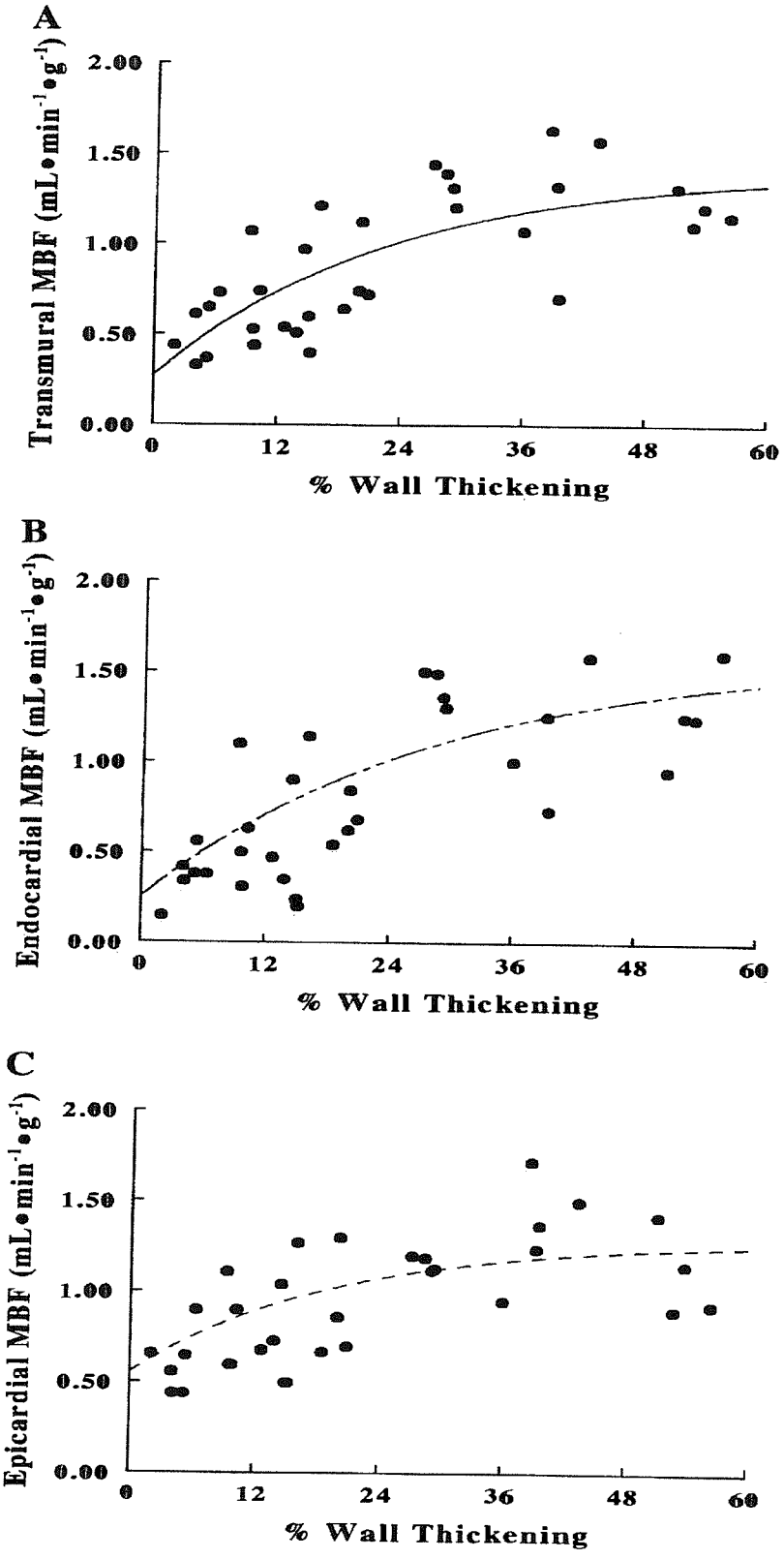
A
Transmural MBF (mL•min-1•g-1)
2.00
1.50
1.00
0.50
0.00
0
12
24
36
48
60
% Wall Thickening
B
Endocardial MBF (mL•min-1•g-1)
2.00
1.50
1.00
0.50
0.00
0
12
24
36
48
60
% Wall Thickening
C
Epicardial MBF (mL•min-1•g-1)
2.00
1.50
1.00
0.50
0.00
0
12
24
36
48
60
% Wall Thickening

Figure 5.7

Figure 5.7

Relation between %WT (x-axis) and regional MBF (y-axis) in regions that ultimately showed a reduction in transmural MBF. **A-C**: relations for transmural, endocardial and epicardial MBF, respectively. Some data points represent more than one observation. See text for details.

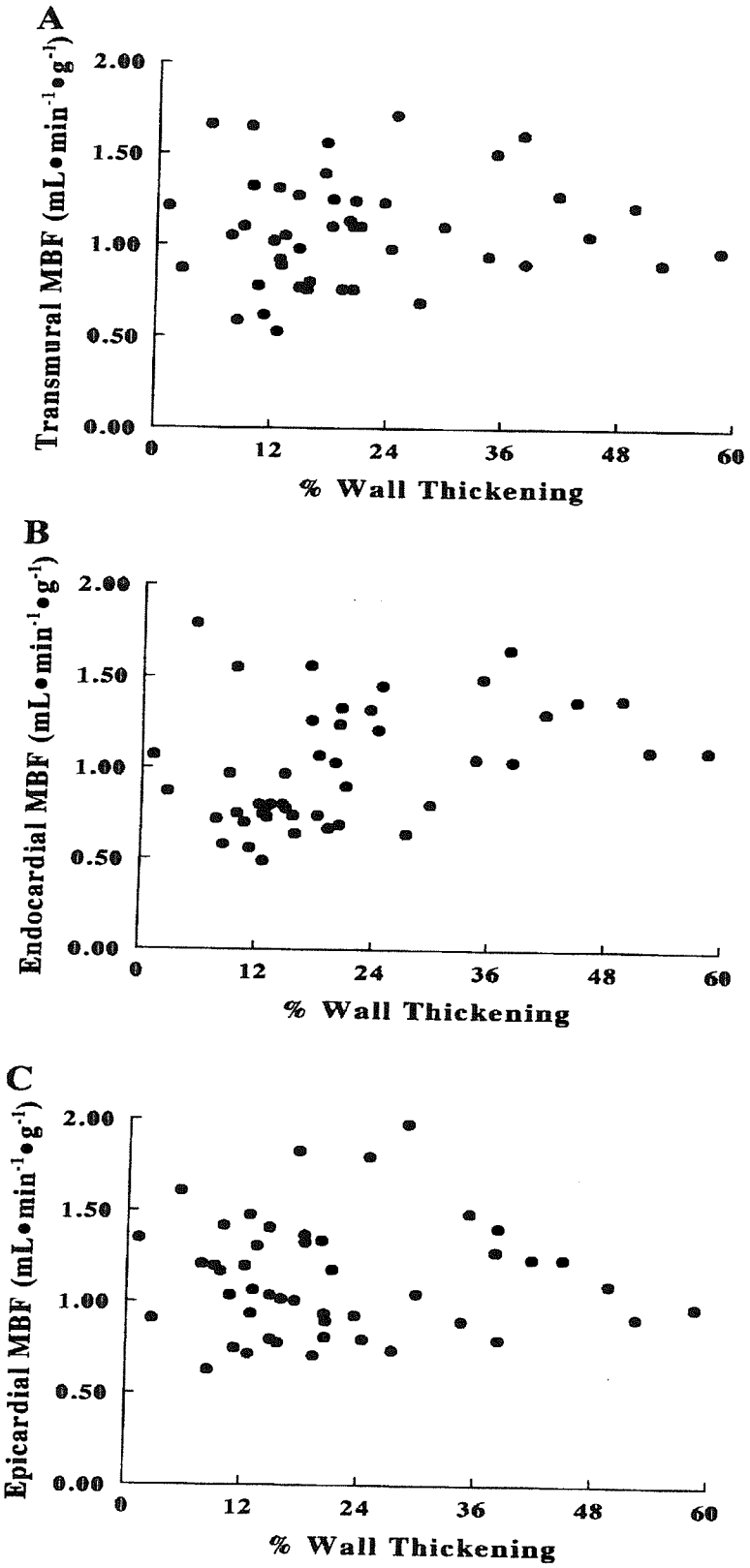
A
Transmural MBF (mL•min-1•g-1)
2.00
1.50
1.00
0.50
0.00
0
12
24
36
48
60
% Wall Thickening
B
Endocardial MBF (mL•min-1•g-1)
2.00
1.50
1.00
0.50
0.00
0
12
24
36
48
60
% Wall Thickening
C
Epicardial MBF (mL•min-1•g-1)
2.00
1.50
1.00
0.50
0.00
0
12
24
36
48
60
% Wall Thickening

Figure 5.8

Figure 5.8

Relation between %WT (x-axis) and regional MBF (y-axis) in regions that ultimately did not show a reduction in transmural MBF. **A-C**: relations for transmural, endocardial and epicardial MBF, respectively. Some data points represent more than one observation. See text for details.

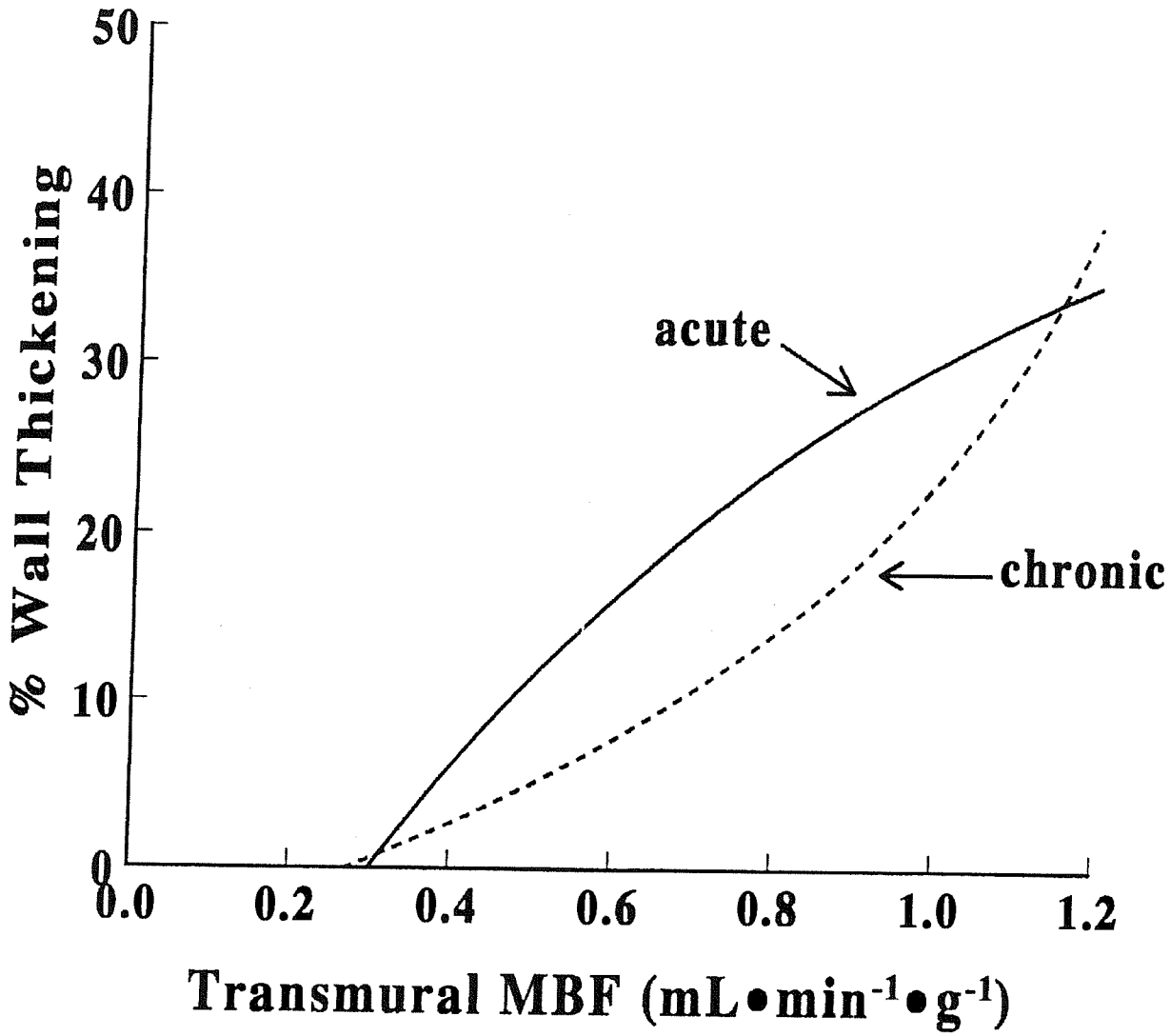
50
40
30
20
10
0
% Wall Thickening
acute
chronic
0.0
0.2
0.4
0.6
0.8
1.0
1.2
Transmural MBF (mL•min-1•g-1)

Figure 5.9

Figure 5.9

Relation between MBF (x-axis) and %WT (y-axis) in the setting of acutely placed (solid line) and chronic (dashed line) stenosis. Data for the solid line have been taken from the literature and those for the dashed line from figure **5.7A** where the axes have been reversed. See text for details.

REFERENCES

Albers, V. M. (1960). Underwater acoustics handbook. State College PA, The Pennsylvania State University Press.

Anderson, C. and S. Bergman (1994). "In search of the perfect PET flow tracer." *Journal of Nuclear Cardiology* **35**: 1122-4.

Arai, A. E., S. E. Grauer, et al. (1995). "Metabolic adaptation to a gradual reduction in myocadial blood flow." *Circulation* **92**: 244-252.

Bergmann, S., S. Hack, et al. (1980). "The dependence of accumulation of 13NH3 by myocardium on metabolic factors and its implications for quantitative assessment of perfusion." *Circulation* **61**: 34-43.

Bergmann, S., P. Herrero, et al. (1989). "Noninvasive quantitation of myocardial blood flow in human subjects with oxygen-15-labeled water and positron emission tomography." *Journal of the American College of Cardiology* **14**: 639-52.

Berman, M., A. J. Fischman, et al. (1996). "Myocardial adaptation during and after sustained, demand-induced ischemia." *Circulation* **94**: 755-62.

Bolukoglu, H., A. J. Liedtke, et al. (1992). "An animal model of chronic coronary stenosis resulting in hibernating myocardium." *Am J Physiol* **263**(1 Pt 2): H20-9.

Braunwald, E. and R. A. Kloner (1982). "The stunned myocardium: prolonged, postischemic ventricular dysfunction." *Circulation* **66**(6): 1146-9.

Braunwald, E. and J. D. Rutherford (1986). "Reversible ischemic left ventricular dysfunction: evidence for the "hibernating myocardium"." *J Am Coll Cardiol* **8**(6): 1467-70.

Brunken, R. C., S. Kottori, et al. (1989). "PET detection of viable tissue in myocardial segments with persistent detects with Tl-201 SPECT." *Radiology* **172**: 65-73.

Burns, P. N., J. E. Powers, et al. (1996). "Harmonic imaging: Principles and preliminary results." *Clinical Radiology* **51(Suppl I)**: 50-55.

Canty, J. M. and F. Klocke (1985). "Reduced regional myocardial perfusion in the presence of pharmacologic vasodilator reserve." *Circulation* **71**: 370-377.

Chen, C., L. Chen, et al. (1996). "Functional and structural alterations with 24-hour myocardial hibernation and recovery after reperfusion. A pig model of myocardial hibernation." *Circulation* **94**(3): 507-16.

Cigarroa, C. C., C. R. deFillipi, et al. (1993). "Dobutamine stress echocardiography identifies hibernating myocardium and predicts recovery of left ventricular function after coronary revascularisation." *Circulation* **88**: 430-436.

Cohen, M. V. (1985). Morphological considerations of the coronary collateral circulation in man. Coronary collaterals . New York, Futura. 1-91.

Crystal, G. J., H. F. Downey, et al. (1981). "Small vessel and total coronary blood volume during intracironary adenosine." *Am J Physiol* **241**: H194-H206.

deJong, N. (1993). Higher harmonics of vibrating gas-filled microspheres. Acoustic properties of ultrasound contrast agents . Woerden, Zuidam & Zonen bv. 61-78.

DiCarli, M. F., F. Asgarzadie, et al. (1995). "Quantitative relation between myocardial viability and improvement in heart failure symptoms after revascularization in patients with ischaemis cardiomyopathy." *Circulation* **92**: 3436-3444.

Eigler, N. L., H. Schunlen, et al. (1991). "Digital angiographic impulse response analysis of regional myocardial perfusion: estimation of coronary flow, flow reserve, and distribution volume by compartmental transit time measurement in a canine model." *Circ res* **68**: 870-880.

Eliasen, P. and O. Amtrop (1984). "Effect of intracoronary adenosine upon regional blood flow, microvascular blood volume and haematocrit in canine myocardium." *Int J Microcirc* **3**: 3-12.

Fallavolita, J. A., B. J. Perry, et al. (1997). "18F-2-deoxyglucose deposition and regional flow in pigs with chronically dysfunctional

myocardium. Evidence for transmural variations in chronic hibernating myocardium." *Circulation* **95**: 1900-1909.

Firschke, C., J. Lindner, et al. (1997-1). "Myocardial contrast echocardiography in acute myocardial infarction using aortic root injections of microbubbles in conjuction with harmonic imaging: potential application in the cardiac catheterization laboratory." *Journal of the American College of Cardiology* **29**: 207-16.

Firschke, C., J. R. Lindner, et al. (1997-2). "Myocardial perfusion imaging in the setting of coronary artery stenosis and acute myocardial infarction using venous injection of a second generation echocardiographic contrast agent." *Circulation* **96**: 959-976.

Fukuyama, T., M. Nakamura, et al. (1978). "Reduced reflow and diminished uptake of 86Rb after temporary coronary occlusion." *American Journal of Physiology* **234**: H724-9.

Gallagher, K. P., M. Matsuzaki, et al. (1984). "Regional myocardial perfusion and wall thickening during ischaemia in conscious dogs." *American Journal of Physiology* **247**: H727-H738.

Gensini, G. G. (1969). "The coronary collateral circulation in living man." *American Journal of Cardiology* **24**: 393-400.

Gerber, B. L., J. J. Vanoverschelde, et al. (1996). "Myocardial blood flow, glucose uptake, and recruitment of inotropic reserve in chronic left ventricular ischemic dysfunction: Implications for the pathology of chronic myocardial hibernation." *Circulation* **94**: 651-59.

Gewirtz, H., A. J. Fischman, et al. (1994). "Positron emission tomographic measurements of absolute regional myocardial blood flow permits identification of nonviable myocardium in patents with chronic myocardial infarction." *J Am Coll Cardiol* **23**: 851-859.

Gheorghiade, M. and R. O. Bonow (1998). "Chronic heart failure in the United States. A manifestation of coronary artery disease." *Circulation* **97**: 282-289.

Goldman, M. E. and B. P. Mindich (1984). "Intraoperative cardioplegia contrast echocardiography for assessing myocardial perfusion during open heart surgery." *Journal of the American College of Cardiology* **4**: 1029-.

Gould, K. L. and K. Lipscombe (1974). "Effects of coronary stenoses on coronary flow reserve and resistance." *American Journal of Cardiology* **34**: 48-55.

Hauser, A., V. Ghangadharan, et al. (1985). "Sequence of mechanical, electrocardiographic and clinical effects of repeated coronary occlusion in human beings :echocardiographic observations during coronary balloon angioplasty." *Journal of the American College of Cardiology* **5**: 193-97.

Hess, O., M. Mcgillem, et al. (1990). "Determination of coronary flow reserve by parametric imaging." *Circulation* **82**: 1438-48.

Heymann, M. A., B. D. Payne, et al. (1977). "Blood flow measurements with radionuclide-labeled particles." *Prog Cardiovasc Dis* **20**: 52-79.

Homans, D. C., E. Sublett, et al. (1986). "Persistence of regional left ventricular dysfunction after exercise-induced myocardial ischaemia." *J Clin Invest* 77: 66-73.

Hood, W. P., C. Rackley, et al. (1968). "Wall stress in the normal and hypertrophied left ventricle." *Am J Cardiol* **22**: 550-558.

Hutchins, G. D. and M. Schwaiger (1993). Quantifying myocardial blood flow with PET. Nuclear Cardiology: State-of-the-art and future directions . St Louis, CV Mosby Co. 305-313.

Ikeda, H., Y. Koga, et al. (1986). "Quantitative evaluation of regional myocardial blood flow by videodensitometric analysis of digital substraction coronary arteriography in humans." *Journal of the American College of Cardiology* **8**: 809-16.

Ismail, S., A. R. Jayaweera, et al. (1996). "Relation between air-filled albumin microbubble and red cell rheology in the human myocardium: Influence of echocardiographic systems and chest wall attenuation." *Circulation* **94**: 445-451.

Ito, H., K. Iwakura, et al. (1995). "Temporal changes in myocardial perfusion patterns in patients with reperfused anterior wall myocardial infarction." *Circulation* **91**: 656-662.

Ito, H., T. Tomooka, et al. (1992). "Lack of myocardial pefusion immediately after successful thrombolysis: A predictor of poor recovery of left ventricular function in anterior myocardial infarction." *Circulation* **85**: 1699-1705.

Jayaweera, A. R., N. Edwards, et al. (1994). "In vivo myocardial kinetics of air-filled albumin microbubbles during myocardial contrast echocardiography:comparison with radiolabelled red blood cells." *Circulation* **74**: 1157-65.

Jayaweera, A. R., S. Ismail, et al. (1994). "Attenuation deforms time-intensity curves during contrast echocardiography: Implications for the asessment of transit rates." *J Am Soc Echocardiogr* **7**: 590-597.

Jayaweera, A. R., T. L. Matthew, et al. (1990). "Method for the quantitation of myocardial perfusion during myocardial contrast two-dimensional evhocardiography." *J Am Soc Echocardiogr* **3**: 91-98.

Jayaweera, A. R., J. Sklenar, et al. (1994). "Quantification of images obtained during myocardial contrast echocardiography." *Echocardiography* **11**: 385-396.

Jayaweera, A. R., D. M. Skyba, et al. (1995). "Technical factors that influence the determination of microbubble transit rate during contrast echocardiography." *J Am Soc Echocardiogr* **8**(2): 198-206.

Kassab, G. S., D. H. Lin, et al. (1994). "Morphometry of pig coronary venous system." *Am J Physiol* **267**: H2100-H2113.

Kaul, S. (1989). "A look at 15 years of planar thallium-201 imaging." *Am Heart J* **118**: 581-601.

Kaul, S. (1990). "Echocardiography in coronary artery disease." *Curr Probl Cardiol* **15**: 239-298.

Kaul, S. (1995-1). "Assessment of coronary microcirculation with myocardial contrast echocardiography: current and future clinical applications." *British Heart Journal* **73**: 490-5.

Kaul, S. (1995-2). "There may be more to myocardial viability than meets the eye!" *Circulation* **92**: 2790-93.

Kaul, S. (1996). "Response of dysfunctional myocardium to dobutamine. "The eyes see what the mind knows!"[editorial; comment]." *J Am Coll Cardiol* **27**(7): 1608-11.

Kaul, S. and A. R. Jayaweera (1997). "Coronary and myocardial blood volumes: Noninvasive tools to assess the coronary microcirculation?" *Circulation* **96**: 719-724.

Kaul, S., P. Kelly, et al. (1989). "Assessment of regional myocardial blood flow with myocardial contrast two dimensional echocardiography." *Journal of the American College of Cardiology* **13**: 468-82.

Kaul, S., R. Senior, et al. (1997). "Detection of coronary artery disease using myocardial contrast echocardiography: Comparison with ^{99m}Tc-Sestamibi single photon emission computed tomography." *Circulation* **96**: 785-92.

Kaul, S., W. D. Spotnitz, et al. (1991). "Mechanism of ischaemic mitral regurgitation: an experimental evaluation." *Circulation* **84**: 2167-2180.

Keller, M. W., W. Glasheen, et al. (1988). "Myocardial contrast echocardiography without significant haemodynamic effects or reactive hyperaemia: A major advantage in the imaging of regional myocardial perfusion." *Journal of the American College of Cardiology* **12**: 1039-47.

Keller, M. W., S. S. Segal, et al. (1989). "The behavior of sonicated albumin microbubbles within the microcirculation: A basis for their use during myocardial contrast echocardiography." *Circulation Research* **65**: 458-67.

Keller, M. W., W. D. Spotnitz, et al. (1990). "Intraoperative assessment of regional myocardial perfusion using quantitative myocardial contrast echocardiography: an experimental evaluation." *Journal of the American College of Cardiology* **16**: 1267-79.

Klitzman, B. and B. R. Duling (1979). "Microvascular haematocrit and red cell flow in resting and contracting striated muscle." *Am J Physiol* **237**: H481-H490.

Kloner, R. A., J. Allen, et al. (1991). "Stunned left ventricular myocardium after exercise treadmill testing in coronary artery disease." *Am J Cardiol* **68**: 329-334.

LaCanna, G., O. Alfieri, et al. (1994). "Echocardiography during infusion of dobutamine for identification of reversible dysfunction in patients with chronic coronary artery disease." *J Am Coll Cardiol* **23**: 617-626.

Leppo, J. A. and D. J. Meerdink (1989). "Comparison of the myocardial uptake of a technetium-labeled isonitrile analogue and thallium." *Circulation Research* **65**: 632-9.

Lindner, J. R., C. Firschke, et al. (1998). "Myocardial perfusion characteristics and haemodynamic profile of MRX-115, a venous echocardiographic contrast agent , during acute myocardial infarction." *J Am Soc Echocardiogr* **11**: 36-46.

Lindner, J. R. and S. Kaul Myocardial perfusion imaging using tracers other than radioisotopes and detectors other than gamma cameras. Nuclear Cardiology: State-of-the-art and future directions (2nd Ed) Eds. G. A. Beller and B. L. Zaret. St Louis, CV Mosby Co. (in pres).

Lindner, J. R. and S. Kaul (1995). "Insights into the assessment of myocardial perfusion offered by different cardiac imaging modalities." *Journal of Nuclear Cardiology* **2**: 446-60.

Lindner, J. R., D. M. Skyba, et al. (1997). "Changes in myocardial blood volume with graded coronary stenosis." *American Journal of Physiology* **272**: H567-H575.

Litvak, J., L. E. Siderides, et al. (1957). "Experimental production of coronary artery insufficiency and occlusion." *Am Heart J* **53**: 505-518.

Ludman, P. F. and P. A. Poole-Wilson (1993). "Myocardial perfusion in humans : What can we measure?" *British Heart Journal* **70**: 307-314.

Maddahi, J., H. Kiat, et al. (1993). Technetium-99m-sestamibi myocardial perfusion for evaluation of coronary artery disease. Nuclear Cardiology: State-of-the-art and future directions . St Louis, CV Mosby Co. 191-200.

Marcus, M. L. (1983). Metabolis regulation of coronary blood flow. The coronary circulation in health and disease . New York, McGraw Hill &Co. 65-92.

Marinho, N. V. S., B. E. Keogh, et al. (1996). "Pathophysiology of chronic left ventricular dysfunction: Insights from the measurement of absolute myocardial blood flow and glucose utilization." *Circulation* **93**: 737-744.

Meyer, S. L., G. C. Curry, et al. (1976). "Influence of dobutamine on haemodynamics and coronary blood flow in patients with and without coronary artery disease." *Am J Cardiol* **38**: 103-108.

Mills, I., J. T. Fallon, et al. (1994). "Adaptive responses of the coronary circulation and myocardium to chronic reduction in perfusion pressure and flow." *American Journal of Physiology* **266**: H447-H457.

Mulvagh, S. L., D. A. Foley, et al. (1996). "Second harmonic imaging of an intravenously administered echocardiographic contrast agent. Visualisation of coronary arteries and measurement of coronary blood flow reserve." *J Am Coll Cardiol* **27**: 1519-1525.

Pagley, P. R., G. A. Beller, et al. (1997). "Improve outcome after coronary bypass surgery in patients with ischaemic cardiomyopathy and residual viability." *Circulation* **96**: 793-800.

Parodi, O., R. D. Maria, et al. (1993). "Myocardial blood flow distribution in patients with ischaemic heart disease or dilated cardiomyopathy undergoing heart transplantation." *Circulation* **88**: 509-522.

Passamani, E., K. B. Davis, et al. (1985). "A randomised trial of coronary artery bypass surgery: Survival of patients with low ejection fraction." *New England Journal of Medicine* **312**: 1655-1671.

Porter, T. R. and F. Xie (1995). "Transient myocardial contrast after initial exposure to diagnostic pressures with minute doses of intravenously injected microbubbles. Demonstration and potential mechanisms." *Circulation* **92**: 2391-2395.

Porter, T. R., F. Xie, et al. (1996). "Improved myocardial contrast with second harmonic transient ultrasound response imaging in humans using intravenous perfluorocarbon-exposed sonicated dextrose albumin." *Journal of the American College of Cardiology* **27**: 1497-501.

Ragosta, M., G. A. Beller, et al. (1993). "Quantitative planar rest-redistribution 201Tl imaging in detection of myocardial viability and prediction of improvement in left ventricular function after coronary bypass surgery in patients with severly depressed left ventricular function." *Circulation* **87**: 1630-=1641.

Rahimtoola, S. H. (1985). "A perspective on the three large multicentre randomised clinical trials of coronary bypass surgery for chronic stable angina." *Circulation* **72(Suppl V)**: V123-V135.

Rahimtoola, S. H. (1996). "Hibernating myocardium has reduced blood flow at rest that increases with low-dose dobutamine [editorial; comment]." *Circulation* **94**(12): 3055-61.

Rauch, B., F. Helus, et al. (1985). "Kinetics of 13N-ammonia uptake in myocardial single cells indicating potential limitations in its applicability as a marker of myocardial blood flow." *Circulation* **71**: 387-93.

Ross, J. (1986). "Assessment of ischaemic regional myocardial dysfunction and its reversibility." *Circulation* **74**: 1186-1190.

Sabia, P. J., E. R. Powers, et al. (1992). "Functional significance of collateral blood flow in patients with recent acute myocardial infarction." *Circulation* **85**: 2080-89.

Sabia, P. J., E. R. Powers, et al. (1992). "An association between collateral blood flow and myocardial viability in patients with recent myocardial infarction." *New England Journal of Medicine* **327**: 1825-31.

Schelbert, H. R. and J. Czernin (1993). PET studies of myocardial blood flow and metabolism in patients with acute myocardial infarction. Nuclear Cardiology: State-of-the-art and future directions . St Louis, CV Mosby Co. 294-302.

Schrope, B., V. L. Newhouse, et al. (1992). "Simulated capillary blood flow measurement using a nonlinear ultrasonic contrast agent." *Ultrason Imaging* **14**: 134-158.

Schulz, R., J. Rose, et al. (1993). "Development of short-term myocardial hibernation: Its limitation by the severity of ischemia and inotropic stimulation." *Circulation* **88**: 684-95.

Senior, R., B. Glenville, et al. (1995). "Dobutamine echocardiography and thallium -201 imaging predict functional improvement after revascularization in severe left ventricular dysfunction." *Br Heart J* **74**: 358-364.

Shen, Y. and S. F. Vatner (1995). "Mechanism of impaired myocardial function during progressive coronary stenosis in conscious pigs: Hibernation versus stunning?" *Circulation Research* **76**: 479-488.

Sherman, A. J., K. R. Harris, et al. (1997). "Proportionate reversible decreases in systolic function and myocardial oxygen consumption after modest reductions in coronary flow: Hibernating versus stunning." *J Am Coll Cardiol* **29**: 1623-1631.

Sklenar, J., G. Camarano, et al. (1996). "Contractile versus microvascular reserve for the determination of the extent of myocardial salvage after reperfusion: the effect of residual stenosis." *Circulation* **94**: 1430-1440.

Sklenar, J., A. R. Jayaweera, et al. (1992). "A computer aided approach for the quantitation of left ventricular function using two-dimensional echocardiography." *J Am Soc Echocardiogr* **5**: 33-40.

Skyba, D. M., G. Camarano, et al. (1996). "Haemodynamic characteristics, myocardial kinetics, and microvascular rheology of FS-069, a second generation echocardiographic agent capable of producing myocardial opacification from a venous injection." *Journal of the American College of Cardiology* **28**: 1292-300.

Skyba, D. M., A. R. Jayaweera, et al. (1994). "Quantification of myocardial perfusion with myocardial contrast echocardiography during left atrial injection of contrast." *Circulation* **90**: 1513-21.

Spotnitz, W. D., M. W. Keller, et al. (1988). "Success of internal mammary bypass grafting can be assessed intraoperatively using myocardial contrast echocardiography." *Journal of the American College of Cardiology* **12**: 196-201.

Tennant, R. and C. J. Wiggers (1935). "The effect of coronary occlusion on myocardial contraction." *American Journal of Physiology* **112**: 351-61.

Tillisch, J., R. Brunken, et al. (1986). "Reversibility of cardiac wall motion abnormalities predicted by positron tomography." *New England Journal of Medicine* **314**: 884-9.

Vanoverschelde, J. J., W. Wijns, et al. (1997). "Chronic myocardial hibernation in humans. From bedside to bench." *Circulation* **95**: 1961-1971.

Vanoverschelde, J. J., W. Wijns, et al. (1993). "Mechanisms of chronic regional post ischaemic dysfunction in humans." *Circulation* **87**: 1513-23.

Varnauskas, E. (1988). "Twelve year followup of survival in the randomised European Coronary Surgery Study." *New England Journal od Medicine* **319**: 332-337.

Versano, T. and L. C. Becker (1985). "Persistence of coronary vasodilator reserve despite functionally significant flow reduction." *Am J Physiol* **248**: H403-H411.

Villanueva, F. S., G. Camarano, et al. (1996). "Coronary reserve abnormalities in the infarcted myocardium: Assessment of myocardial viability immediately versus late after reflow by contrast echocardiography." *Circulation* **94**: 748-754.

Villanueva, F. S., W. D. Spotnitz, et al. (1992). "On-line intraoperative quantitation of regional myocardial perfusion during coronary artery bypass graft operations with myocardial two-dimensional echocardiography." *Journal of Thoracic and Cardiovascular Surgery* **104**: 1524-31.

Wang, T., X. Wu, et al. (1989). "Myocardial blood flow estimated by synchronous, multislice, high speed computed tomography." *Trans Med Imaging* **8**: 70-77.

Wei, K., S. Firoozan, et al. (1997-1). "Quantification of the severity of coronary stenoses using venous injection of minute amounts of AFO150 during intermittent harmonic imaging." *Journal of the American College of Cardiology* **29(Suppl A)**: 222A.

Wei, K., S. Firoozan, et al. (1997-2). "Detection of coronary stenosis from intravenous administration of microbubbles: Bolus injection or continuous infusion." *Circulation* **96 (Suppl 1)**: I-213.

Wei, K., S. Firoozan, et al. (1997-3). "Use of microbubble destruction as a novel method for the qauntification of myocardial perfusion with contrast echocardiography during venous infusion of contrast." *Journal of the American College of Cardiology* **29(Suppl A)**: 2(A).

Wei, K., A. R. Jayaweera, et al. (1998). "Quantification of myocardial blood flow with ultrasound-induced destruction of microbubbles administered as a constant infusion." *Circulation* **97**: 473-483.

Wei, K., D. M. Skyba, et al. (1997). "Interactions between microbubbles and ultrasound: in vitro and in vivo observations." *J Am Coll Cardiol* **29**: 1081-1088.

Weintraub, W. S., S. Hattori, et al. (1981). "The relation between myocardial blood flow and contraction by layer in the canine left ventricle during ischaemia." *Circ Res* **48**: 430-438.

Wu, C. C., M. D. Feldman, et al. "Myocardial contrast echocardiography can be used to quantify intramyocardial blood volume: new insights into structural mechanisms of coronary autoregulation." *Circulation* : in press.

Wu, X., D. L. Ewert, et al. (1992). "In vivo relation of intra-myocardial blood volume to myocardial perfusion: evidence supporting microvascular site for autoregulation." *Circulation* **85**: 730-737.

BIBLIOGRAPHY

Dawson D, **Firoozan S.** Assessment of myocardial perfusion using ultrasound. *Int J Cardiol (in press)*

Firoozan S, Wei K, Linka A, Gaffey M, Goodman NC, Kaul S. A canine model of chronic ischaemic cardiomyopathy: Characterization of regional flow- function relations.*Am J Physiol* 1999; **276 :** H446-H455

Wei K, Jayaweerea AR, Lindner Jr, **Firoozan S,** Linka AZ, Kaul S. Quantification of myocardial perfusion with contrast echocardiography. *J Invest Radiol* (in Press)

Firoozan S, Forfar JC. Exercise training and the coronary collateral circulation: Is its value underestimated in man? *European Heart J* 1996;**17**:1791-95

Firoozan S, Kaul S. Echocardiography in acute myocardial infaction: Today and tomorrow. *Indian Heart J* 1996; **48** : 23-32

Firoozan S, Ates G, Wei K, Goodman NC, Skyba DM, Kaul S: Quantification of myocardial Perfusion with myocardial contrast echocardiography during venous injection of contrast. *Journal of the American Coll of Cardiology (In press)*

Forfar JC, **Firoozan S.** Application of coronary angiography in the UK: disease severity or physician preference? *Q J Med* 1995; **88**:147-8

Wei K, **Firoozan S,** Jayaweera AR, Skyba DM, Goodman NC, Kaul S: Use of microbubble destruction as a novel method for the quantification myocardial perfusion with contrast echocardiography during venous infusion of contrast *Circulation* 1998;**98** :473-483

Wei K, Jayaweera A R, **Firoozan S**, Linka A, Skyba D, Kaul S. Basis for detection of stenosis using venous administration of microbubbles during myocardial contrast echocardiography: Bolus or continuous infusion? *J Am Coll Cardiol* **1998** ;32: 252-60

Linka A, Ates G, Wei K, **Firoozan S**, Skyba DM, Kaul S: Three-dimensional myocardial contrast echocardiography: Validation of in-vivo risk and infarct volumes *Journal of the American College of Cardiology*1997;30:1892-9

Abstracts

Firoozan S, Wei K, Ates G, Linka A, Goodman NC, Kaul S: A Canine model of ischaemic Cardiomyopathy: Characterization of regional flow-function relations. *Journal of the American College of Cardiology* **1998**; 31(Suppl A): 256(A)

Firoozan S, Wei K, Ates G, Linka A, Goodman NC, Kaul S: Flow-function relations in a model of progressive ischaemic Cardiomyopathy. *Heart* **1998** 79: p20

Pelberg RA, **Firoozan S**, Linla AZ, Goodman C, Kaul S: Myocardial contrast echocardiography can detect viability in chronic ischaemic left

ventricular dysfunction : comparison with dobutamine echocardiography. *JASE* **1998**

Firoozan S, Wei K, Ates G, Linka A, Goodman NC, Kaul S: Quantification of the severity of coronary stenoses during bolus intravenous injection of contrast during contrast echocardiography. October **1996** 11th Annual Symposium on Echocardiography, Chicago, Illinois .

Firoozan S, Wei K, Linka A, Ates G, Goodman NC, Kaul S: Both repetitive stunning and hibernation are present in chronic ischaemic left ventricular dysfunction: Serial flow function studies in a chronic canine model. *Journal of the American College of Cardiology* **1997**; 29(Suppl A): 480(A)

Wei K, **Firoozan S**, Jayaweera AR, Skyba DM, Goodman NC, Kaul S: Use of microbubble destruction as a novel method for the quantification myocardial perfusion with contrast echocardiography during venous infusion of contrast. *Journal of the American College of Cardiology* **1997**; 29(Suppl A): 2(A)
Winner of Investigator Prize in Physiology, ACC 1997

Firoozan S, Wei K, Jayaweera, Skyba DM, Goodman NC, Kaul S: Quantification of myocardial blood flow with contrast echocardiography using intravenous infusion of contrast. *Journal of Nuclear Cardiology* **1997**; 4 (1): S115

Wei K, **Firoozan S,** Ates G, Linka A, Goodman N, Kaul S: Quantification of the severity of coronary stenoses using venous injection of minute amounts of AFO150 during intermittent harmonic imaging. *Journal of the American College of Cardiology* **1997**; 29(Suppl A): 222(A)

Firoozan S, Wei K, Ates G, Skyba DM, Goodman N, Kaul S. Quantification of myocardial perfusion with contrast echocardiography during venous administration of contrast. *Heart* 1997; 77 **(Suppl 1)**:p 41

Linka A, Ates G, **Firoozan S**, Wei K, Skyba DM, Kaul S: Three-dimensional myocardial contrast echocardiography using a new deposit contrast agent: An experimental study with implications for the cardiac catheterization laboratory. **1997** *American Society of Echocardiography*

Firoozan S, Wei K, Ates G, Goodman N, Skyba D, Kaul S: Requirements for quantification of myocardial perfusion with echocardiography during venous injection of contrast. **1997** *European Society of Cardiology*

Firoozan S, Wei K, Ates G, Linka A, Goodman N, Kaul S. The severity of coronary stenoses can be quantified with intravenous injection of contrast during intermittent harmonic imaging. **1997** *European Society of Cardiology*

Firoozan S, Wei K, Jayaweera AR, Skyba DM, Goodman NC, Kaul S. Quantification of myocardial blood flow with contrast echocardiography during venous infusion of contrast. **1997** *12th Symposium on Echocardiology* (Rotterdam)

Wei K, **Firoozan S,** Jayaweera A, Skyba D, Kaul S. Detection of coronary stenoses from venous administration of microbubbles: Bolus injection or continuous infusion? **1997** *American Heart Asscoiation*

Firoozan S, Wei K, Ates G, Linka A, Skyba D, Kaul S. Flow-function relations in a canine model of progressive ischaemic cardiomyopathy **1998** *British Cardiac Society*